

Magnus Skramstad

Anode-free Lithium Metal Batteries with High-Concentration Ether Electrolytes

Master's thesis in Materials Science and Engineering

Supervisor: Ann Mari Svensson

July 2021

Magnus Skramstad

Anode-free Lithium Metal Batteries with High-Concentration Ether Electrolytes

Master's thesis in Materials Science and Engineering
Supervisor: Ann Mari Svensson
July 2021

Norwegian University of Science and Technology



Preface

This thesis is written as part of the course "TMT4905 - Materials Technology, Master's Thesis", and is the final course of a five year materials science and engineering Master's degree program (MTMT) at the Norwegian University of Science and Technology (NTNU). The work described in this thesis has been done during spring 2021. All experimental work presented has been conducted by the author.

First and foremost I would like to thank my supervisor Ann Mari Svensson for excellent guidance, helpful discussions, and feedback. Thanks to PhD candidates Heidi Thuv and Harald Norrud Pollen for practical help in the lab and insightful discussions. Thanks to Staff Engineer Pei Na Kui and Senior Engineer Agnes Christina Diagrane for practical help in the lab and equipment training. Thanks to all people involved in the battery group at NTNU for sharing their battery research, providing interesting insights to the battery world. I would like to thank my fellow co-students in material science, especially Joachim Sebastian Bjørklund for interesting battery related discussions over the last year.

This thesis is intended for readers with a background in electrochemistry and material science.

Trondheim, 2021

Magnus Skramstad

Abstract

As the demand for batteries is growing rapidly, new batteries capable of storing more energy are needed. Replacing the graphite anode with lithium metal is a promising solution to increase the energy density of lithium-ion batteries. However, there are many problems associated with lithium metal due to its high reactivity and tendency to grow non-uniformly.

An anode-free configuration has been tested in this work, seen as a promising configuration for the practical realization of the lithium metal anode. The cells used had an LFP - Cu structure. The thesis has investigated the use of highly concentrated electrolytes using ether solvents (TEGDME or DME), LiFSI salt, and LiNO₃ additive. The influence of ether solvent, additive, and cycling conditions have been explored, trying to achieve high lithium reversibility. A total of four electrolytes were tested.

Pouch cells and PAT-cells were made and cycled electrochemically to determine the performance of each electrolyte. Some cells were opened and investigated, either in SEM or XRD. SEM analysis was done to identify the morphology of deposited lithium, while XRD was performed to determine the amount of lithium delithiated from the LFP cathode.

Results show excellent properties for several of the electrolytes used. The most promising electrolyte, 3.2 M LiFSI + LiNO₃ in DME, achieved an average CE of 99.4 % when cycled at intermediate current densities, with a slow charge and fast discharge (C/5, D/2). The actual lithium reversibility is believed to be even slightly better than this, as cross talk is suspected of influencing the measured coulombic efficiencies.

Cycling performances identify DME as a better solvent than TEGDME, and show that LiNO₃ causes improved cycling performance. SEM images show that the morphology significantly improves when adding LiNO₃, contributing to a more even deposition morphology. The cycling conditions proves to be critical. This work advocates a slower charge and faster discharge, cycled at mediocre current densities.

Sammendrag

Med en raskt voksende etterspørsel for batterier, trengs det nye batterier som kan lagre mer energi. Å erstatte dagens grafittanode med litiummetall er en potensiell løsning for å øke energitettheten til litium-ionbatterier. Det er imidlertid mange problemer assosiert med litiummetall, på grunn av dets høye reaktivitet og tendens til å vokse ujevnt.

En anodeløs konfigurasjon har blitt testet i dette arbeidet, sett på som en lovende kandidat for praktisk realisering av litium-metall-anoden. Cellene som ble brukt hadde en LFP-Cu struktur. Rapporten har utforsket bruken av høykonsentrerte elektrolytter ved bruk av etersolventer (TEGDME eller DME), LiFSI-salt, og LiNO₃-tilsetningsstoff. Påvirkningen av etersolvent, tilsetningsstoff og sykleforhold har blitt utforsket, for å oppnå høy litium-reversibilitet. Fire ulike elektrolytter har blitt testet.

Poseceller og PAT-celler har blitt laget og syklet elektrokjemisk for å se på ytelsen til hver elektrolytt. Noen celler ble åpnet og analysert, enten i SEM eller XRD. SEM-analysen ble gjort for å se på morfologien til litiumdeponeringen, mens XRD ble gjort for å bestemme hvor mye litium som hadde blitt delitiert fra LFP-katoden.

Resultatene viser gode egenskaper for mange av elektrolyttene. Den mest lovende elektrolytten, 3.2 M LiFSI + LiNO₃ i DME, oppnådde en effektivitet på 99.4 %, når den ble syklet på mellomstore strømtettheter, med en sakte oppladning og rask utladning (C/5, D/2). Den faktiske litium-reversibiliteten antas å være enda litt høyere enn dette, ettersom ”cross talk” mistenkes å ha påvirket den målte coulombiske effektiviteten.

Sykleytelsene identifiserer DME til å være den beste solventen, og viser at LiNO₃ har en forbedrende effekt. SEM-bildene viser at morfologien forbedres kraftig, ved å tilsette LiNO₃ ettersom den bidrar til at litiumdeponeringen får en jevnere morfologi. Sykleforholdene viser seg å være betydelige. Dette arbeidet taler for bruken av en sakte oppladning og rask utladning, syklet på middels strømtettheter.

Table of Contents

List of Figures	x
List of Tables	xii
1 Introduction	1
2 Theory	3
2.1 Fundamentals of Batteries	3
2.1.1 Lithium ion batteries	4
2.2 Parameters and terminology	6
2.3 Metallic Lithium	9
2.3.1 Dendrite formation	12
2.4 Solid Electrolyte Interface	14
2.4.1 SEI in Lithium Metal Batteries	16
2.5 Electrolyte: Salt, Solvent and Additives	17
2.5.1 Concentrated Electrolytes	19
2.6 Cycling conditions	20
2.7 The Anode-free Battery Cell	21
2.8 LiFePO ₄	24
2.9 Beyond Lithium Ion Batteries	26
3 Experimental	29
3.1 Electrolyte preparation	30
3.2 Cell assembly	31
3.2.1 Pouch cell assembly	33
3.2.2 PAT-cell assembly	35
3.3 Cycling	37
3.3.1 Galvanostatic cycling	37
3.3.2 Cyclic Voltammetry and Electrochemical Impedance Spectroscopy	39
3.4 X-ray Diffraction and Scanning Electron Microscopy	40
3.4.1 X-ray Diffraction	40
3.4.2 SEM	41

4	Results	43
4.1	Galvanostatic Cycling	43
4.1.1	Program 1	43
4.1.2	Program 2	48
4.1.3	Cycling conditions, Program 2-5 comparison	53
4.2	Electrochemical Impedance Spectroscopy	56
4.3	Cyclic voltammetry	56
4.4	SEM	58
4.4.1	3 minutes deposition	59
4.4.2	One charge discharge cycle/stripped	60
4.5	XRD	61
5	Discussion	65
5.1	Comparison of ether solvents	65
5.2	Effect of LiNO ₃ additive	71
5.3	The importance of cycling conditions	73
5.4	The anode free cell configuration, The LFP-Cu system	75
6	Conclusion	79
7	Further work	81
	Bibliography	83
	Appendices	93
A	Supplementary results, electrochemical cycling	93
B	Supplementary results, SEM	97
C	Supplementary results, XRD	99

List of Abbreviations

CE	Coulombic efficiency
CV	Cyclic voltammetry
DME	Dimethoxyethane
DoD	Depth of Discharge
EIS	Electrochemical impedance spectrometry
E_{OC}	Open circuit voltage
SEI	Solid electrolyte interface
SEM	Scanning electron microscopy
LIB	Lithium ion battery
LFP	Lithium iron phosphate
LMB	Lithium metal battery
LiFSI	Lithium bis(fluorosulfonyl)imide
TEGDME	Tetraethylene glycol dimethyl ether
XRD	X-ray diffraction

List of Figures

2.1	Working Principle LIB	5
2.2	Overview anode materials, capacity	10
2.3	Lithium metal anode challenges	11
2.4	Open-circuit energy diagram of electrolyte.	15
2.5	Working principle, Anode free LMB	23
2.6	LFP and FP, unit cell	25
2.7	XRD of Li_xFePO_4 from $x = 0$ to $x = 1$	26
3.1	Configuration of cells produced	32
3.2	Assembly and sealing done outside glove box	33
3.3	Illustration of finished cell + sealing order	34
3.4	Pouch cell pictures	35
3.5	Illustration of PAT-cell	36
3.6	Pressure plates, pouch cells	39
4.1	CE comparison, Program 1	44
4.2	CE comparison, zoomed in, Program 1	44
4.3	Average CE, Program 1	45
4.4	Capacity retention, Program 1	46
4.5	CE, initial cycles, Program 1	46
4.6	Voltage curves, first ten cycles, Program 1	47
4.7	Voltage curves overview, Program 1	47
4.8	CE comparison, Program 2	49
4.9	Average CE, Program 2	50
4.10	Capacity retention, Program 2	50
4.11	CE, initial cycles, Program 2	51
4.12	Voltage curves, Program 2	51
4.13	Voltage curves, PAT-cells, Program 2*	52
4.14	CE, different cycling conditions, Program 2-5	53
4.15	Capacity retention, different cycling conditions, Program 2-5	54
4.16	Average CE, different cycling conditions, Program 2-5	55
4.17	Average CE, zoomed in, different cycling conditions, Program 2-5	55

4.18 CV, SEI region	56
4.19 CV, first cycle comparison	57
4.20 CV, individual samples, all six cycles	57
4.21 SEM images, 3 min plating	59
4.22 SEM images plating and stripping	60
4.23 XRD of LFP, comparison	62
4.24 Pictures of opened cells	63
5.1 Voltage profile, initial cycle, LiNO ₃ -less electrolytes	68
5.2 CE-capacity retention, vs actual lifetime	77
A.1 CE, individual plots, Program 1	93
A.2 CE, individual plots, Program 2	94
A.3 Average CE with standard deviation, Program 2	94
A.4 CE, PAT-cells, Program 2*	95
A.5 Voltage curve, 3.2M LiFSI-TEGDME with 3.5mAh LFP, Program 2 .	95
A.6 Average CE with standard deviation, Program 2-5	96
B.1 Additional SEM images 3-min plating	97
B.2 Additional SEM images, plating and stripping	98
C.1 Individual X-ray diffractograms	99
C.2 Unit cells of LFP and FP from PDF-database	100

List of Tables

3.2	Electrolyte compositions	30
3.1	Details of the chemicals utilized in work	31
3.3	Details of cycling program 1 and 2	38
3.4	Details of cycling program 3, 4, and 5	38
3.5	Details of cycling programs, SEM	41
4.1	Average CE, Program 1	45
4.2	Average CE, Program 2	49
4.3	Average CE, different cycling conditions, Program 2-5	54
4.4	Ohmic resistances, EIS	56
5.1	Linear CE values given CE measurements and observed lifetime	78

1 Introduction

With the world consuming an increased amount of energy every year, it has become clear that depending on coal and oil is not a sustainable or scalable solution to meet future energy demand. As a result, the attention has shifted towards renewable energy and sustainable energy storage solutions, with rechargeable batteries playing a vital role in this transition.

Lithium-ion batteries have been in the forefront of battery technology since its introduction in 1991, as it has the highest energy density battery. However, to meet future demand, batteries with higher energy densities using more abundant materials are necessary.

One of the potential solutions that has attracted a lot of attention is using lithium metal as the anode material, replacing the currently used graphite. This replacement has several advantages, with the main one being the possibility of higher energy

densities, due to lithium metal being the theoretical best anode with low potential and theoretically maximum capacity. However, further research is needed as batteries using lithium metal anode suffer from poor performance and the lithium forming dendrites when cycled.

Many strategies have been proposed and tested to improve performance. Identifying an ideal electrolyte suitable with lithium metal is one of the effective strategies to improve the performance of the lithium metal battery [1]. The conventional carbonate LiPF_6 electrolyte used in lithium-ion batteries is shown not to work well with lithium metal [2]. Ether-based electrolytes have received attention as it is believed to be better suited for lithium metal batteries.

One of the promising strategies to achieve commercial lithium metal batteries is to use a so-called anode-free configuration. This configuration uses only the lithiated anode as the lithium source, eliminating the need to produce a thin lithium film. This is seen as a cheaper and more realistic solution, as producing a thin enough film to realize sufficiently higher energy densities can be costly [3, 4].

Aim of work

This thesis aims at investigating different electrolytes and their impact on the cell performance in anode free LMBs. Four electrolyte composition are compared investigating the impact of each of the electrolyte components. Comparing the two ether solvents TEGDME and DME, to identify the most suitable solvent of the two when using of a high concentration of LiFSI salt. The comparison aims at investigating parameters such as the stability, rate performance and coulombic efficiency.

The work also aims at investigating the effect of LiNO_3 on the coulombic efficiency and lifetime of the cell, as well as how it effects the deposition morphology of lithium. The electrolyte compositions tested in this work are 3.23M LiFSI in TEGDME or DME solvent with or without LiNO_3 additive.

The goal is to achieve a cell with good reversible cycling and high lifetime by identifying an optimal electrolyte composition as well as optimal cycling parameters given the anode free configuration.

A general investigation of the anode free configuration is also within the scope of the work, to attain further knowledge if this is a reliable and realistic approach for potential commercialization of LMBs.

2 Theory

2.1 Fundamentals of Batteries

A battery is defined as a device that can convert chemical energy into electrical energy. This is made possible by electrochemical reactions in electrochemical cells by separating the electron transfer from the redox reactions occurring. The electrochemical cell consists of three main components: the anode, cathode, and electrolyte. The anode and cathode are also known as electrodes, defined as where the electrochemical reactions occur. A separator is also used when using liquid electrolytes to assure physical spacing between the two electrodes to avoid short circuit. A battery consists of one or several electrochemical cells. However, this work will only consider single cells.

Batteries are divided into two main categories: primary and secondary batteries. Primary batteries are non-rechargeable batteries, while secondary batteries are rechargeable. For this reason, they are also commonly called non-rechargeable and rechargeable batteries which is the terminology used in this work. Rechargeable batteries are receiving great interest as they can find use in several applications, with the breakthrough of the lithium-ion battery enabling portable high power electronic devices such as phones, computers, and electric vehicles. Therefore, most research in the field of batteries focuses on secondary batteries, which is also the case in this work.

Charging and discharging a battery involves redox reactions occurring at the anode and cathode with migration of electrons from one of the electrodes to the other through the outer circuit. When a battery is discharged, electrons are traveling from the anode to the cathode with a driving force equal to ΔV . At the same time, an oxidation process occurs at the anode while a reduction process occurs at the cathode. The ions produced or consumed are transported through the electrolyte.

The theoretical energy a battery can deliver is given by the difference in Gibbs free energy of the total reaction, which can be expressed in terms of the difference between the electrochemical potential of electrons in the cathode and anode [5].

The electrolyte in a battery cell has the requirement of being a poor electronic conductor while being a good ionic conductor. The result of this is that the electrons are forced through an external circuit where the electrical current can be used to power electrical devices like phones or vehicles. The purpose of good ionic conductivity is to allow the ions to move between the electrode, preferably with low ohmic resistance.

2.1.1 Lithium ion batteries

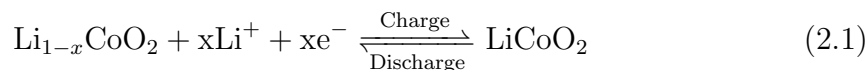
The lithium-ion battery (LIB) is a type of rechargeable battery. It is not one specific type of battery, but a common term used for a range of batteries where Li-ions is a core part of the battery's working principle. LIB has dominated the battery market since its first appearance in 1991, and for a good reason. They are the rechargeable batteries with the best properties overall, with high energy density, high energy output, and the fact that they can last for thousands of cycles with the battery still retaining a sufficient amount of the initial battery capacity.

As LIBs do not refer to one specific battery chemistry, there are several unique LIBs depending on the electrode materials and electrolyte. However, in conventional LIBs, most of the distinctive features between the various technologies lie in the choice of cathode material. The different cathode materials have their advantages and disadvantages. Some have better lifetime and working temperature window, while others have greater energy density. This results in the different technologies being suitable for various applications.

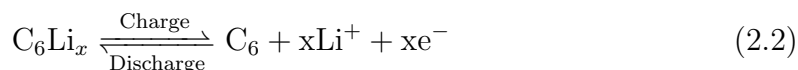
Even though there exists a broad range of LIBs, all of them work more or less the same way. The working principle of a LIB is to convert chemical energy to electrical energy by moving Li-ions between the cathode and the anode. The large difference in the energy state of lithium in the anode and cathode makes it possible to convert a lot of energy per Li-ion. Both the anode and cathode have a layered or tunnel structure. This is to enable reversible storage of the Li-ions. This way of storing ions into a layered structure is called intercalation and is, interestingly, something quite unique for LIBs compared to other battery technologies. The anode is graphite,

while the cathode is a complex structure, usually a metal oxide. In 1991 when Sony commercially released the first LIB, the cathode was LiCoO_2 , but today other cathode structures are more dominating such as LiNiMnCoO_2 and LiFePO_4 , commonly known as NMC and LFP. Using LiCoO_2 as the cathode, the total reactions when discharging and charging the battery can be written as:

Positive electrode:



Negative electrode:



Over LIBs' 30-year lifespan, graphite has exclusively been used as the anode, even though it has a mediocre capacity since it can store no more than one Li-ion per six carbon atoms. The explanation for not finding a graphite replacement is that graphite shows little volume expansion when cycled and enables the formation of a highly stable Solid Electrolyte Interface (SEI) at the graphite/electrolyte interface. The SEI is a passive layer kinetically protecting the electrolyte from decomposing enabling reversible cycling of the battery (for more detail on SEI, see Section 2.4). No potential anode material has been able to compete with graphite, which is why graphite is the anode material commercially used today [6, 7].

The working principle of a typical LIB is illustrated in Fig. 2.1.

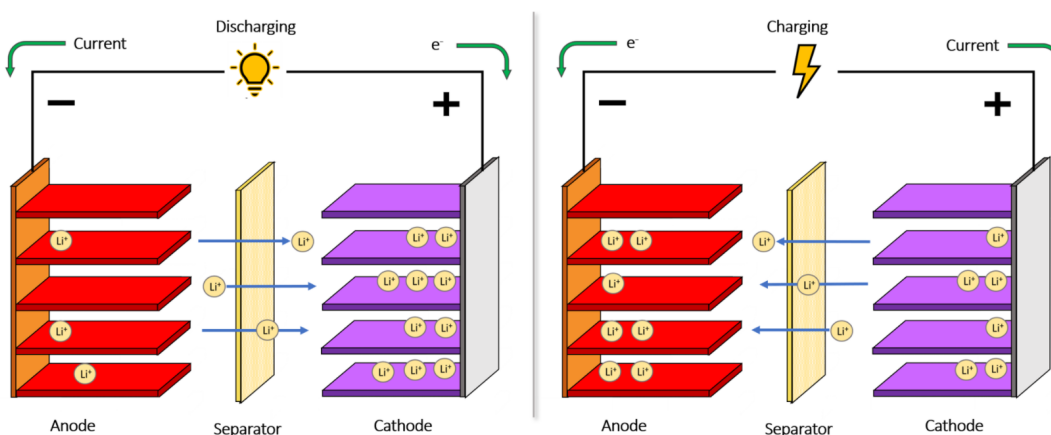


Figure 2.1: Working principle of a lithium-ion battery [8]

2.2 Parameters and terminology

An overview of the terminology of common parameters used to describe batteries is given in the section below.

Anode/Cathode definition:

According to the electrochemical definition, the anode and cathode are defined with respect to the reaction occurring on each electrode. This being that the oxidation reaction occurs at the anode, and the reduction reaction occurs at the cathode. Given this terminology, the two electrode materials in a battery switch between being the anode or cathode depending on whether the battery is charging or discharging.

However, terminology commonly used when discussing batteries refers to the anode and cathode with respect to the reactions happening upon discharge. Consequently, the electrode undergoing oxidation at discharge is referred to as the anode, and the electrode undergoing reduction at discharge is referred to as the cathode. This is the terminology used in this report.

The terms positive and negative electrode might be used instead, when referring to the electrodes in the cells. The negative electrode being the electrode with the lowest potential and the positive electrode the one with the highest potential. Using the latter terminology, the cathode would equal the positive electrode and the anode would equal the negative electrode.

Current:

An electric current is defined as charge per unit time

$$I = \frac{dq}{dt} \tag{2.3}$$

Where the unit is ampere which is also coulombs per second.

Theoretical specific capacity:

The specific capacity, often also referred to as theoretical capacity, describes the total amount of charge an electrode can convert per unit weight. It is given as:

$$\frac{It}{m} = \frac{nF}{M} \quad (2.4)$$

Where I = current, t = time, m = mass, n = charge number (1 in the case of lithium), F = Faraday's constant and M = molar mass. It is typically measured in Ah/kg or mAh/g.

C-rate:

The C-rate is the current corresponding to a certain charge/discharge rate of a battery. 1C = charge/discharged in 1 hour, 2C = charge/discharged in 1/2 hour etc.

Battery capacity:

The capacity of a battery is defined as the amount of charge a battery can supply given a certain discharge current. It is a function of the C-rate as a higher C-rate will give a lower capacity due to higher overpotentials at high current densities.

DoD and SoC:

Depth of Discharge is the percentage of the capacity that has been removed from the fully charged battery. State of Charge is the inverse of Depth of Discharge.

Coulombic efficiency:

The coulombic efficiency is the yield of charge in one charge/discharge cycle. It is the amount charge you release when discharging the cell divided by the charge supplied upon when charging. The coulombic efficiency indicates how much charge is lost irreversibly for each discharge/charge cycle. It is given as:

$$CE(\%) = \frac{Q_{discharge}}{Q_{charge}} * 100\% \quad (2.5)$$

Understandably, the coulombic efficiency should be as close to a hundred percent as possible for batteries.

Open circuit voltage:

The open circuit voltage V_{oc} is an important parameter of a battery cell. It is defined as the difference in electrochemical potential between the anode and the cathode. Consequently the expression becomes:

$$V_{oc} = \frac{\mu_a - \mu_c}{e} = E_c^0 - E_a^0 \quad (2.6)$$

where μ_c and μ_a is the electrochemical potential of the cathode and anode respectively, and e is the elementary charge. E_c^0 and E_a^0 is the equilibrium reversible potential of the cathode and anode respectively.

Overpotential:

The overpotential represents the overall voltage losses in a battery. These losses mainly originates from the ohmic resistance as well as the charge transfer resistance.

Energy supplied by a cell:

The energy supplied by a cell is given as the capacity times the voltage, often given in Wh. Over a time t with a voltage V , and current I , it can be expressed as:

$$Energy = \int_0^t V(t) * I dt \quad (2.7)$$

Specific energy:

The specific energy is the energy of a battery per unit mass given in Wh/kg. It is also referred to as gravimetric energy density.

Energy density:

The energy density is the energy of a battery per unit volume and is given in Wh/l. It is also referred to as volumetric energy density

Cost

The cost of production is a very important parameter, usually given in cost/kWh, or cost/kWh/Cycle if the batteries is for stationary applications.

2.3 Metallic Lithium

The anode component of a battery cell is undoubtedly a crucial part of every battery. The anode material has a significant influence on the electrochemical performance of the battery. Currently, conventional anode and cathode material are made up of host structures used to store the lithium reversibly through intercalation.

However, the theoretically optimal anode for lithium-based batteries is lithium metal. This is due to lithium in its metal form having an exceptionally low electrochemical potential, even lower than LiC_6 . Additionally, using a lithium metal anode would eliminate the need for an anode host structure like graphite. This would drastically increase the energy density to its theoretical limit, as you have only the active component and no dead-weight material. Graphite needs six carbon atoms to store one lithium atom. By using lithium metal anode, all this excess carbon is effectively removed.

The consequence of the host material removal is metallic lithium in the battery, something which introduces several considerations. Consequently, a thin lithium film has to be produced as the active anode material. Another possible solution for implementing a lithium metal anode is using a lithiated cathode as the only lithium source, creating the metallic lithium anode in situ. This concept is called the anode-free lithium metal battery (anode-free LMB).

Using lithium metal anode is an attractive solution to potentially increase the energy output per weight and volume compared to current battery technology. In general, there are certain requirements the anode material has to fulfill if it is to be used in batteries. Eftekhari presents three main requirements for anode materials that should be met for practical development [9]:

- Low potential against cathode materials
- High capacity
- High cyclability

Metallic lithium fulfills the first requirement excellently as it possesses one of the lowest potentials of any anode material. It has a potential of -3.04 V vs. standard hydrogen electrode, which is remarkably low, making it suitable towards a variety of cathode materials. The electrochemical potential of the electrodes is also commonly given in reference to Li/Li^+ , where, e.g, lithium metal has a potential of 0 V vs. Li/Li^+ . Lithium metal is the best material in terms of capacity, as it does not carry any dead weight. It has both a high specific capacity as well as a high volumetric capacity. A specific capacity of 3860 mAh/g and a volumetric capacity of 2061 mAh/cm³, respectively [10, 11]. In comparison, conventional graphite has a specific capacity of 372 mAh/g and a volumetric capacity of 850 mAh/cm³ [6]. A comparison between potential anode materials in respect to the potential vs. Li/Li^+ and theoretical specific capacity can be observed in Fig. 2.2.

Lithium metal's high capacity and its low potential, could facilitate batteries with higher energy densities.

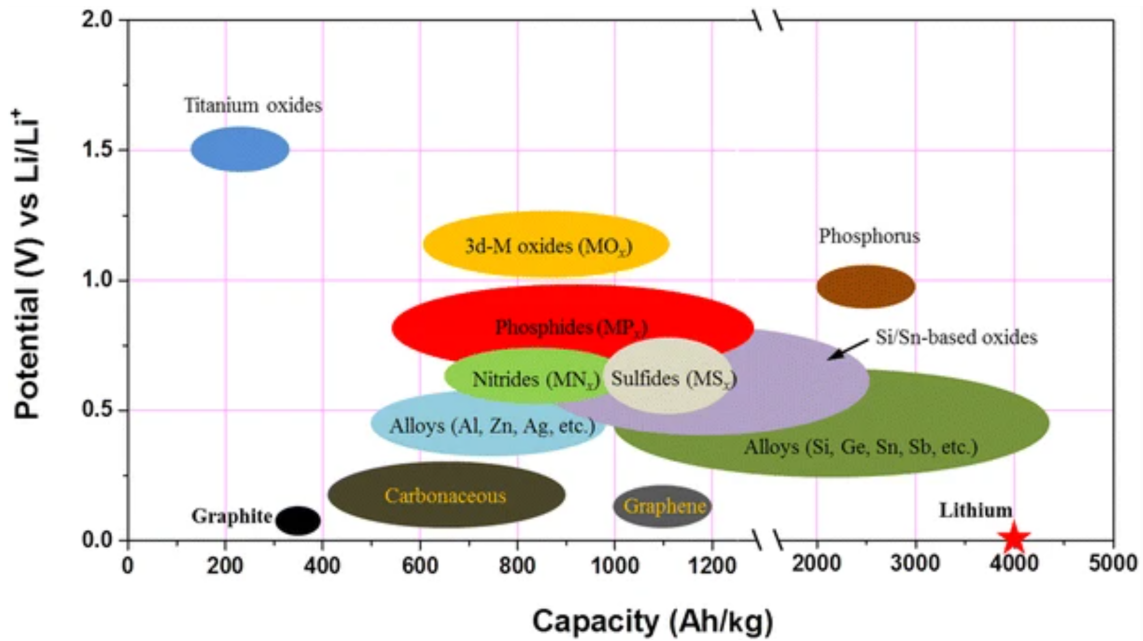


Figure 2.2: Overview of anode materials and their theoretical specific capacity [10]

Although lithium metal scores excellently on the first two requirements, the achievement of good cyclability has proven to be a significant challenge when dealing with lithium metal. Battery cells using lithium metal anode commonly experience low coulombic efficiency due to irreversible losses when cycling. As there is no anode

host material, the losses at the anode are associated with the stripping and plating of lithium. Lithium tends not to grow uniformly when electrodeposited, as some sites are more energetically favored than others. Consequently, the lithium forms local mossy or tree-like structures during cycling commonly referred to as dendrites. These dendrites could eventually short circuit the cell, which could involve serious safety hazards. The dendrites could also be detrimental to the battery performance, as it could lead to increased electrolyte consumption, resulting in lower cycle life. An overview of the problems associated with lithium metal anode, is found in Fig. 2.3. For the lithium metal anode to be competitive, these cyclability issues must be figured out.

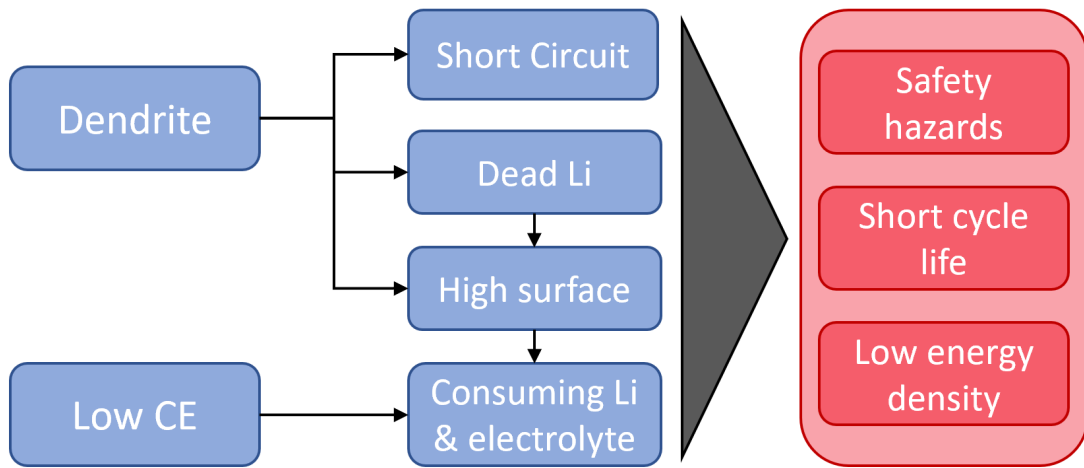


Figure 2.3: Challenges related to the use of lithium metal anode

Additional features of lithium metal worth attention are cost and environment. Concerning cost, lithium is reasonably good as it is cheaper per mAh compared to conventional graphite. From an environmental point of view, using lithium metal has several benefits. It eliminates the dependency of graphite, which is defined as a critical material according to the EU. Using pure lithium also makes the lithium more recyclable, which potentially can reduce our dependency of mining lithium in the future as lithium, similarly to graphite, is classified as a critical raw material. Using lithium metal anode can, as a result, facilitate more sustainable battery production.

2.3.1 Dendrite formation

For metallic lithium to be sufficient as anode material in secondary batteries, the lithium cycled needs to strip and deposit reversibly. A uniform deposition and a uniform stripping is preferred, as this promotes less surface area exposed to the electrolyte and better electrical contact between lithium and the copper current collector.

Unfortunately, this is often not the case, as lithium tends not to deposit uniformly, but rather forming dendrites during cycling. The uneven deposition introduces multiple issues reducing the cycling performance of the battery, preventing metallic lithium from being acceptable for use in rechargeable batteries. These issues are a large surface area exposed to the electrolyte, an uneven SEI layer, and dead lithium, all of which reduce the overall performance. Short-circuiting the battery is another potential issue that happens when a dendrite reaches the counter electrode.

It should be noted that a lot of these issues are highly connected, meaning that solving one of these can significantly or entirely solve another issue as well. For example, achieving less dendrite formation would also reduce the surface area of lithium metal towards the electrolyte, leading to the formation of a better SEI layer. There are undoubtedly several factors determining the morphology and distribution of lithium when stripping/plating. Chang et al. presented the following influencing factors [12].

- SEI
- Electrodes
- Separators
- Electrolytes
- Current density
- Stack pressure
- Electrolyte concentration gradient
- Temperature

There has been put a lot of effort into understanding the growth mechanisms causing dendrite formation better. One of the widely accepted models predicting dendrite growth is the Sand's time/Chazalviel model, which predicts dendrite growth triggered by ion depletion in the electrolyte close to the electrode [13].

The model starts with the following equation calculating concentration gradients in the cell:

$$\frac{dC}{dx}(x) = \frac{J\mu_a}{eD(\mu_a + \mu_{Li^+})} \quad (2.8)$$

Where C is the ionic concentration, J is the current density, e is the elemental charge, D is the diffusion coefficient, and μ being the mobilities for the anion and the Li-cation.

Two separate regimes are considered for the ionic concentration gradient:

- (a) When $dC/dx < 2C_0/L$, the ionic concentration in the electrolytes evolves to a steady state.
- (b) When $dC/dx > 2C_0/L$, the ions are continuously depleted, leading to the ionic concentration eventually going to zero at the negative electrode at a time τ . This is known as Sand's time and is thought to be highly correlated to when dendritic growth starts to occur.

Sand's time is given in the following expression:

$$\tau_s = \pi D \left(\frac{C_0 e}{2J t_a} \right)^2 \quad (2.9)$$

Where τ_s is Sand's time, C_0 is the initial concentration, and t_a is the transport number of the anion.

This model predicts dendrite growth to occur only at high current densities. However, Chang et al. reported dendrite formation at low current densities, suggesting a different mechanism for low current densities which was not due to concentration gradients that the Chazalviel model predicts [12].

The transport number of the Li-cation can be expressed as:

$$t_{Li} = 1 - t_a = \frac{\mu_a}{\mu_a + \mu_{Li}} \quad (2.10)$$

Eq. 2.9 and 2.10 indicate that Sand's time is highly correlated with the transport numbers. A high lithium transport number and low anion transport number are preferred as this increases Sand's time.

Bai et al. reported another fundamental constrain that needs to be considered related to dendrite formation. They reported a threshold in capacity from when lithium dendrites growth occurs, referred to as Sand's capacity, where dendrites are able to cross the separator, potentially shorting the cell. The current dependent Sand's capacity then becomes another important metric when considering dendrite formation in addition to Sand's time [14].

2.4 Solid Electrolyte Interface

The solid electrolyte interface (SEI) is a crucial part of many batteries and is an essential component of all LIBs. The SEI is a passive layer formed on the electrode/electrolyte interface consisting of decomposition products originating from the electrolyte. Peled first recognized it in 1979 as an electric insulating but ionic conducting layer of about 20 nm consisting of inorganic and organic compounds [15].

The formation of an SEI arises due to limitations of electrochemical stability of the electrolyte relative to the electrode materials. If the electrode material's potential is outside the electrolyte's electrochemical window, the cell is not thermodynamically stable, causing reactions to occur spontaneously at the electrode/electrolyte interface during operation. An illustrative explanation of this is found in Fig. 2.4.

By themselves, these degradation reactions are unfavorable, as they are parasitic reactions consuming lithium and electrolyte, therefore reducing the overall capacity of the battery cell. However, suppose the degradation products create a dense uniform film between the electrode and the electrolyte. In that case it can potentially act as a passivation layer that kinetically stabilizes the battery and prevents further electrolyte consumption. Consequently, the SEI layer enables the possibility of galvanic cells with very high cell voltages, higher than the electrochemical window of the electrolyte.

Therefore, most high voltage batteries require a few "formation cycles" for the stable SEI to form before it is commercially ready. The ability to establish a stable SEI on the graphite anode in LIBs is one of the main reasons LIBs are used today, as it makes reversible intercalation of lithium into graphite possible.

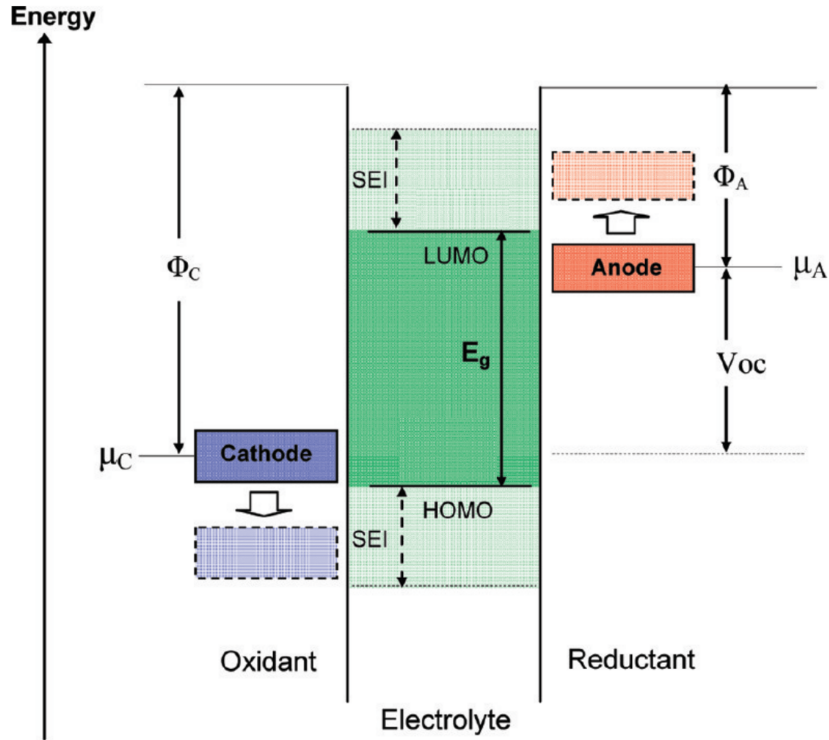


Figure 2.4: Schematic showing the electrochemical potential of the electrodes and the electrochemical window of the electrolyte [5]

As the SEI acts as a separate component, the composition and properties of the SEI are crucial for battery performance. Therefore, the formation of the SEI layer is a critical step that will affect the cyclability, rate capacity, and capacity loss of the battery [16]. As a result, a lot of work has gone into optimizing the SEI in LIBs over the years to improve the performance. In general, a SEI as thin as possible is preferred, as this means less irreversible losses and less ohmic resistance in the cell.

Like graphite, lithium metal does not find itself within the electrochemical window of any conventional liquid electrolyte, meaning there will be electrolyte consumption at the lithium/electrolyte surface. Optimizing the conditions creating a stable SEI enabling reversible cycling is of high importance.

2.4.1 SEI in Lithium Metal Batteries

As in LIBs, the SEI has a significant influence on the performance of lithium metal batteries (LMBs). Compared to graphite, there exist additional requirements the SEI has to fulfill in LMBs owing to the fundamental differences between graphite and lithium metal anode. The two main differences being the potential dendritic growth of lithium metal and the potential infinite relative volume change of lithium metal anode during cycling [17, 18]. To prevent dendritic growth, the SEI preferably must have enough mechanical strength to prevent this from occurring. In addition to having high strength, good flexibility is also needed to avoid cracking in the SEI layer, which, if it occurs, would cause additional electrolyte and lithium consumption. This is undesirable as it represents an overall irreversible loss in the battery [19].

The challenges mentioned above make the creation of a stable SEI a difficult task when dealing with LMBs. The SEI arguably has an even higher significance in LMBs as it not only impedes the continuous parasitic reactions, but also governs the morphology of the deposited lithium. The case in LMBs is commonly the formation of a thick unstable SEI while having repeated formation of SEI-products during cycling, causing a low CE and short cycle life.

Another distinction worth discussing regarding lithium metal anode compared to graphite is the addition of chemical SEI formation processes in addition to electrochemical due lithium being chemically unstable towards the electrolyte, unlike graphite. This additional SEI contribution should undoubtedly be kept in mind when researching LMBs [20].

There have been extensive efforts to find a stable SEI and better understanding the formation mechanisms. This has led to various strategies attempting to form a stable SEI layer. These efforts include: Mechanical reinforcement layers [21, 22], ex situ SEI formation [23, 24], functional additives to the electrolyte [1], anode structure design [25], high salt concentration, and multiple salt electrolytes [26].

In most of these efforts, the electrolyte is an essential factor. For all in situ SEI

layers, the electrolyte directly influences the composition of the SEI, causing it to have a substantial impact on the performance of the cell. This, while also being at a relatively low cost compared to alternative measures is a clear reason why most works have gone into optimizing the electrolyte [27]. Ideally, an electrolyte with an electrochemical window including lithium's potential would be preferable, but as this is not realistically achievable, the formation of the SEI has to be considered when choosing electrolyte.

Even though there has been significant progress in improving the SEI layer, there is still a lack of understanding of the SEI, especially surrounding the formation mechanisms. This is owing to the SEI layer's complex and dynamic nature. The SEI's complex nature makes it challenging to find the optimal composition of the SEI, having no clear answer. However, some indications/trends have been seen by previous work. For instance, a LiF-rich SEI seems to have a good ability to stabilize the Li-metal [28, 29, 30].

2.5 Electrolyte: Salt, Solvent and Additives

The compounds formed in the SEI are largely determined by the electrolyte composition and its electrochemical properties [16]. The conventional electrolytes used in lithium batteries consist of an organic solvent and a Li-salt. When considering these organic electrolytes, all the electrolyte components would influence the composition of the SEI and the Li-metal surface. Those being the lithium salt, solvent, and possible additives in the electrolyte. Other influencing factors worth mentioning include current density, pressure, temperature, and cut-off voltage [20].

The organic solvent is the source of the organic salts in the SEI [31]. These SEI compounds originate from the chemical reactions between solvents and the lithium metal, and the electrochemical reduction of solvents. As a result, the SEI can vary greatly depending on the solvent utilized.

Conventional carbonate solvents have proven not ideal for use in battery systems containing Li-metal anodes [32, 33]. These carbonate-based electrolytes typically achieve a CE of no more than 90 % in LMB systems, when stripping/plating lithium

[34, 35]. Ether-based electrolytes have proven to be more promising as better cyclability can be achieved with these [36]. The improved performance of ether solvents naturally originates from the difference in SEI components contributing to a better SEI.

However, one downside with ether solvents is the expected instability at high voltages of $> 4\text{V}$ (vs. Li/Li^+), causing ether electrolyte decomposition [37, 38]. This instability can prevent the use of high voltage cathode materials like NMC, NCA, and LCO, limiting it to lower voltage materials such as LFP and sulfur.

The Li-salt utilized is the source for inorganic salts in the SEI, such as LiF [31]. The SEI components are largely determined by the salt reduction products originating from the salt anion. This is one of the reasons that the LiFSI salt is considered such a promising salt for battery purposes. The FSI^- anion being fairly easily reduced, compared to similar salts, such as LiTFSI , which promotes formation of an SEI rich in inorganic salts.

These salts include LiF in particular, but also LiOH , Li_2O , and LiSO_2F , which are compounds promoting good ionic conductivity and mechanical strength [27, 39]. Additionally, LiFSI is discovered to promote a thinner SEI than other salts, such as the conventional LiPF_6 [40]. LiFSI is also seen as a better salt for LMB purposes compared to LiPF_6 as it exhibits a lower sensitivity to hydrolysis and has no HF emissions [41].

Aurbach et al. presents the following considerations when choosing a salt for lithium batteries: **1)** Should be highly stable and compatible with Li and cathode, **2)** Safe and non-toxic, **3)** Have good ionic conductivity, and **4)** Have good lithium cycling efficiency [42].

Given these considerations, particularly the first one, there is a limited amount of lithium salts realistically available for use. The limited amount of suitable electrolyte salts available makes introducing additives to the electrolyte an attractive option to improve the battery performance. The additives are mainly introduced to passivate the lithium anode surface, protecting the lithium from reacting with the electrolyte [43].

The modified reaction products can improve the passivation of the lithium surface, allowing improved cycling. In addition to altering the SEI, functional additives can also contribute to a more uniform lithium deposition [1, 20]. Introducing functional additives in the electrolyte is seen as one of the most effective and economical approaches in preventing the problems associated with LMBs [1]. Only a small amount of additive, even in the ppm range, can substantially influence cycling performance [18, 20].

Commonly the additives utilized have a reduction potential higher than the salt and solvent. Consequently, additives can modify and adjust the chemical environment and therefore change the SEI compared to the same electrolyte without any additives [18]. These changes can result in differences in composition and morphology, i.e., something that could lead to a denser or more flexible SEI.

There exist a broad range of additives, both organic such as VC, FEC [1, 18, 44, 45, 46], and inorganic additives such as LiNO_3 , LiBr , Li_2S_n , HF , and LiF [18, 27, 31, 47]. LiNO_3 is a specifically interesting additive proven to be an effective reagent in passivating the lithium surface, creating an in situ protective layer. LiNO_3 is considered especially attractive towards Li-S chemistries as it has proven to suppress the shuttle effect, known to be one of the main challenges associated with Li-S batteries [43, 48, 49, 50].

2.5.1 Concentrated Electrolytes

An especially high interest has developed in electrolytes with a high salt concentration, commonly referring to electrolytes with salt concentrations $> 3\text{M}$. Highly concentrated electrolytes are believed to give enhanced SEI properties compared to regular electrolytes, resulting in better interfacial stability between electrode and electrolyte [30, 51].

The salt concentration increase induces a shift in the SEI determining reactions, which can be partially described by the change in activities. The SEI layer goes from being dominated by the reduction of solvent molecules over to being determined by the decomposition of the salt. When using concentrated electrolytes, the SEI layer

is derived mainly from salt reduction products and is typically rich in LiF, believed to be thinner, denser, and with enhanced mechanical properties [30, 52].

Mandai et al. also reported some interesting results regarding ether solvents with lithium salt [53]. They reported an abnormality for the equimolar composition between the ether solvent and Li-salt, where the solvent molecule and the Li⁺ ion would create a complex cation. In the equimolar composition, this would result in a solution with only anions and complex cations. This would classify as a solvate ionic liquid and is believed to have extraordinary high stability, especially with the use of long molecule ether solvents [53, 54].

There exist additional implications with highly concentrated electrolytes compared to regular electrolytes. One of them is that they are less flammable due to higher thermal stability [55]. The high concentration of Li⁺ in high concentrated electrolytes enables a high rate of plating/stripping of lithium as more lithium-ions are available in solution [56].

According to Eq. 2.9, Sand's time is proportional to the $[C_{Li^+}]^2$, implying that a higher concentration can further delay the start of dendritic growth of Li. The work of Bai et al. also concluded with this, implying that higher salt concentrations would be preferred delaying dendrite growth [14].

2.6 Cycling conditions

Similar to the electrolyte, the choice of cycling conditions has a significant effect on cycling performance, especially for lithium metal anodes. Parameters such as temperature, pressure, current density, depth of discharge, and impurities are all parameters determining the cell's overall performance.

Generally, a low charge/discharge rate is predicted to give the least capacity loss in LIBs [57], partly owing to a more rapid volume change of the electrode materials at higher rates as well as a higher overpotential [58]. However, a consequence of using lithium metal anode is a different mechanism when charging and discharging the cell [59]. The main difference between conventional LIBs and LMBs in terms of cycling

mechanisms is that LMBs involve stripping and plating of lithium when cycling the cell, instead of intercalation in graphite. These mechanisms are fundamentally different. Consequently, it would be natural to expect a divergence in optimal cycling conditions between the two.

When discussing charge and discharge rates, it is intuitive that the current density, by itself, is the most critical factor. Despite this, Louli et al. proposed that the relative difference between the charge and discharge rate is more important than the current densities themselves for LMBs [59]. Currently, LIBs are mostly tested using symmetrical cycling protocols. However, Louli and his group investigated asymmetric cycling conditions, reporting that a slow charge and a faster discharge current density improved CE, with significantly lower capacity fade in their anode-free LMB setup [59].

The depth of discharge is also essential. A higher DoD is known to give an increased capacity fade and, therefore, a shorter lifetime. Limiting the depth of discharge is, thus, a way of increasing the lifetime. However, the depth of discharge should exceed 60 % to achieve practical energy densities [59].

2.7 The Anode-free Battery Cell

The anode-free cell is a cell configuration eliminating the active anode material during cell assembly. The problem in academic research investigating lithium metal anodes is the use of thick lithium films, practically causing a near infinite lithium reservoir. A major concern with this is that it does not reflect a potential commercial LMB as the thick lithium metal film will give high costs and reduce the energy density, which is the primary reason for investigating LMBs in the first place.

Using a lithium film thinner than about 50 μm is needed for LMBs with higher energy densities than state-of-the-art LIBs [3]. Secondly, the use of a near infinite lithium reservoir can artificially contribute to seemingly good efficiencies for a significant amount of cycles, which would never occur using a limited lithium source [60].

One of the main advantages of anode-free LMBs, making it an attractive concept,

is that there is no need to produce an active anode material, such as a lithium film or graphite. Consequently, one only requires the bare current collector on the anode side, paired with a lithiated cathode as the lithium source. This can potentially cut production costs significantly, ultimately lowering the cost/kWh [2]. This is one of the reasons the anode-free LMB is seen as the clear realistic approach for the commercialization of LMBs. The working principle of anode-free LMB is illustrated in Fig. 2.5.

There are, however, some important considerations associated with the anode-free LMB. Due to the copper being bare initially, limiting the depth of discharge during the first cycle, effectively creating a small lithium reservoir, is advantageous for the CE and lifetime of the cell. It is shown that limiting the depth of discharge, ergo "sacrificing" a bit of capacity to achieve a small lithium reservoir at the copper is advantageous for the cells' CE and overall lifetime [59]. This can be controlled in the cycling program by adjusting the cut-off voltage when discharging the cell.

The depth of discharge consideration can be seen as a compromise between energy density and CE/lifetime of the cell. This is because no reservoir would cause a short lifetime, while a too large lithium reservoir lowers the cell's energy density significantly.

Previous work has also shown that mechanical pressure is also shown to have an influence, with higher pressure exhibiting better reversible cycling. The extent of the improved effect depends on the system used [61].

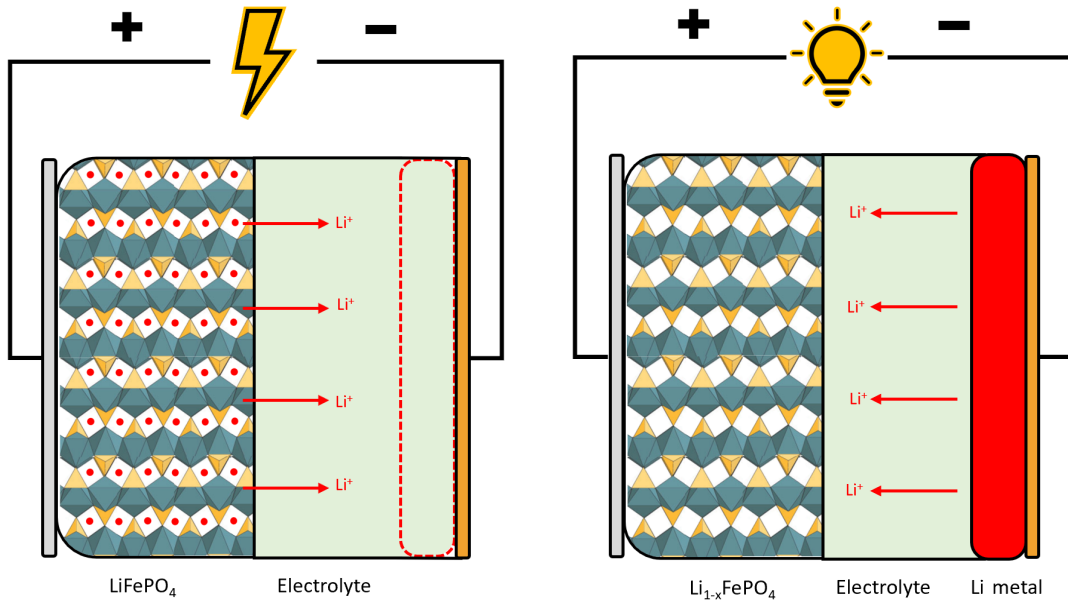


Figure 2.5: Working principle of an anode-free LMB

As a result of the anode-free LMB containing a limited amount of lithium, research on the subject has primarily focused on the coulombic efficiency, trying to achieve as high capacity retention as possible, keeping the lithium inventory loss to a minimum.

Qian et al. investigated the anode-free LMB configuration using a Cu-LiFePO₄ cell structure [2]. They tested a traditional carbonate electrolyte, 1M LiPF₆ in EC/DMC, and an ether-based electrolyte, 4M LiFSI in DME. They reported poor reversibility of lithium in the carbonate electrolyte, but achieved coulombic efficiencies of over 99 % with a capacity retention of 60 % after 50 cycles with the ether-based electrolyte. They reported a further increase in CE values when changing the cycling protocol, from symmetrical to a slow charge, fast discharge protocol, in agreement with what Louli's group reported [59].

Louli et al. reported a high capacity retention of 85 % after 50 cycles using a dual salt electrolyte, 2 M LiDFOB and 1.4 M LiBF₄ in FEC:DEC, cycled at high pressure and later reported a 99.3 % CE with a 1.4 M LiDFOB and 0.4 M LiBF₄ in FEC/DEC electrolyte [4, 59].

Lin et al. reported a capacity retention of 85 % after 50 cycles using an epitaxially induced Cu current collector using an NMC811 cathode with 6M LiFSI in DME

as electrolyte [62]. Coulombic efficiencies of 98.9 % were reported by Beyene et al. using a stable dual salt electrolyte [26]. The electrolyte being 2 M LiFSI + 1 M LiTFSI in DME/DOL using a Cu-LiFePO₄ cell structure.

Nanda et al. researched lithium-sulfur battery in the anode free cell configuration, using Li₂S-Cu with 2 M LiCF₃SO₃ + 0.1 M LiNO₃ in DOL/DME (1:1) electrolyte. They reported a coulombic efficiency of 96 % with a capacity retention of 51.5 % at 100 cycles [63].

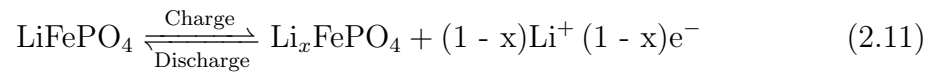
2.8 LiFePO₄

LiFePO₄, commonly called LFP, is a layered olivine structured material used as active cathode material in lithium-based batteries. It is currently a popular commercial product with an expected increase in popularity [64, 65]. This is because of LFP's excellent qualities, such as being environmentally friendly, a superbly high cycle life, stability, and a wide SOC window [66, 67].

As the host structure of LFP is made from Iron Phosphate(*FePO*₄), LFP is regarded as a very environmentally friendly material. The use of abundant materials like iron is an advantage that should be emphasized. With an increased focus on sustainable solutions, a cathode material like LFP is an attractive option removing our dependency on scarce materials like cobalt and nickel, with cobalt being classified as a critical raw material as of EU's latest report [68].

However, the significant downside of LFP, compared to high energy density cathode materials, is the electrochemical potential, which is about 3.4V vs. Li/Li+. The lower potential of LFP makes it difficult to compete with cathode materials like NMC and NCA in terms of pure energy density. Arguably this is not that low, still making it viable in many applications, increasingly in applications like grid energy storage etc, where the energy density is not as an important factor compared to e.g electric vehicles.

The delithiation process in LFP works as follows:



In the composition Li_xFePO_4 , the material consists of two phases: the lithiated triphylite phase, LiFePO_4 , and the delithiated heterosite phase, FePO_4 . These are structurally very similar, but as the lithium is removed, the unit cell shrinks about 7 percent. The unit cells for the respective phases are presented in Fig. 2.6.

Li_xFePO_4 having two phases makes it possible to distinguish between LiFePO_4 and FePO_4 in XRD measurements, consequently observing how much Li there is left in the cathode material.

Dodd reported the difference in X-ray diffractograms as a function of the amount of lithium x , shown in Fig. 2.7.

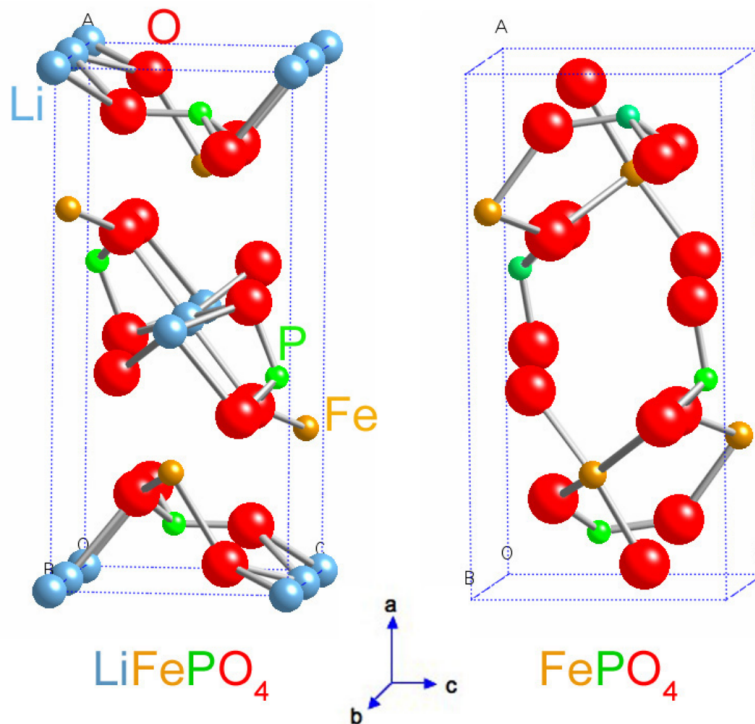


Figure 2.6: Unit cell of LiFePO_4 and FePO_4 . Taken from [69]

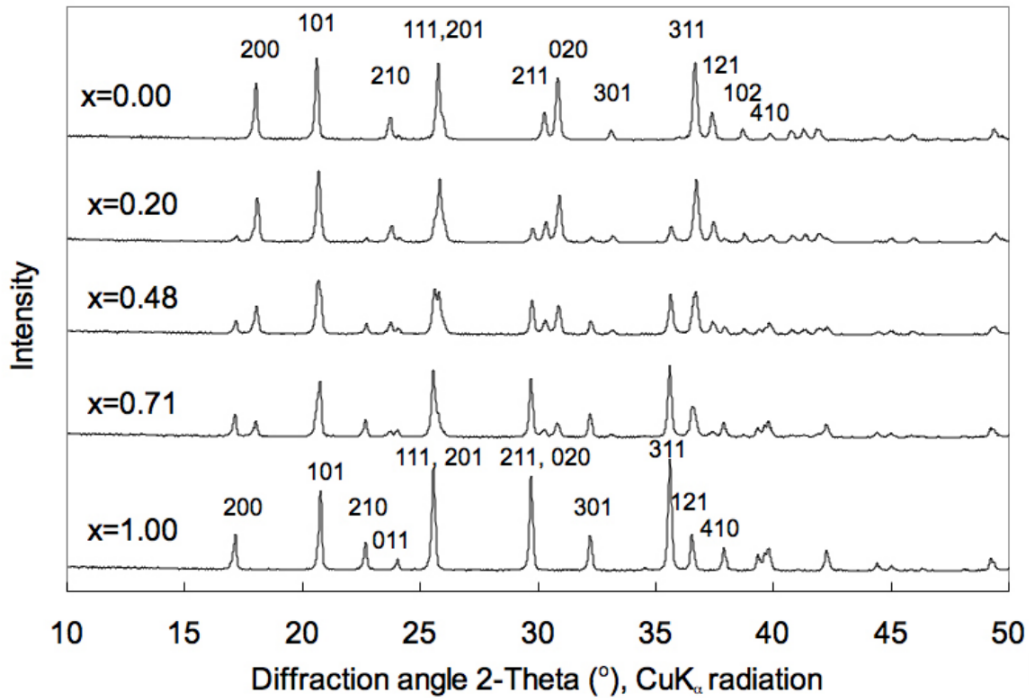


Figure 2.7: XRD of Li_xFePO_4 from $x = 0$ to $x = 1$. Taken from [69].

2.9 Beyond Lithium Ion Batteries

The increased demand for higher energy density storage has led to researchers looking beyond the LIB [70]. Other battery chemistries using lithium metal anodes are attractive solutions, as this could potentially enable the development of batteries with significantly higher energy densities than state-of-the-art LIBs.

This search has led to the interest in new concepts such as the Li-air and Li-sulfur battery. The aspects that make these batteries attractive are the possibility of very high energy density and the use of relatively abundant and cheap materials in the cathode.

Li-air and Li-S have an extraordinary high theoretical specific energy density of 3,505 Wh/kg (non-aqueous) and 2,567 Wh/kg, respectively, compared to LIBs' 387 Wh/kg (LiCoO_2). The theoretical volumetric energy density is 3,436 Wh/l and 2,199 Wh/l for Li-air and Li-S, respectively, compared to 1,015 Wh/l of the LIB (LiCoO_2) [11, 71]. However, these are theoretical values. For practical batteries, these val-

ues seem unrealistic. State-of-the-art LIBs usually have a specific energy of 120-270 Wh/kg [72, 73, 74].

Before commercialization, there exist certain challenges of Li-air and Li-S batteries that one has to solve. These include issues related to the cathodes, in addition to the challenges associated with metallic lithium, as discussed previously. One of the critical challenges for Li-air batteries is the degradation of the electrolyte by reduced oxygen species. The corresponding electrolyte degradation can significantly reduce the cycle life of the battery [11, 71, 75]. The presence of moisture is also a significant challenge, as only small amounts are shown to affect the performance of Li-air batteries in a negative manner [70, 76].

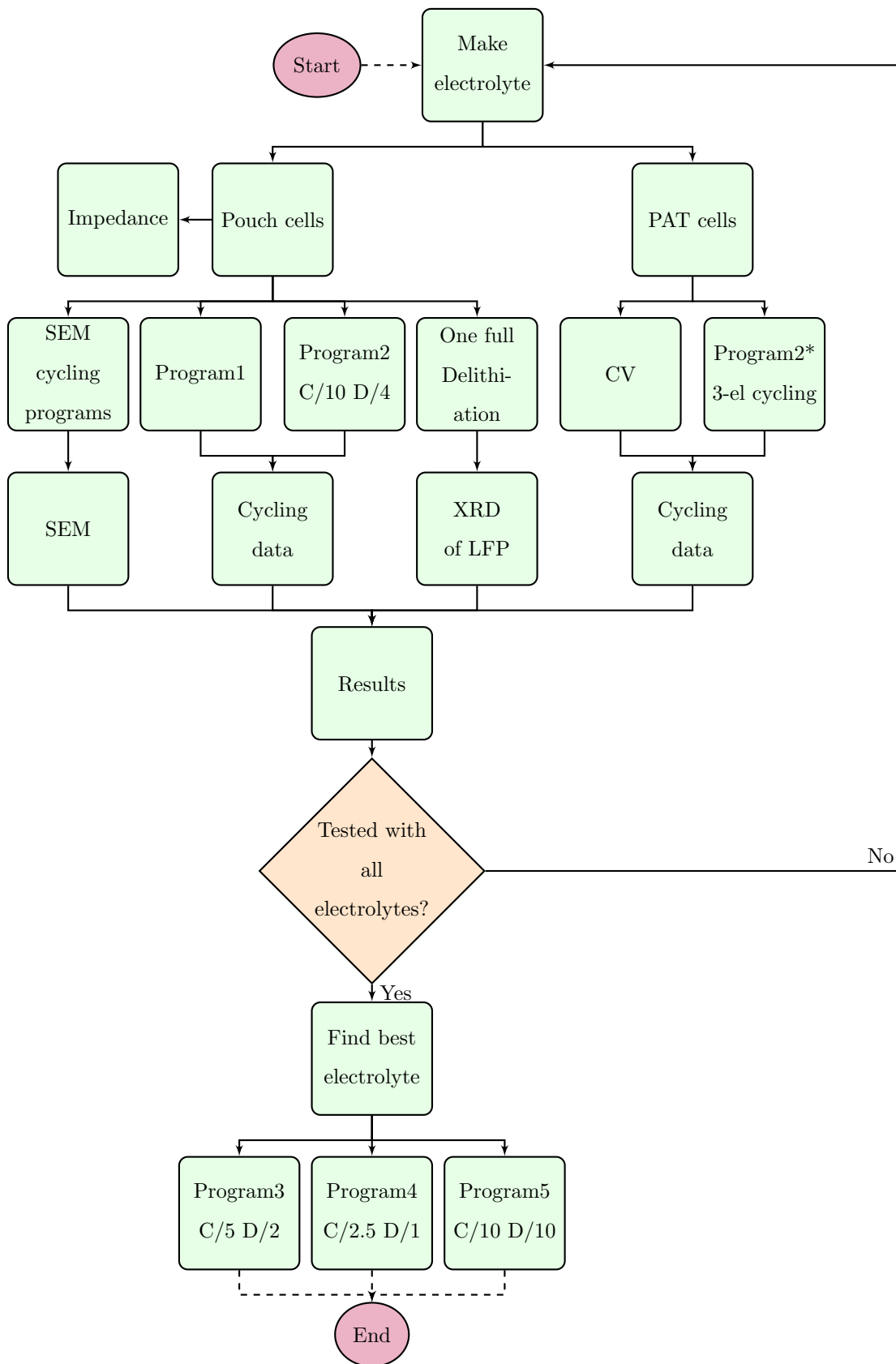
For Li-S, the main problem is the so-called shuttle effect involving dissolution of polysulfides from the sulfur cathode. Polysulfides means lithiated sulfur species, Li_2S_x . The polysulfides shuttling between cathode and anode reduces the coulombic efficiency and the cyclability [77, 78]. The volume change on the cathode of about 80% between charge/discharge is another challenge worth mentioning [79].

If the aforementioned challenges are resolved, it is believed that one could see commercialization of Li-air and Li-S batteries with a possible energy density of about 500 Wh/kg [3, 77]. To put this into perspective, one could consider an electric car with a range of 400 km. If one assumes a LIB with a specific energy of 250 Wh/kg, an increase to 500 Wh/kg, by the commercialization of Li-air or Li-S, would result in the same car having 800 km range.

Ether-based electrolytes such as DME and TEGDME have proven to be more suitable for these systems than carbonate electrolytes [80]. In the case of Li-air, they are ideal due to improved stability against reduced oxygen species [70, 71, 75]. LiNO_3 , especially towards Li-S batteries, has become a common additive as it enables stable cycling with a higher coulombic efficiency [17, 48, 77].

3 Experimental

A flow chart describing the work flow is shown below:



3.1 Electrolyte preparation

The lithium salt used was lithium bis(fluorosulfonyl)imide (LiFSI). Chemical formula: $F_2LiNO_4S_2$. The LiFSI salt was dried at $80\text{ }^\circ\text{C}$ for 48 hours under active vacuum. Two distinct ether solvents were used in this work. Of the four electrolytes produced, two consisted of the solvent tetraethylene glycol dimethyl ether, commonly called TEGDME, while the other two consisted of dimethoxyethane, commonly called DME. The latter terms for both solvents will be utilized in this work. Their respective chemical formulas are given in Table 3.1.

Additionally, lithium nitrate, $LiNO_3$, was added to half of the electrolytes. It was added in one of each of the same solvent electrolytes, resulting in four unique electrolyte compositions. $LiNO_3$ was dried at $140\text{ }^\circ\text{C}$ for 34 hours under active vacuum. A detailed description of these components can be found in Table 3.1.

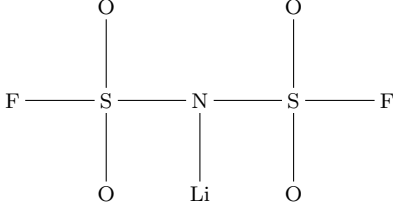
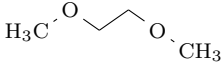
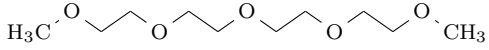
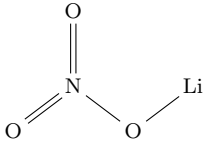
The concentration of LiFSI was 3.23 M for both the TEGDME based and DME-based electrolytes, respectively. 3.23 M being the equimolar composition between LiFSI and TEGDME, meaning they had a 1:1 molar relationship [81]. The concentration of the $LiNO_3$ additive was 0.2 M. Worth noting is that this seemed to reach saturation in the TEGDME electrolyte, something that was not observed with the DME electrolyte.

After adding all electrolyte components, a teflon magnet was added, and the electrolyte bottles were put on a magnetic stirrer to ensure sufficient mixing and dilution of the salts, especially $LiNO_3$. The electrolyte details can be found in Table 3.2.

Table 3.2: Electrolyte compositions used

Electrolyte	Composition
1	3.2 M LiFSI in TEGDME
2	3.2 M LiFSI in TEGDME + 0.2 M $LiNO_3$ (Saturated)
3	3.2 M LiFSI in DME
4	3.2 M LiFSI in DME + 0.2 M $LiNO_3$

Table 3.1: Details of the chemicals utilized in work

Name	Structural formula	Chemical formula	Purity/ Producer
LiFSI		$F_2LiNO_4S_2$	Lithium battery grade 99% FluoroChem
DME		$C_4H_{10}O_2$	99%, Aeros organics, dried
TEGDME		$C_{10}H_{22}O_5$	99%, Aeros organics, dried
Lithium Nitrate		$LiNO_3$	99.99%, Sigma- Aldrich

3.2 Cell assembly

Two types of cells were made in this work, pouch cells and PAT-cells. The reason for utilizing two kinds of configurations is due to the ability of doing three-electrode experiments with the PAT-cells, while for the two electrode experiments, pouch cells were mainly used due to being cheap and easy to manufacture.

The same electrodes and separators were used in all cells tested in this work. The electrode materials utilized were LFP on Al foil and pure Cu foil as a substrate for Li deposition. The LFP cathode was premade from Customcells with an areal capacity of 2 mAh/cm² or 3.5 mAh/cm².

The cut LFP electrodes were dried in vacuum at 110 °C for 16 hours before they were put into the glove box. The copper foil had a thickness of 30 μm with a 99.8% purity produced from Alpha Aesar. After cutting to the correct diameter, it was dried at 60 °C for four hours.

The separator material used was a 260 μm glass fiber (GF/A) from Whatman Corp and was dried in vacuum at 120 °C for 16 hours. The amount of electrolyte used for all cells was 75 μl . The configuration of the cells when fully assembled is illustrated in Fig. 3.1.

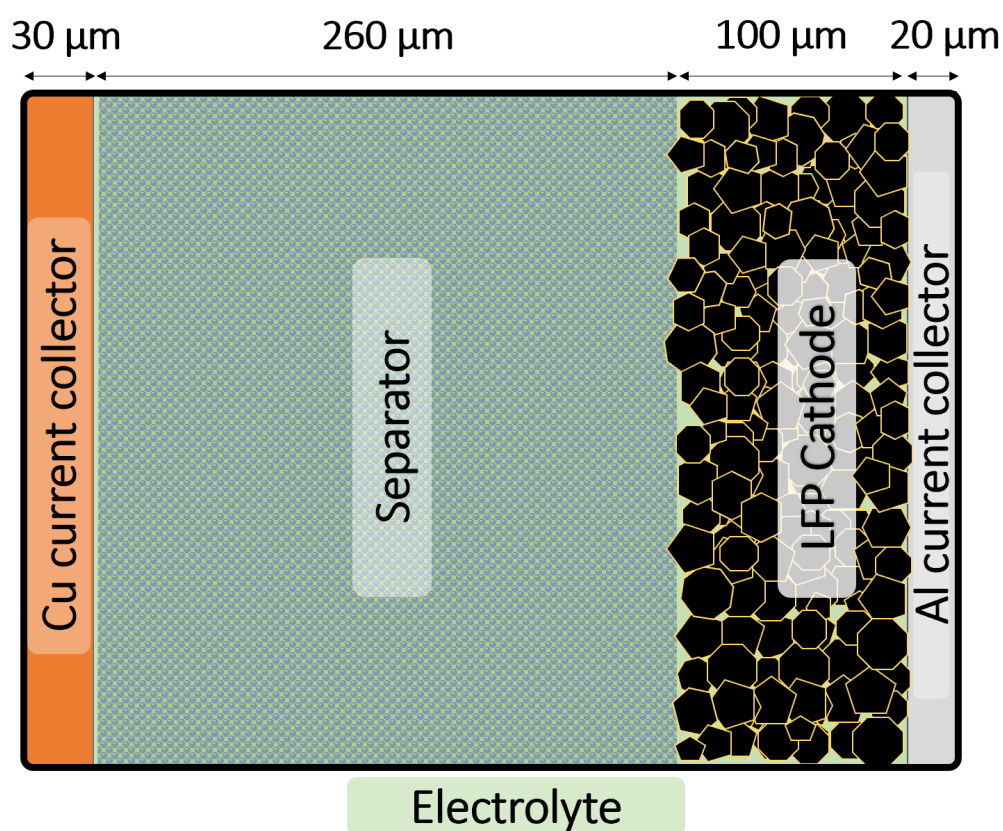


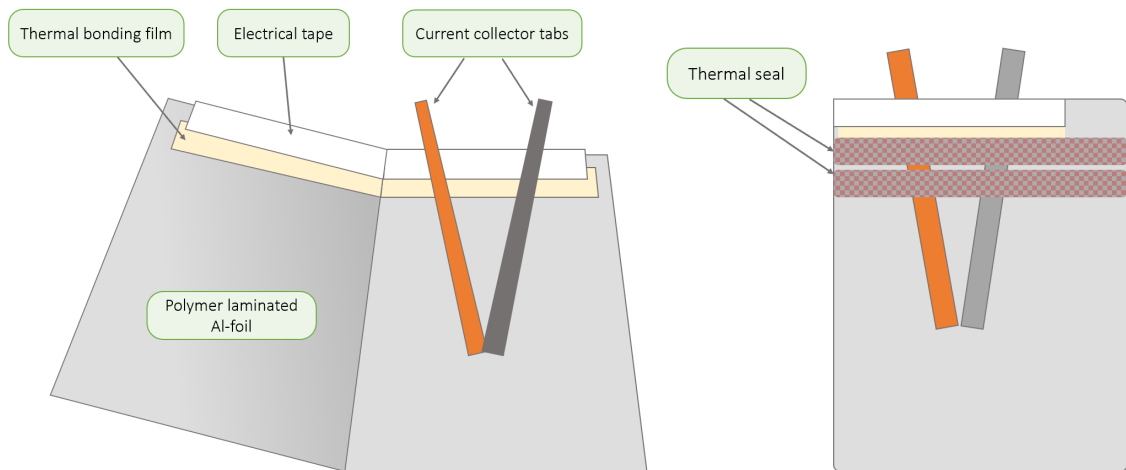
Figure 3.1: General configuration of all cells produced. All cells consisted of a copper current collector, glass fiber separator with added electrolyte, LFP cathode, and aluminium current collector

3.2.1 Pouch cell assembly

The experimental work done involving creating pouch cells can be divided into two steps. The first one being the work done outside the glove box, and the second step being the work done inside the glove box. The work outside the glove box was done in a lab with regular atmosphere. This step involved making the pouch cell body, which consisted of the following five components.

- Laminated aluminium foil
- Thermal bonding film
- Electrical tape
- Copper current collector
- Aluminium current collector

The work consisted of cutting all the parts in the preferred sizes. The laminated Al foil was cut into $8 \cdot 11$ cm before being folded in the middle. The $10 \cdot 1$ cm thermal bonding film was put on the top before the $10 \cdot 2$ cm electrical tape was attached and folded over the top, thereby visible on both sides. Subsequently, the current collectors were lined up before sealing the top twice. The sealing was done with the Audion Magneta MGMIDS sealer. An overview of the pouch cell with the distinct components and the location of the sealing done is illustrated in Fig. 3.2 a and b, respectively.



(a) Components and structure of pouch cell (b) Thermal seal done outside glove box

Figure 3.2: Assembly and sealing of pouch cell done outside glove box

The following work concerning the pouch cell assembly was done in a glove box. The glove box used was a Braun glove box with < 0.1 ppm O_2 and < 0.1 ppm H_2O content. The cells consisting of the two electrodes, separator, and electrolyte were assembled outside of the pouch cell before being carefully put inside the pouch cell body between the current collectors. The diameters of the LFP, separator, and copper were 12, 18, and 14 mm, respectively.

Subsequently, the pouch cell was fully sealed, first sealing the side before finally sealing at the bottom. The sealing done inside the glove box was done with AUDIONVAC VMS 53 sealer. An illustration of the finished pouch cell, as well as the sealing and their order, can be observed in Fig. 3.3.

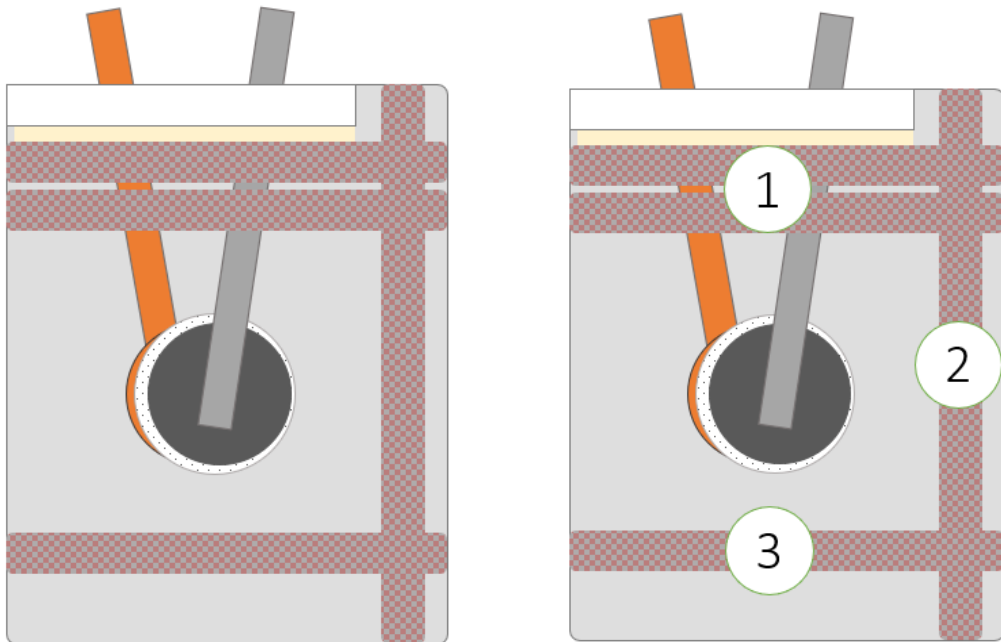


Figure 3.3: Illustration of finished pouch cell as well as sealing in its respective order.
1: Sealing done outside, 2-3 Sealing done inside glove box

Pictures of the cell after the first step and after completely finished can be found in Fig. 3.4



Figure 3.4: Left) Picture of pouch cell after the initial step, Right) Pouch cell when completed, being fully sealed with the active cell inside

3.2.2 PAT-cell assembly

The PAT-cells are a type of cell made from EL-Cell GmbH. It is a test cell with the possibility of doing two and three-electrode measurements. Illustrative pictures of the PAT-cells are found in Fig. 3.5.

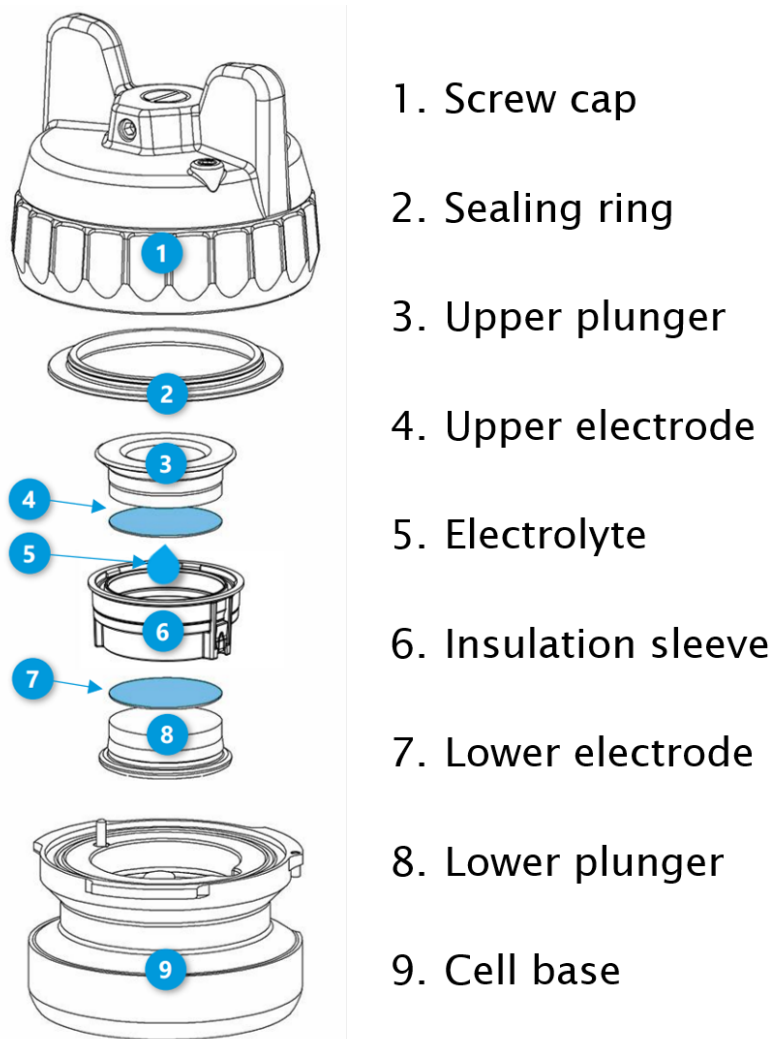


Figure 3.5: Illustration of the PAT-cell from EL-cell used. Taken from EL-cell

The dimension of all the components in this setup was 18 mm diameter for LFP, separator, and Cu foil. The assembly was done inside the glove box and consisted of assembling the core before putting it into the PAT-cell body. The core consisted of the insulation sleeve, electrodes, and plungers. Lastly, it was sealed by tightening the lid of the PAT-cell, which also adjusted the mechanical pressure applied on the cell.

After use, the plungers were carefully washed with acetone and ethanol to assure no electrolyte was present. Then the plungers and PAT-cell body were put into water for any possible lithium remains to react. All the PAT-cell components were later dried before being ready to be used again.

3.3 Cycling

All pouch cells cycled galvanostatically, and were cycled using a Lanhe Battery Test System CT2001A. All PAT-cell cycling, both galvanostatically and cyclic voltammetry were done on a Biologic VMP-300 potentiostat. The electrochemical impedance spectroscopy was also performed on the Biologic VMP-300 Potentiostat.

3.3.1 Galvanostatic cycling

The majority of cells were cycled using one of two cycling programs, where the coulombic efficiency was the main parameter of interest as well as lifetime. The first of them, named Program 1, was used primarily to have a direct comparison with previous work done on the subject where lithium metal was used instead of LFP, as well as being a program with a lower DoD. This program was set at a specific current density where lithium was plated for 1 hour before being stripped until a specific cut-off voltage was reached.

The second program, Program 2, tested an asymmetric charge/discharge cycle while utilizing more of the theoretical capacity available in the LFP electrode. Using a decent amount of the capacity is necessary if the desired energy density increase is to be accomplished. The reason 100% was not delithiated was due to this being an unrealistic approach in terms of reversible cycling as the program used a fixed charging time. 80% was chosen as a “compromise”, achieving a higher energy density while still achieving good reversible cycling.

All electrolytes tested were cycled in both these programs. Program 2 was used in pouch cells mainly, but also in PAT-cells for each electrolyte, unlike Program 1, which was only utilized testing the pouch cells. However, regarding the PAT-cells, there were some differences. The relative dimensions of the two electrodes were a bit different in PAT-cells compared to the pouch cells, and the PAT-cells were cycled in reference to the copper working electrode, which were things that had to be considered in the cycling program. The details of the two programs, as well as the slightly altered Program 2* for PAT-cells, are found in Table 3.3.

Table 3.3: Details of cycling program 1 and 2

Name	Charge			Discharge		
	i(mAh/cm ²)	C-rate	End	i(mAh/cm ²)	C-rate	End
Prgm1	0.500	C/3	1h	0.500	C/3	$E_{oc} < 2.5V$
Prgm2	0.147	C/10	8h	0.367	C/4	$E_{oc} < 2.5V$
Prgm2*	0.147	C/10	10.9h	0.367	C/4	$E_{we} > 1V$

The safety conditions were set to $E_{OC} = -3 V$ and $5 V$, while the cut-off at discharge was set to $2.5 V$.

An additional three programs were used. Two of them were asymmetric, as Program 2, only with faster rates. The last program was symmetric with a slow charge and discharge rate. It should be noted that the cells cycled on the asymmetric higher rate programs went under one formation cycle, equal to the rates in Program 2. The details of these programs are found in Table 3.4.

Table 3.4: Details of cycling program 3, 4, and 5

Name	Charge			Discharge		
	i(mAh/cm ²)	C-rate	End	i(mAh/cm ²)	C-rate	End
Prgm3	0.294	C/5	4h	0.735	C/2	$E_{oc} < 2.5V$
Prgm4	0.588	C/2.5	2h	1.469	C/1	$E_{oc} < 2.5V$
Prgm5	0.147	C/10	8h	0.147	C/10	$E_{oc} < 2.5V$

Before cycling, pressure plates were placed on each side of the pouch cells and kept in place with paper clips. This was done to assure good contact between the electrodes as well adding pressure. A schematic, as well as a real-life picture of how a typical setup looked, is shown in Fig. 3.6 a and b, respectively.

The pressure distribution was measured with pressure paper type SPI SPF-A pressure paper. This revealed that the pressure applied to the cell was about 172 kPa . A picture of the pressure paper showing the stress distribution can be found in Fig. 3.6 c.

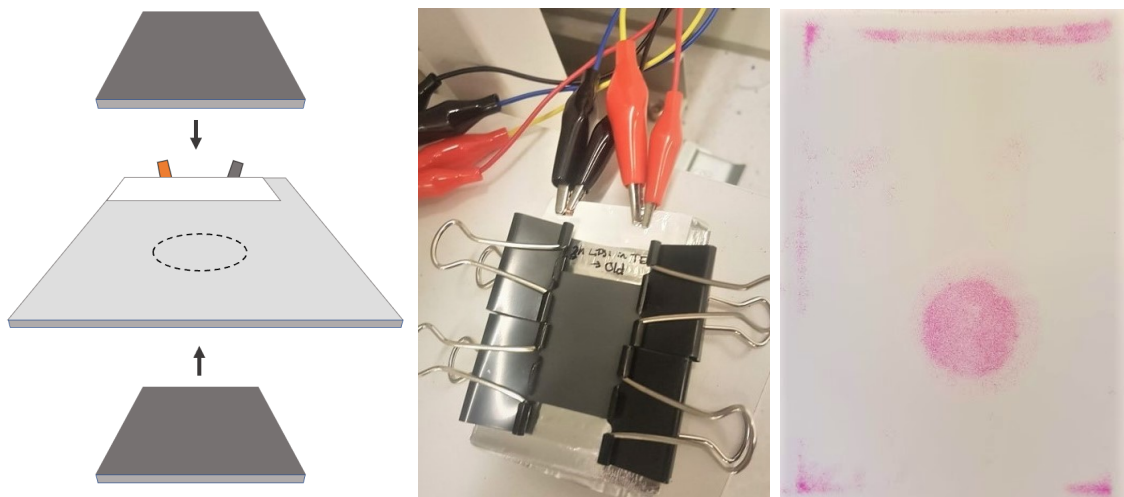


Figure 3.6: Left) Illustration of pressure plates, Middle) Picture of setup, Right) Pressure distribution from applied pressure

3.3.2 Cyclic Voltammetry and Electrochemical Impedance Spectroscopy

The cyclic voltammetry (CV) was performed with respect to the copper working electrode in the three-electrode setup, with the reference being electrode being Li/Li⁺. The cell was cycled from its open circuit potential (2.7 V vs. Li/Li⁺) down to -0.08 V before going back and forth between -0.08 V and 1 V a total of six times before the cycling was stopped.

The scan rate used in all voltammetry experiments was 1 mV/s. In non-aqueous systems, a slow scan rate is commonly used in order to identify reduction and oxidation peaks without transport limitations.

Electrochemical impedance spectroscopy (EIS) was performed on pouch cells containing each of the four electrolytes. The impedance was performed to reveal the resistances of the cells, the main contribution being the electrolyte. Frequencies between 200 kHz and 1 kHz were utilized.

3.4 X-ray Diffraction and Scanning Electron Microscopy

3.4.1 X-ray Diffraction

The crystal structure of the LFP cathode was used as an indicator of the lithium content left in the material and was estimated by X-ray diffraction (XRD). The diffractometer used was of type: Bruker D8 A25 DaVinci X-ray Diffractometer. Pouch cells were cycled for C/10 for 10 hours, equal to 100% theoretical capacity of the LFP.

After cycling, the LFP electrode was extracted and washed thoroughly with DME two times to assure no salt was left. For the TEGDME electrolytes, electrodes were also rinsed with DME to ensure that no TEGDME remained, as TEGDME is more or less non-volatile. Afterward, the samples were put under active vacuum for 1-2 hours to ensure that the samples were dry.

The LFP samples were scanned for two hours from 5-75 2Theta with a fixed slate setting. An uncycled LFP was also analyzed to have a reference of a 100% lithiated sample.

The X-ray penetration depth in the LFP material was calculated using the exponential attenuation law:

$$\frac{I}{I_0} = \exp\left[-\left(\frac{\mu}{\rho} \cdot x\right)\right] \quad (3.1)$$

Where $x = \text{density} \cdot \text{thickness}$ [g/cm^2], and $\frac{\mu}{\rho}$ is the attenuation coefficient [cm^2/g].

The attenuation coefficient was found to be $124.5 \text{ cm}^2/\text{g}$ for 98.5 wt% LFP 1.5 wt% C with K_α radiation using the NIST attenuation database [82]. If one sets the limit I/I_0 to 0.1, the penetration depth in the LFP at an incident angle of 30 degrees is about $20 \mu\text{m}$.

3.4.2 SEM

Samples containing each of the four electrolytes were investigated. Two distinct cycling programs were performed on each sample type, consequently leading to a total of eight samples being investigated. These two programs are described in Table 3.5. It should be kept in mind that the "Stripped" program is only for one cycle in contrast to Program 1-5. The "3-min" program intended to investigate the deposition morphology of the lithium during the initial plating, and the "stripped" program was to examine the leftover material after an entire cycle.

Table 3.5: Details of cycling programs, SEM

Name	Charge			Discharge		
	i(mAh/cm ²)	C-rate	End	i(mAh/cm ²)	C-rate	End
3 min	0.500	C/3	3 min	-	-	-
Stripped	0.500	C/3	1h	0.500	C/3	E _{oc} < 2.5V

The sample preparation procedures were the same as for the pouch cells opened for XRD. When transferring the copper samples from the glove box into the vacuum chamber of the SEM, exposure to air was inevitable, causing oxidation of the deposited material. All samples were kept in tightly sealed bottles in an attempt to keep oxidation to the minimum. The samples were only exposed to air when mounting them to the SEM sample holder, estimated to be 1-2 min.

This is also why only a limited amount of lithium was plated, as an increased amount would oxidize and not give good information about the original deposition morphology and distribution.

4 Results

In the following sections, the results obtained from electrochemical cycling are presented, including the galvanostatic cycling performed on cells, as well as Cyclic Voltammetry(CV) measurements and Electrochemical Impedance Spectroscopy. Presented next are selected SEM images taken of the copper electrodes. Finally, the results obtained from XRD measurements and some visual observations of opened cells are presented.

4.1 Galvanostatic Cycling

4.1.1 Program 1

The results obtained from cycling program 1 are presented in the following section. A comparison of representative coulombic efficiencies(CE) for each sample is presented in Fig. 4.1, with a zoomed in version of the same results presented in Fig. 4.2 to easier distinguish the CE values. See Appendix A Fig.A.1 for individual plots of these. The average coulombic efficiencies from cycle 6 to failure for each electrolyte are listed in Table 4.1. The average CE with standard deviation are presented in Fig. 4.3. The capacity fade, given the CE values in Fig. 4.1, are shown in Fig. 4.4. The dashed line observed is the cycle capacity of Program 1 (DoD). LiFSI + LiNO₃ in DME had the highest efficiencies of $\approx 99\%$ and a lifetime of ≈ 200 cycles.

Fig. 4.5 shows the CE at the first five cycles. The initial cycles, especially the first one being lower due to SEI formation.

The voltage curves of the selected samples are shown in Fig. 4.6 for the initial ten cycles and in Fig. 4.7 for a total overview. The two TEGDME-based electrolytes had higher overpotential compared to DME. All electrolytes saw higher overpotentials at charging close to failure.

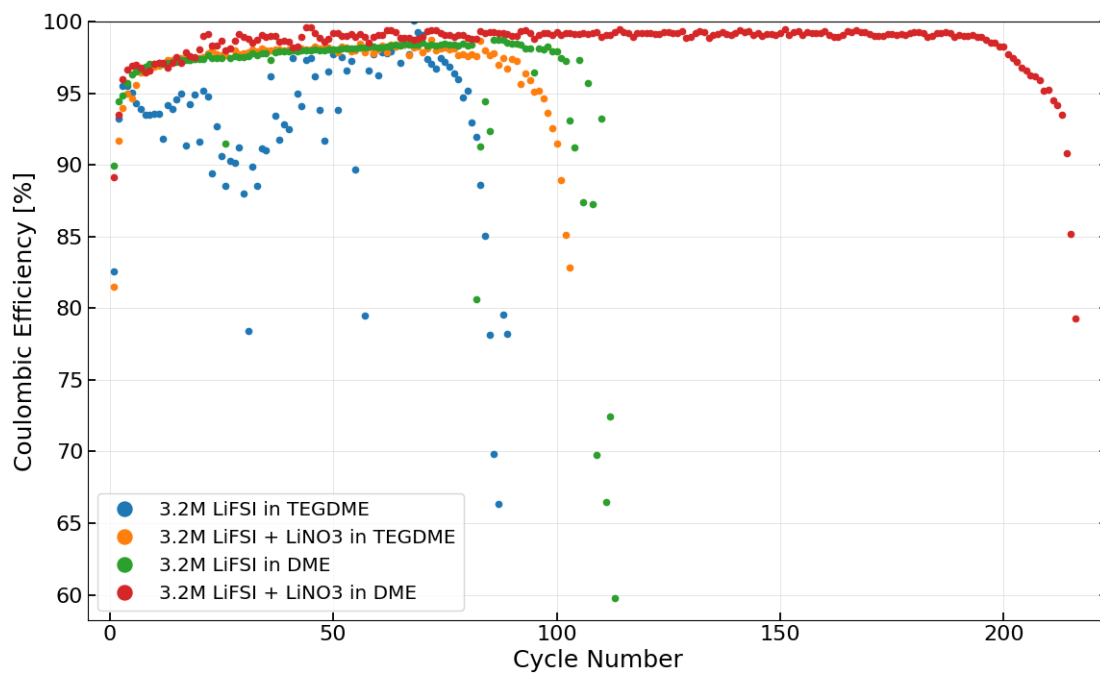


Figure 4.1: Coulombic efficiencies of selected samples containing each electrolyte, cycled on Program 1.

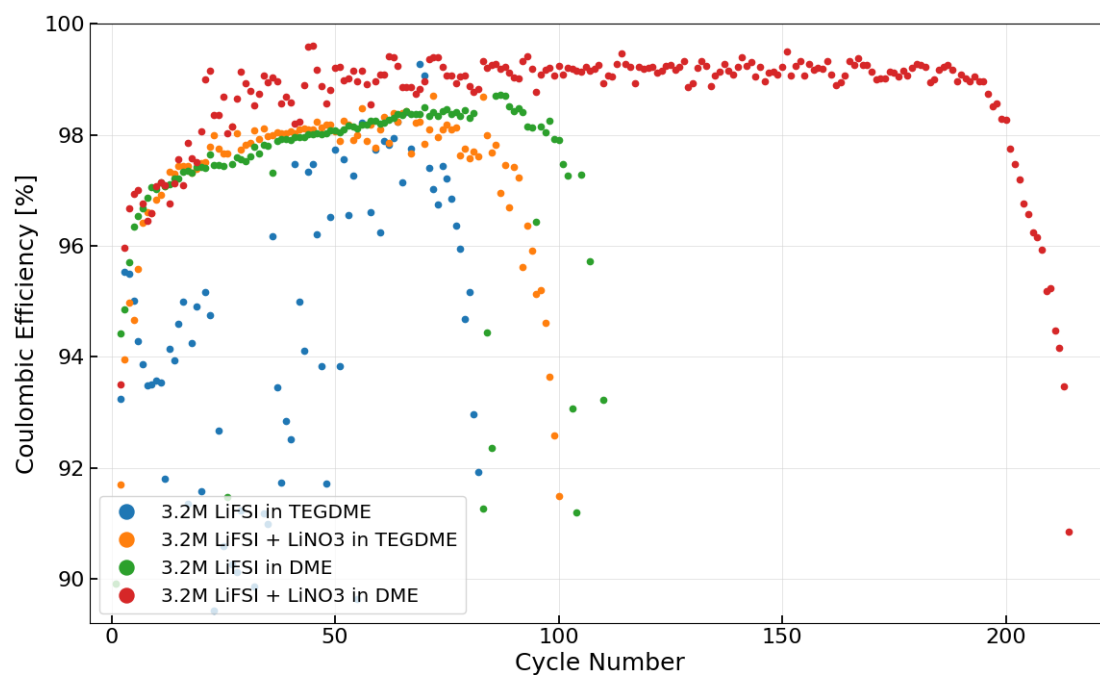


Figure 4.2: Zoomed in version of Fig. 4.1, between 90 and 100% CE.

Table 4.1: Average coulombic efficiency from cycle six until failure of each electrolyte cycled on Program 1.

Electrolyte	CE[%]
LiFSI in TEGDME	94.06
LiFSI + LiNO ₃ in TEGDME	97.84
LiFSI in DME	96.22
LiFSI + LiNO ₃ in DME	98.92

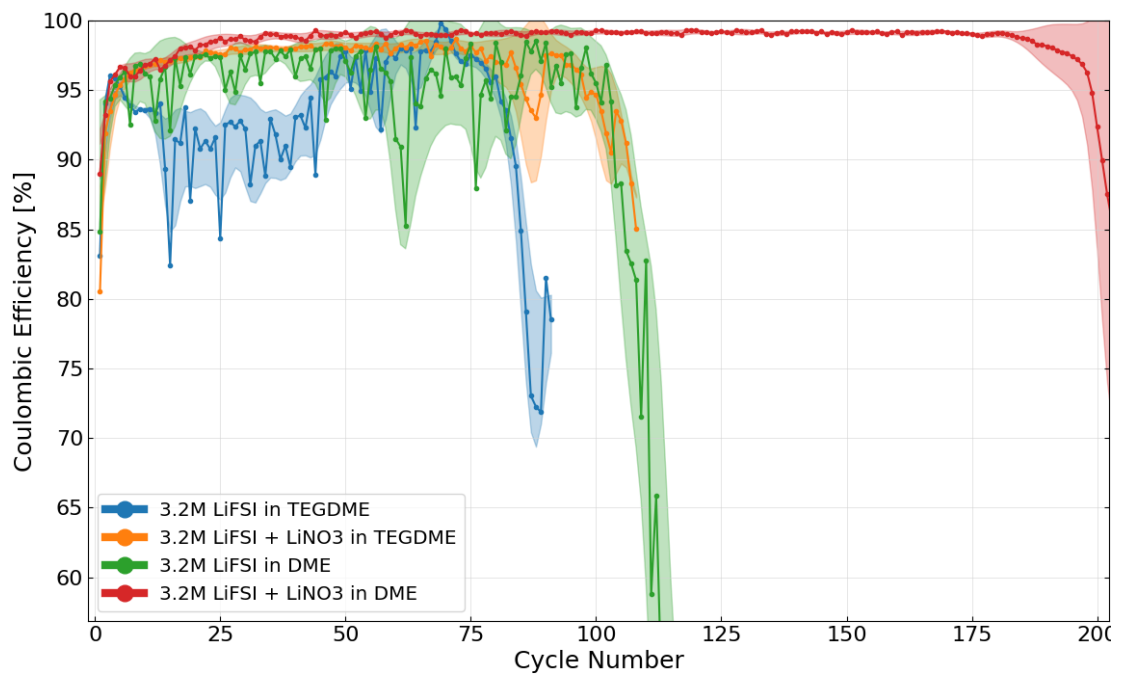


Figure 4.3: Average coulombic efficiencies of all samples cycled on Program 1. The shaded bands is a Gaussian filtered standard deviation of CE values, meant to provide further information on the variance between cells containing the same electrolyte.

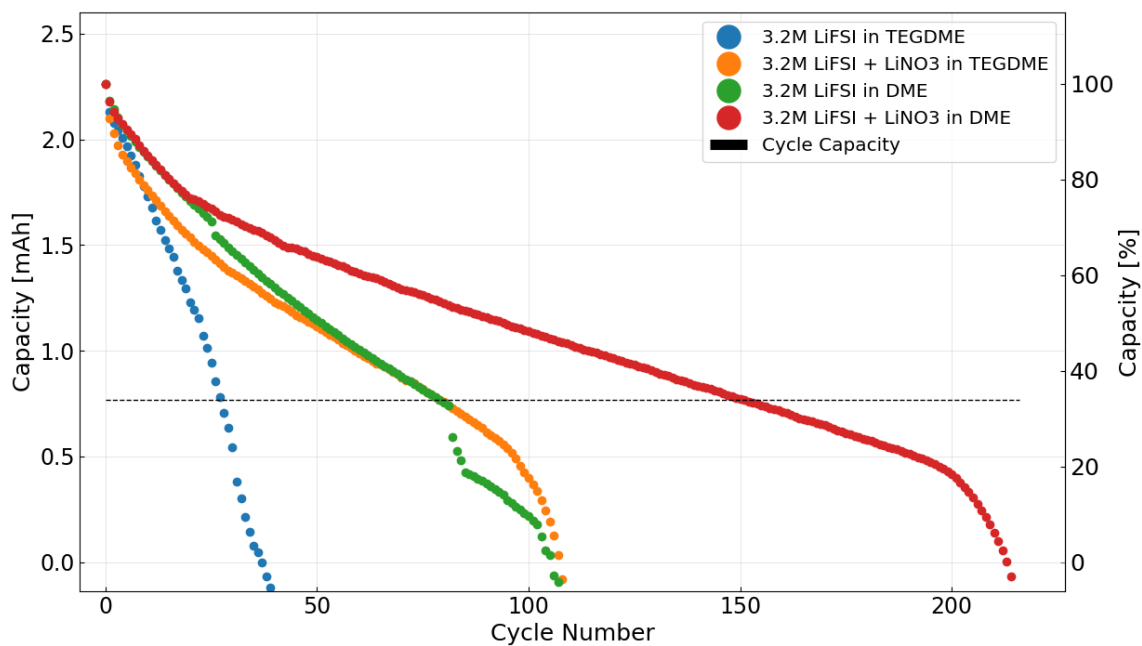


Figure 4.4: Capacity retention given the coulombic efficiencies presented in Fig. 4.1. The dashed line being the cycle capacity, corresponding to the DoD.

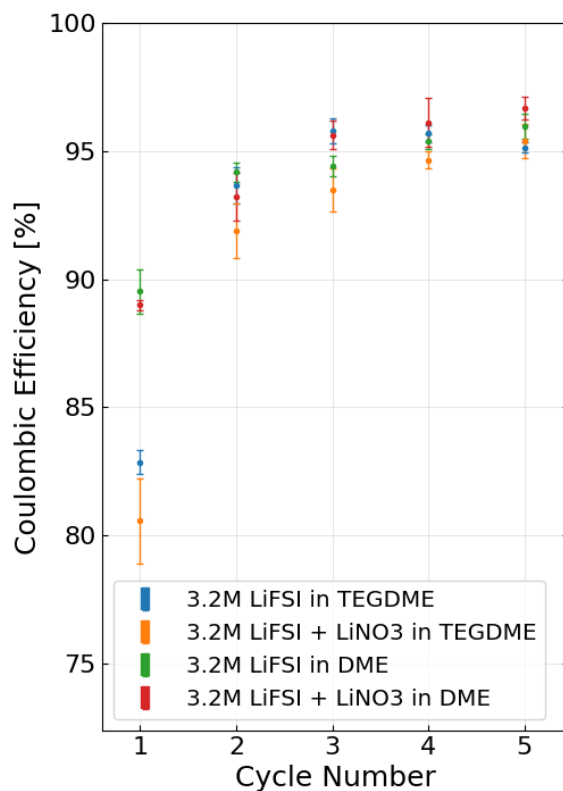


Figure 4.5: Comparison of the coulombic efficiency in the first 5 cycles in Program 1. The values being the average of all cells containing the same electrolyte, including the standard deviation.

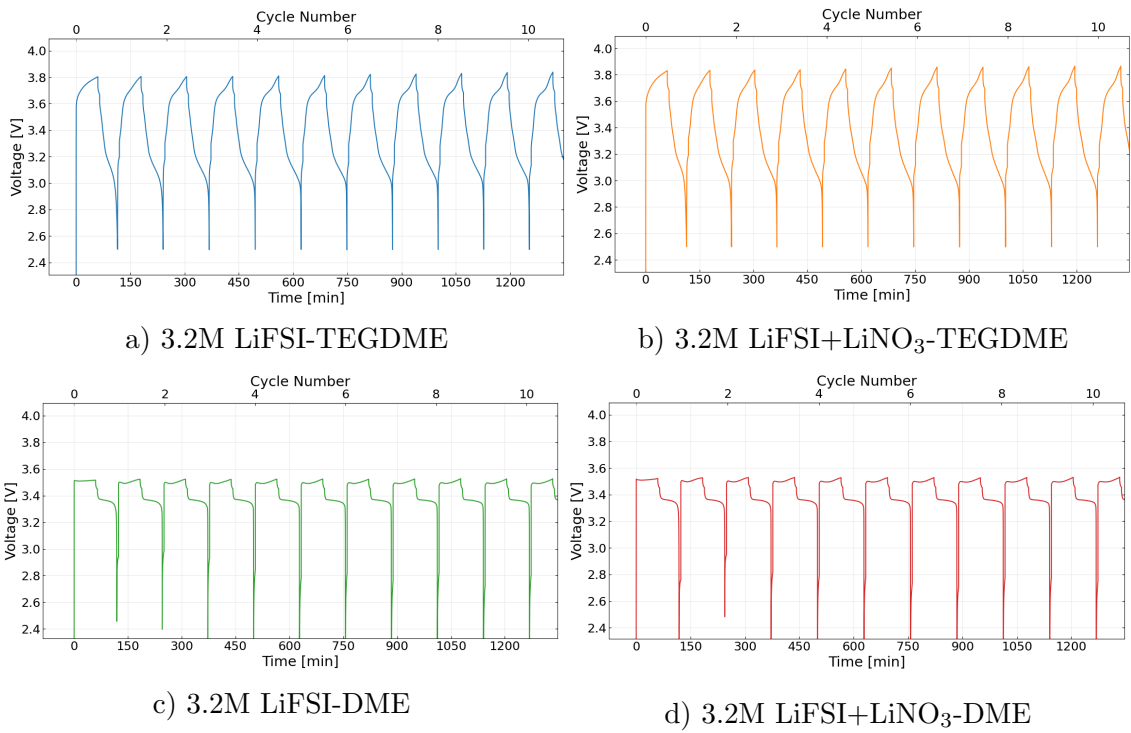


Figure 4.6: Voltage curves of the initial 10 cycles of each of the cells cycled on Program 1.

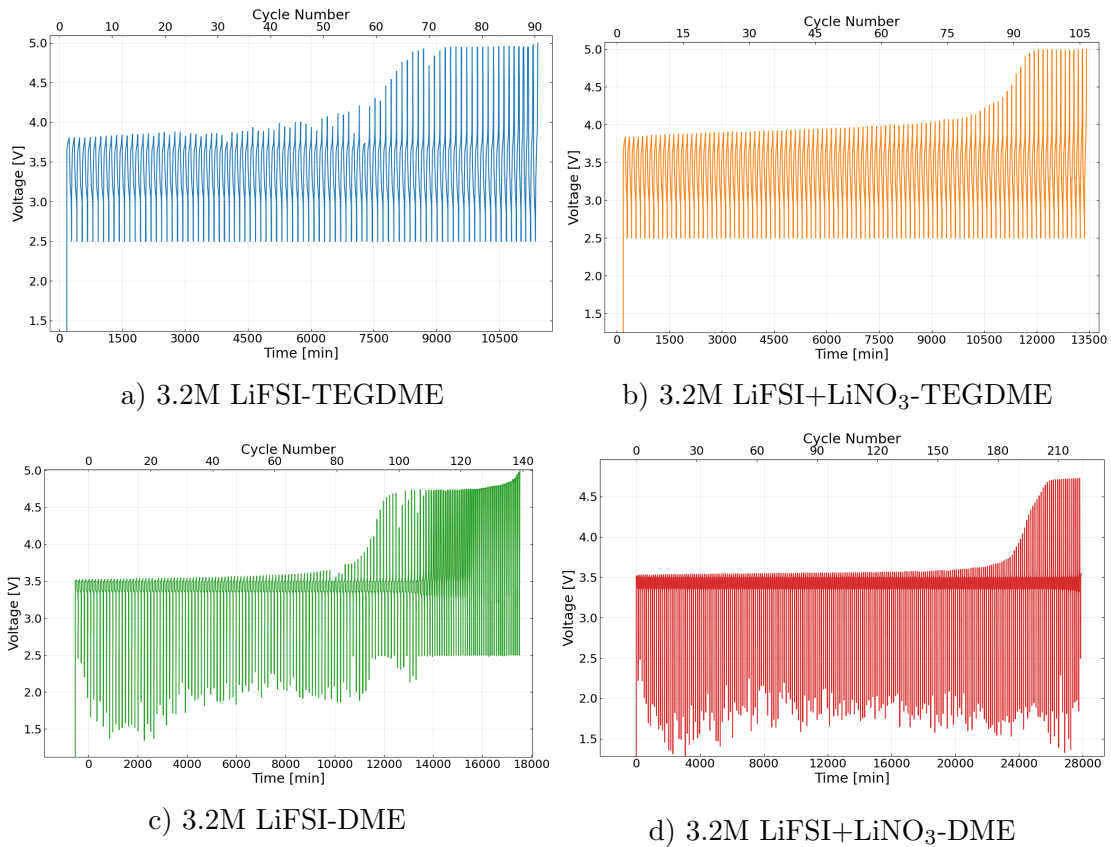


Figure 4.7: Representative voltage curves for each cell cycled on Program 1, including all cycles until failure.

4.1.2 Program 2

The results obtained from pouch cells cycled on Program 2 are presented in Fig. 4.8 - 4.12. A comparison of representative coulombic efficiencies(CE) for each sample is presented in Fig. 4.8. Individual plots of these can be found in Appendix A Fig. A.2. The average coulombic efficiencies from cycle 6 until failure are given in Table 4.2. Electrolyte 1 (LiFSI in TEGDME) is not included here due to giving poor and inconsistent efficiencies.

The average CE for each cycle are presented in Fig. 4.9. The same plot with standard deviation is located in Appendix A. Electrolyte 1 (LiFSI in TEGDME) is not included here either for the same reasons as explained earlier. The capacity fade, given the CE values in Fig. 4.8, are shown in Fig. 4.10, with the dashed line being the cycle capacity of Program 2 (DoD).

The average CE of the first five cycles for each electrolyte is shown in Fig. 4.11. These values are lower, especially in the first cycle, due to SEI formation.

The voltage profiles for the initial ten cycles for respective samples are shown in Fig. 4.12. The voltage curve for Electrolyte 1 (LiFSI in TEGDME) cycled with the higher areal capacity LFP (3.5 mAh/cm^2), on Program 2, is located in Appendix A.

The PAT-cells were cycled with a reference electrode. This made it possible to measure the potential of each electrode. The potential of the copper working electrode(we), and the LFP counter electrode(ce) were measured separately. The potential curves for the working electrode, counter electrode and the difference between them is shown in Fig. 4.13.

The coulombic efficiencies of the PAT-cells containing each electrolyte, cycled on Program 2*, is located in Appendix A Fig. A.1.

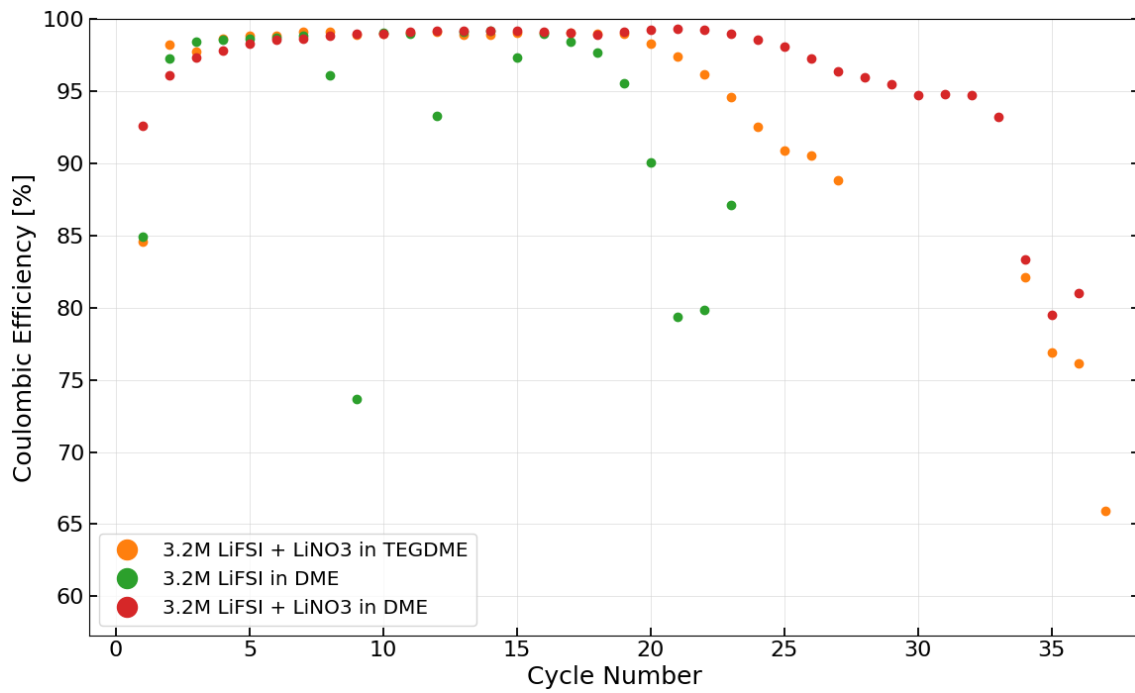


Figure 4.8: Program 2 coulombic efficiencies, comparison of the four electrolytes, selected samples

Table 4.2: Average coulombic efficiency from cycle 6 until failure of each electrolyte cycled on Program 2

Electrolyte	CE[%]
LiFSI in TEGDME	-
LiFSI + LiNO ₃ in TEGDME	98.6
LiFSI in DME	96.7
LiFSI + LiNO ₃ in DME	98.8

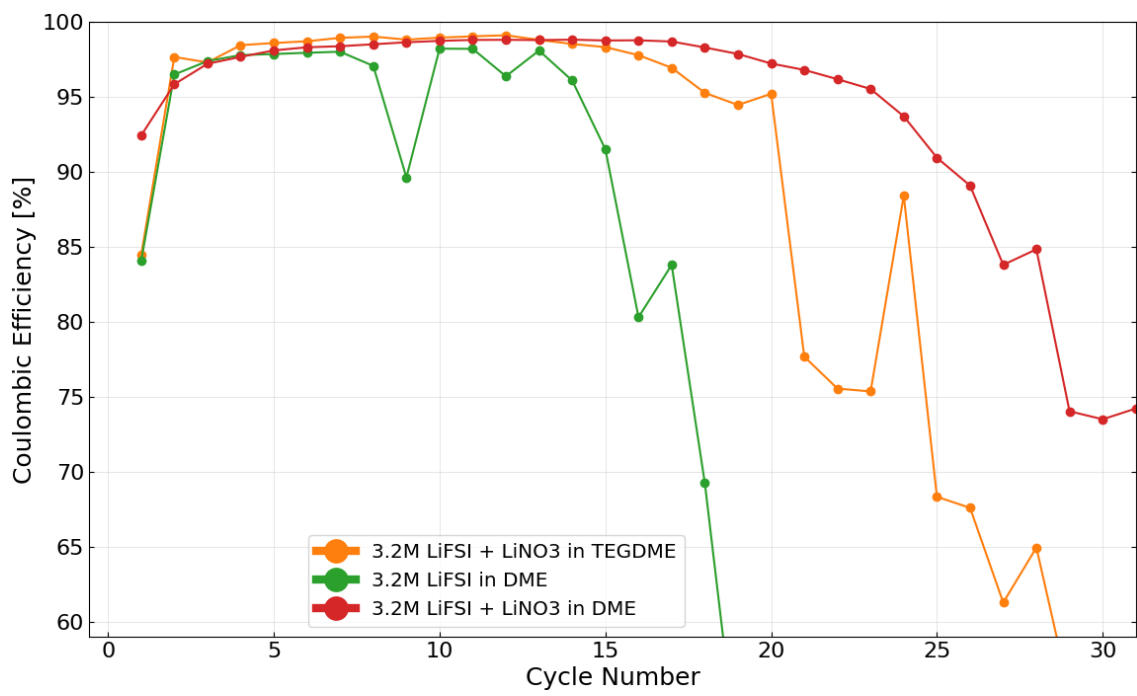


Figure 4.9: Average coulombic efficiencies of all samples, Program 2. Plot including standard deviation is located in Appendix A

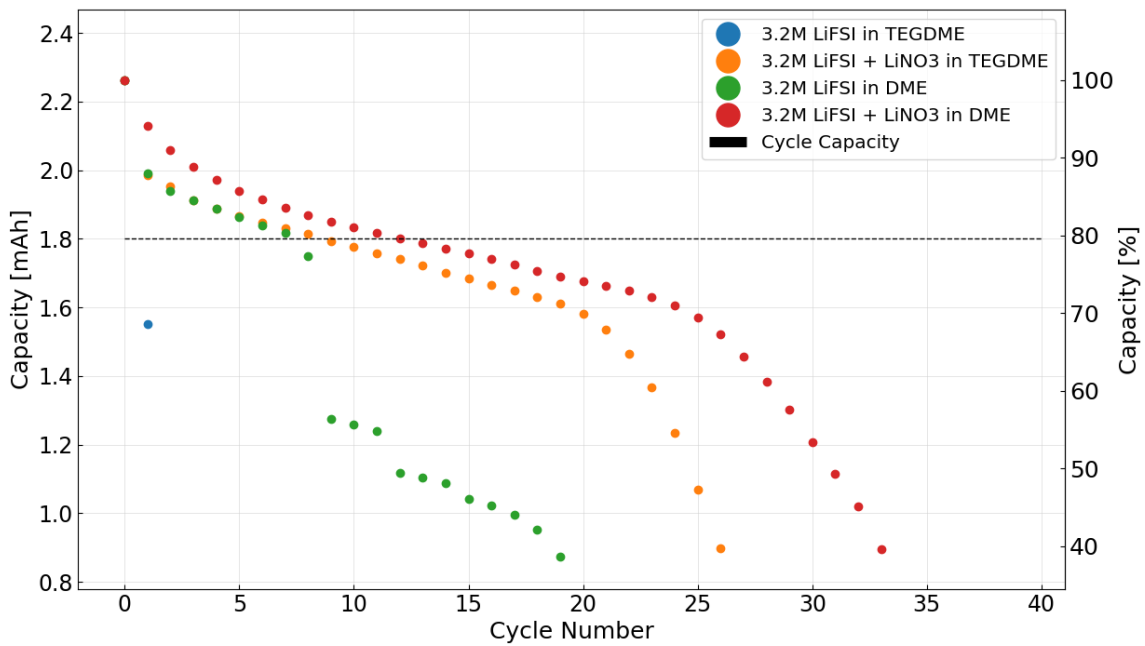


Figure 4.10: Capacity retention given the coulombic efficiency for the samples cycled at Program 2. The dashed line is the cycle capacity of Program 2 (DoD).

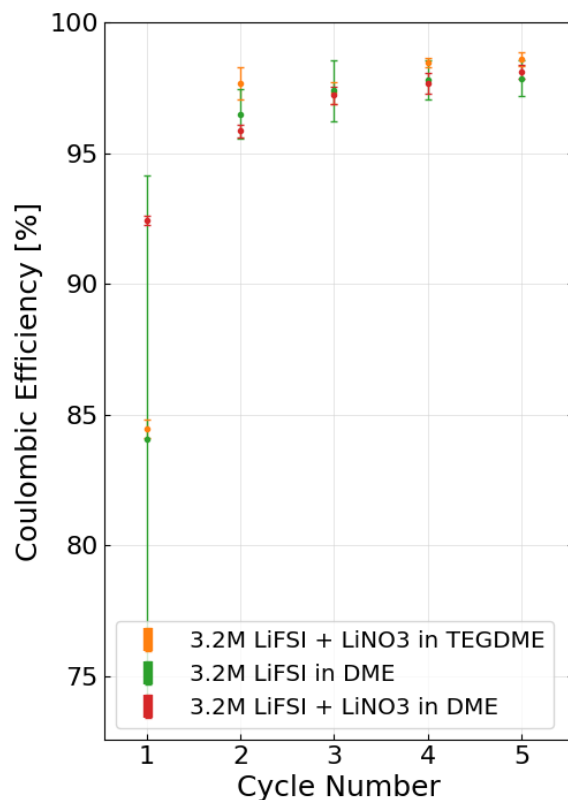


Figure 4.11: Comparison of the coulombic efficiency in the first 5 cycles, Program 2

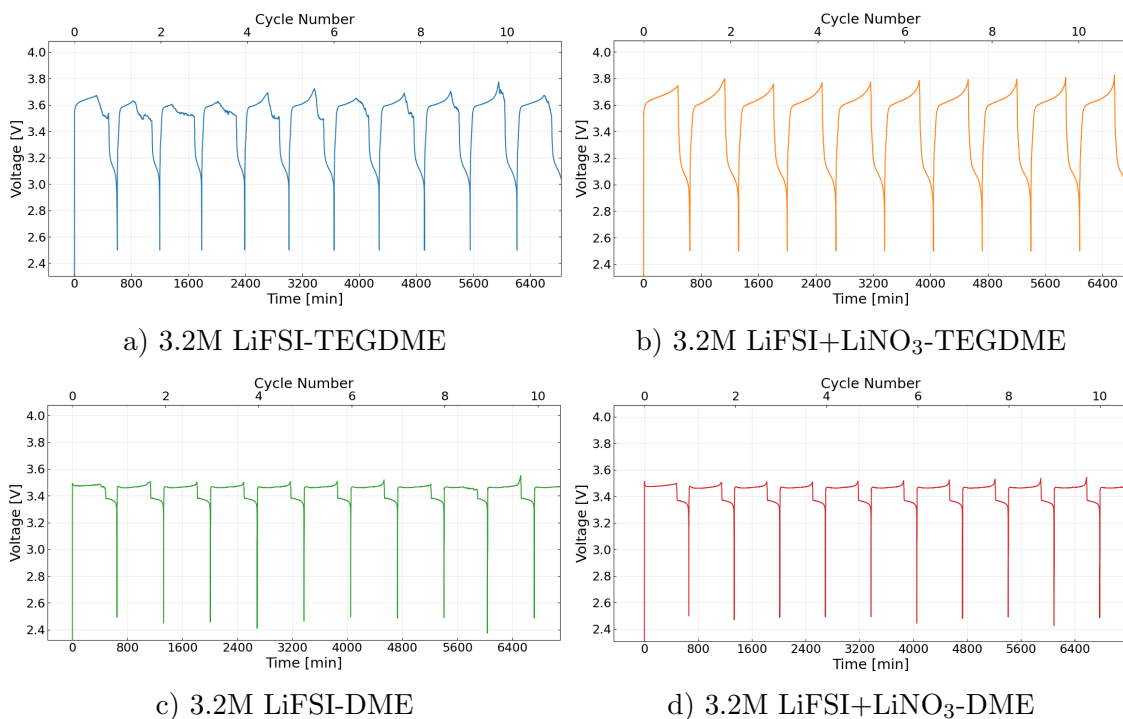


Figure 4.12: Voltage curves for the initial 10 cycles, of each of the samples cycled on Program 2

Program 2*, PAT-cells

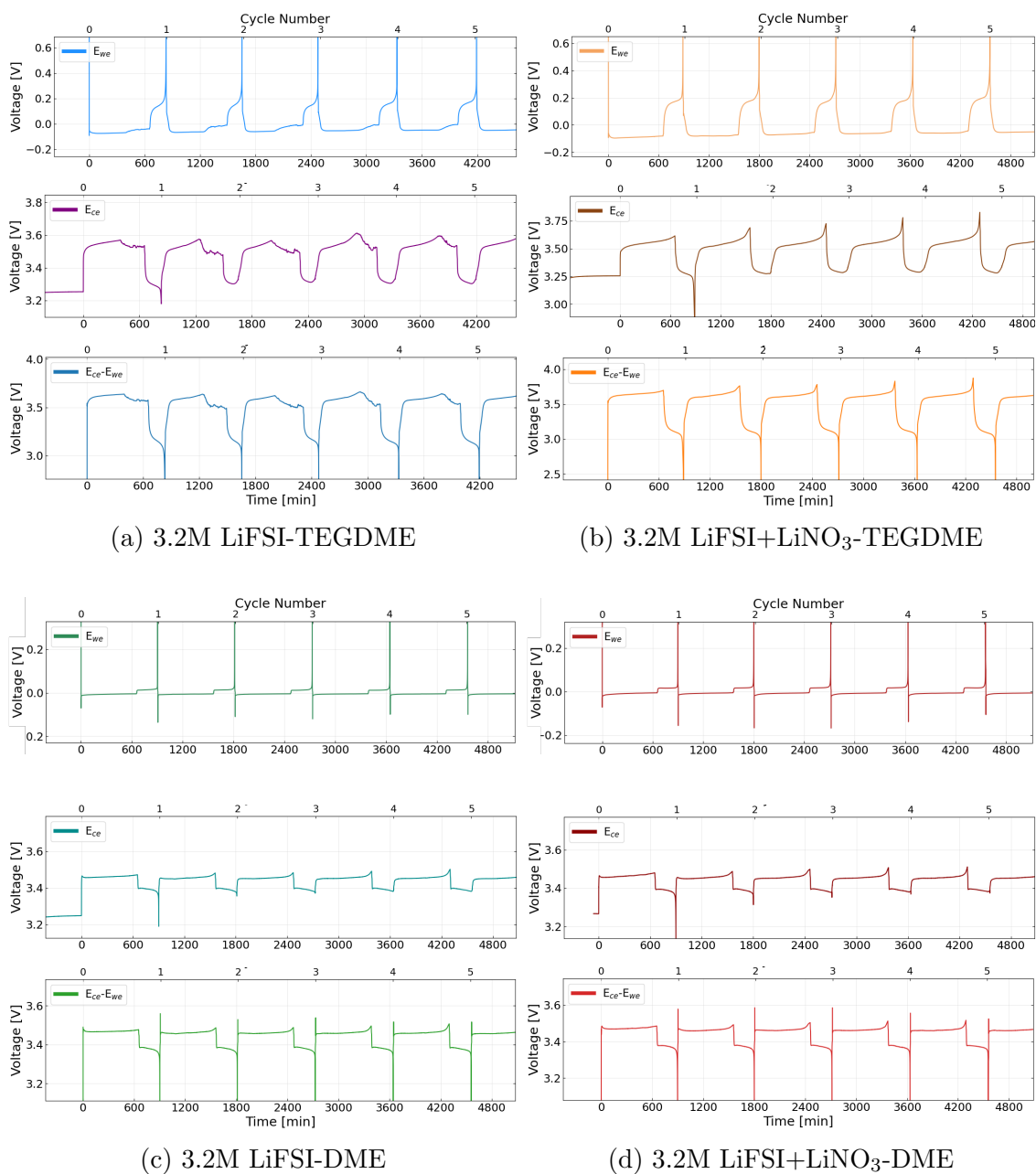


Figure 4.13: Potential curves of the copper working electrode, LFP counter electrode and the difference between the two. PAT-cells containing each of the four electrolytes, cycled on Program 2*

4.1.3 Cycling conditions, Program 2-5 comparison

The following section compares all the different cycling programs tested on Electrolyte 4 (LiFSI + LiNO₃ in DME), testing three asymmetric programs with a slow, medium and fast rate. The slow program being Program 2 presented earlier. Additionally, a symmetric program cycled at very low current densities is presented. The coulombic efficiencies of representative samples are presented in Fig. 4.14. The respective capacity fade given the coulombic efficiency are presented in Fig. 4.15.

The average coulombic efficiencies from cycle 6 to failure is listed in Table 4.3

The average CE values for each cycle are illustrated in Fig. 4.16. A zoomed in version of this between 90 and 100 % CE is shown in Fig. 4.17. The plot with standard deviation included is located in Appendix A.

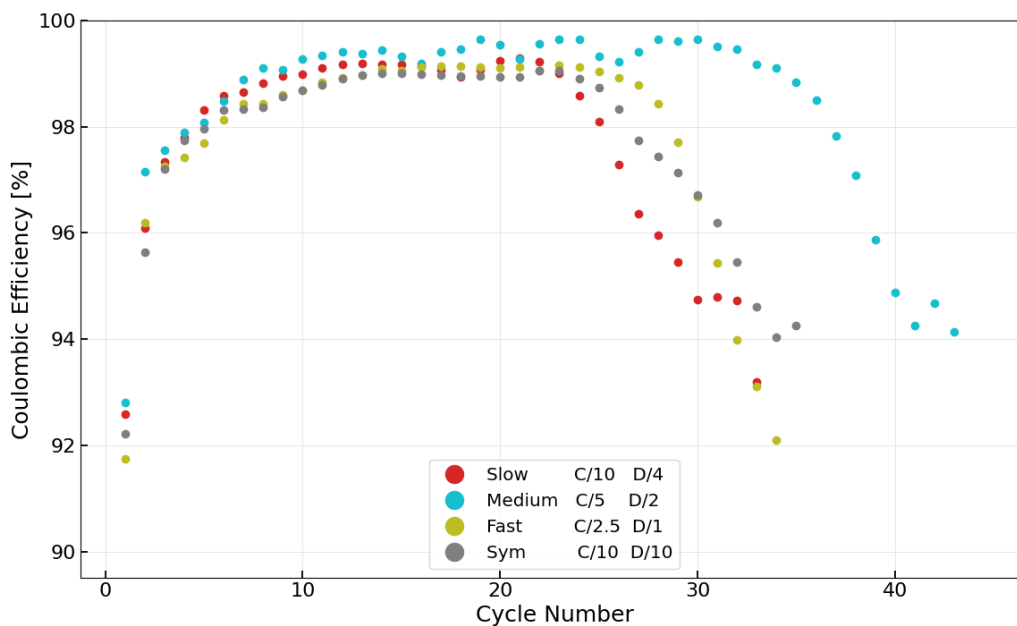


Figure 4.14: Coulombic efficiency of selected samples containing 3.2M LiFSI M in DME at different cycling conditions, including different rates and symmetric/asymmetric protocol

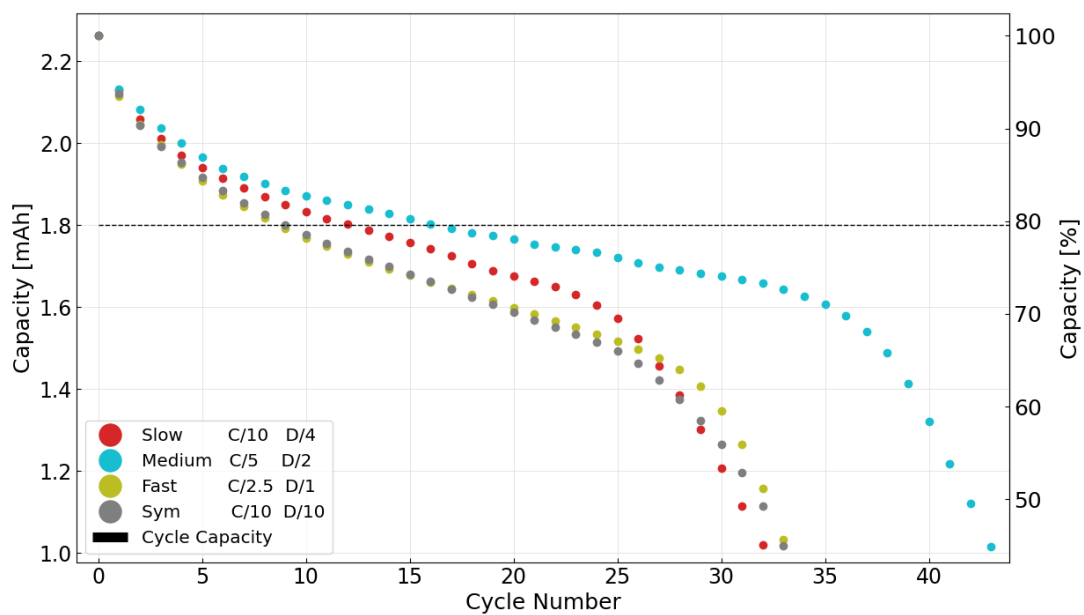


Figure 4.15: The capacity retention given the coulombic efficiencies presented in Fig. 4.14. The dashed line is the cycle capacity of Program 2 (DoD), were failure is expected to happen

Table 4.3: Average Coulombic efficiency from cycle 6 until failure of $3.2\text{M} + \text{LiNO}_3$ in DME under different cycling conditions

Cycling program	CE[%]
Program 2/Slow	98.8
Program 3/Medium	99.4
Program 4/Fast	98.7
Program 5/Symmetric	98.5

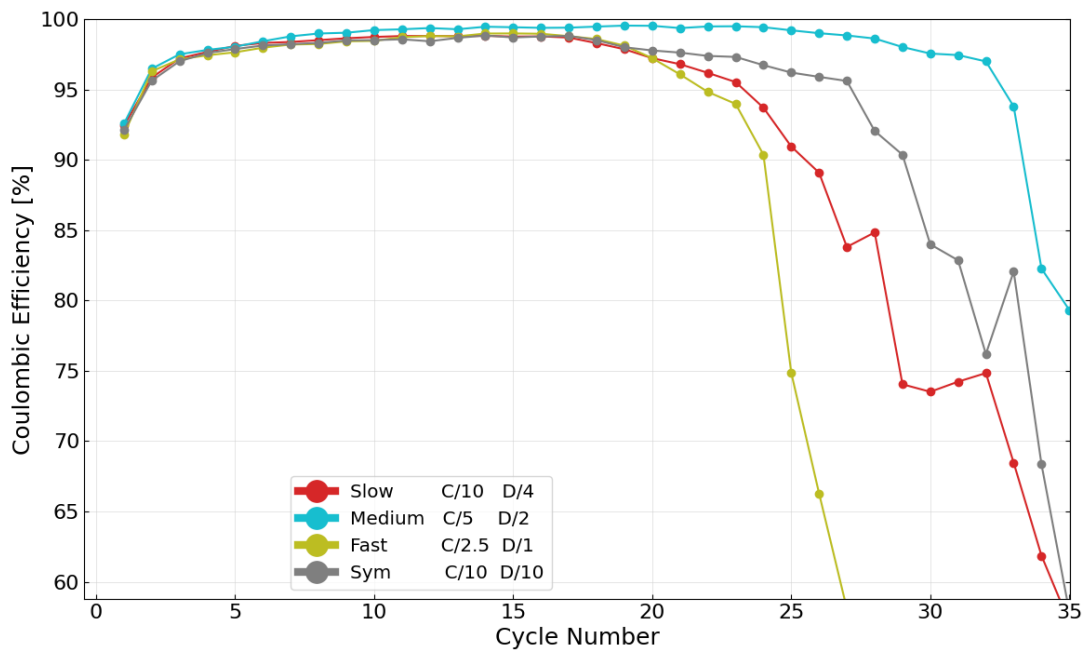


Figure 4.16: Average coulombic efficiencies of the samples cycled at different cycling conditions.

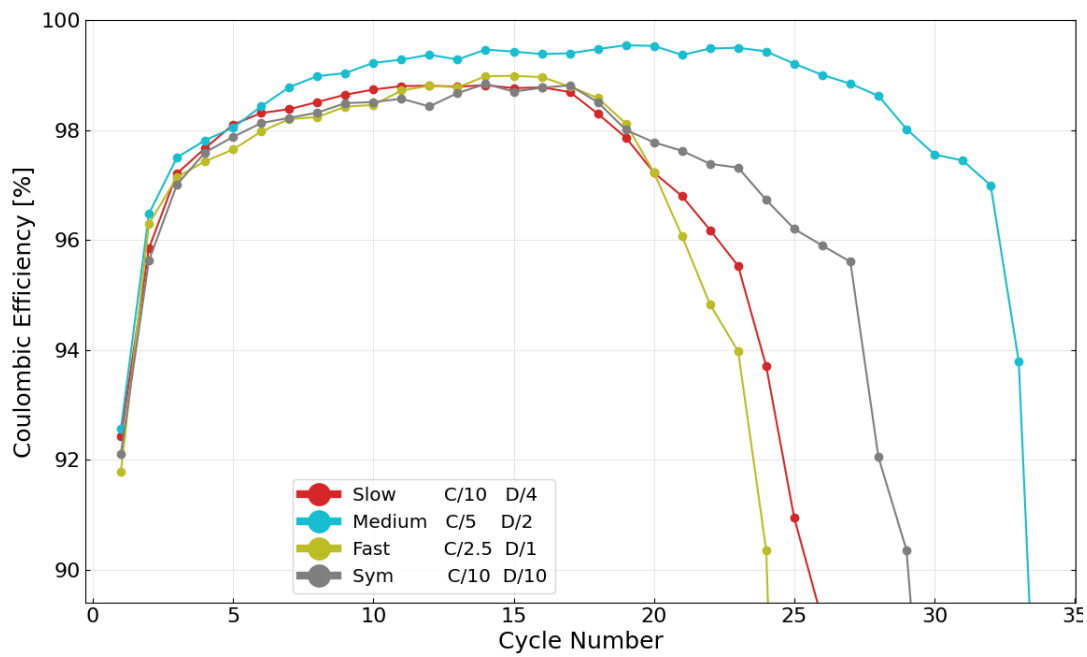


Figure 4.17: Same data as presented in Fig. 4.16, only zoomed in to CE between 90-100%. Same plot with standard deviation included are located in Appendix A

4.2 Electrochemical Impedance Spectroscopy

The ohmic resistances obtained from EIS are listed in Table 4.4

Table 4.4: Ohmic resistances of pouch cells for each electrolyte

Electrolyte	Resistance [Ω]
3.23M LiFSI/TEGDME	$12.6 \pm 0.7 \Omega$
3.23M LiFSI/LiNO ₃ -TEGDME	$14.5 \pm 0.4 \Omega$
3.23M LiFSI-DME	$2.95 \pm 0.3 \Omega$
3M LiFSI/LiNO ₃ -DME	$3.23 \pm 0.2 \Omega$

4.3 Cyclic voltammetry

The results acquired from cyclic voltammetry are included in the following section. A closer look at the initial charge cycle in the region of SEI formation (3.0 - 0 V) is presented in Fig. 4.18. A comparison of the first cycle between the electrolytes is presented in Fig. 4.19. An individual look at the samples, including all six cycles, is shown in Fig. 4.20.

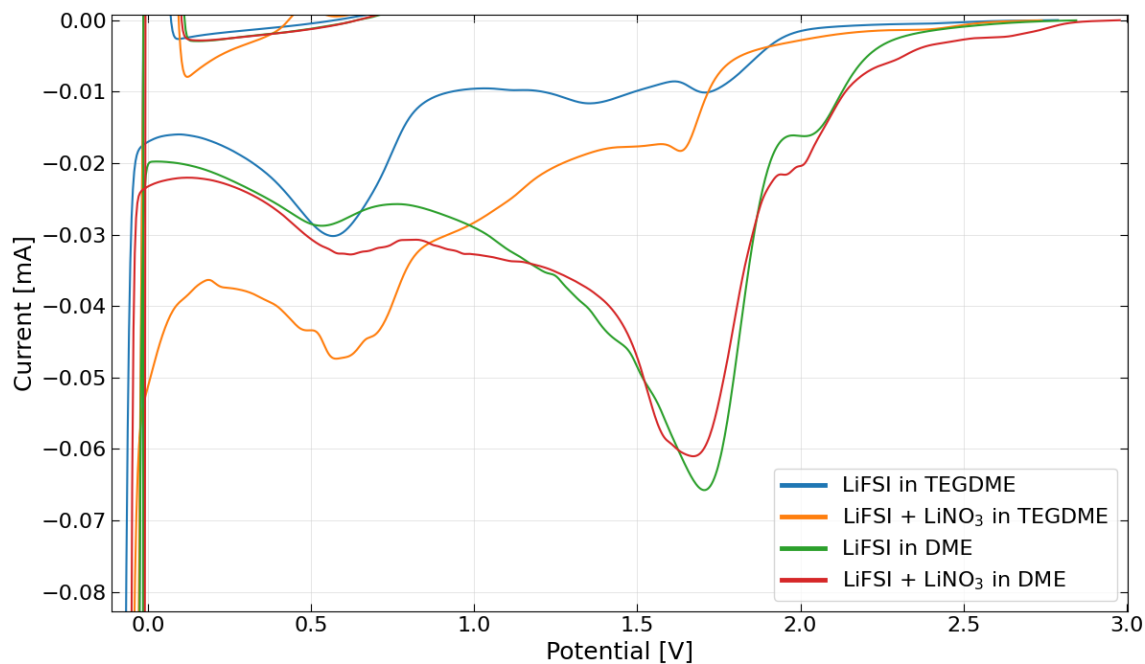


Figure 4.18: Initial cycle from Cu's original potential down to 0V

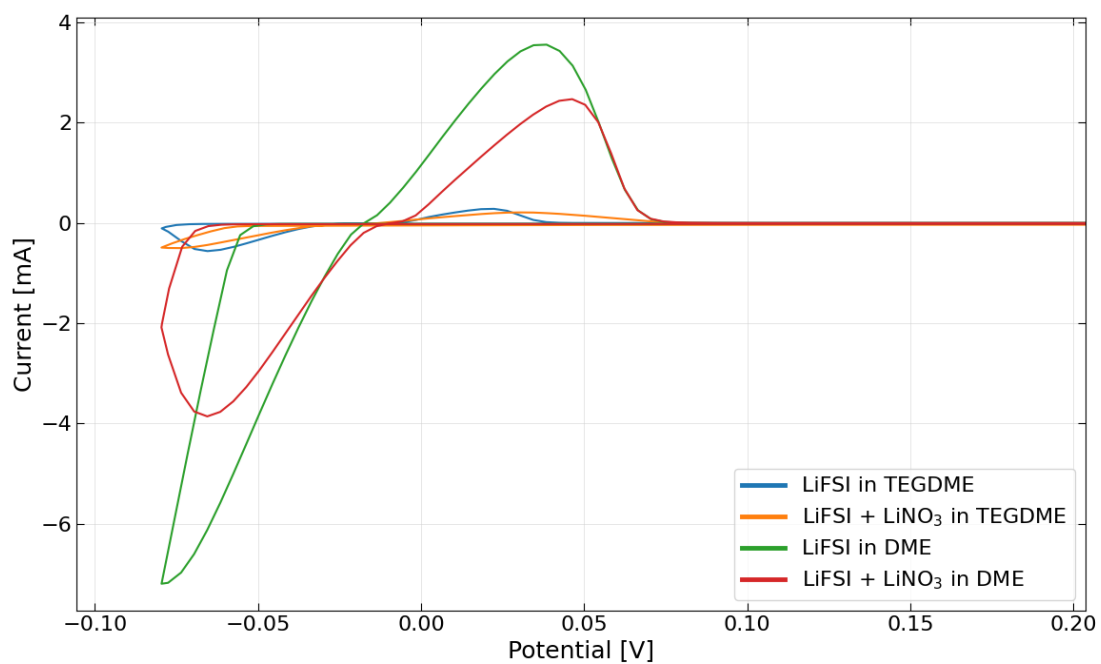


Figure 4.19: CV, first cycle comparison

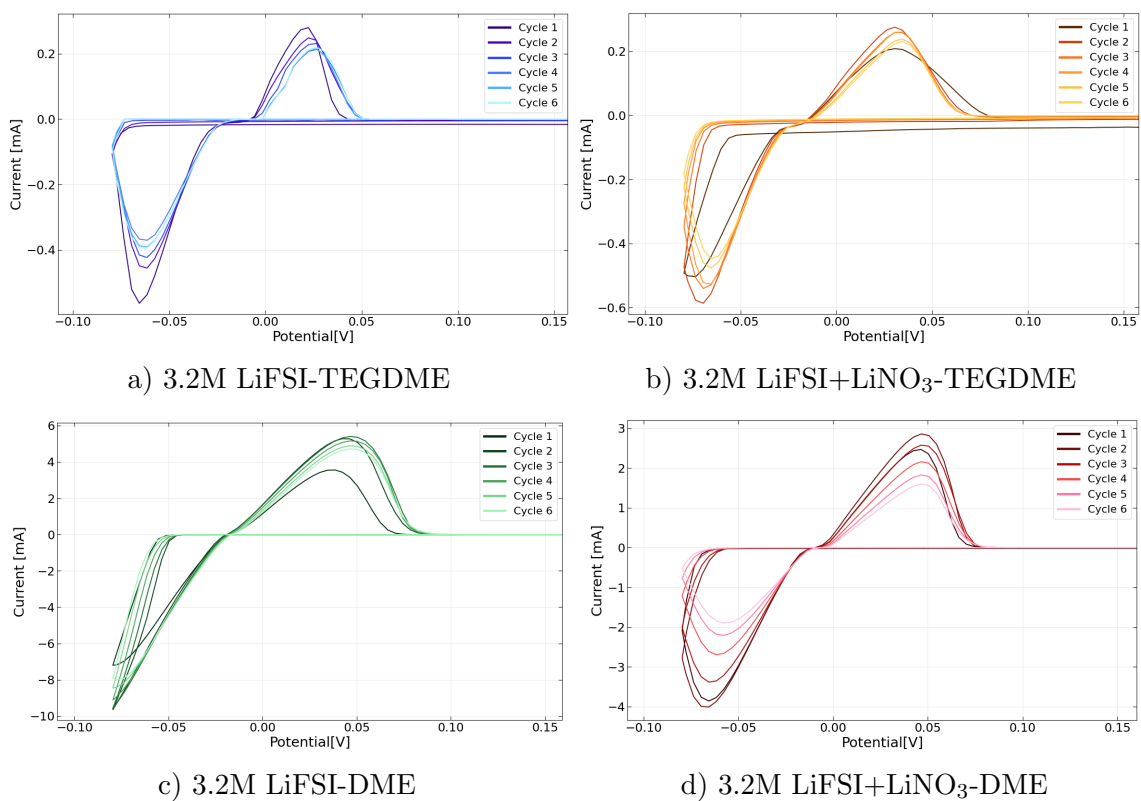


Figure 4.20: Cyclic voltammetry for all electrolytes, including all six cycles

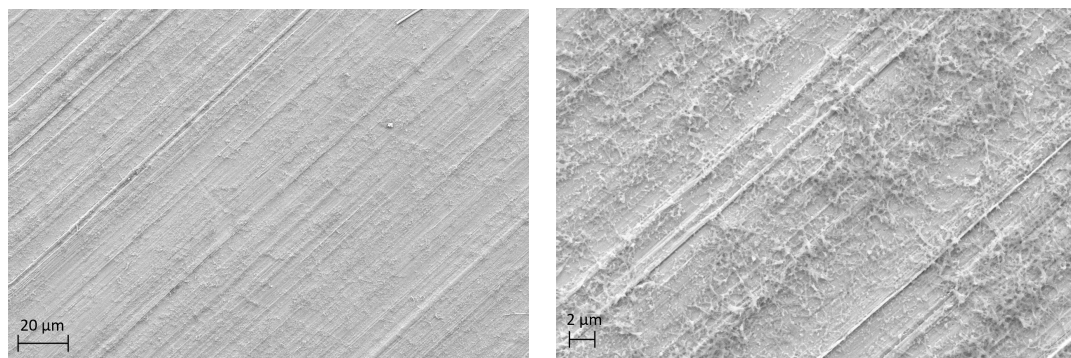
4.4 SEM

The following section includes a selection of SEM images taken of the copper foil after being cycled. All pictures are secondary electron images.

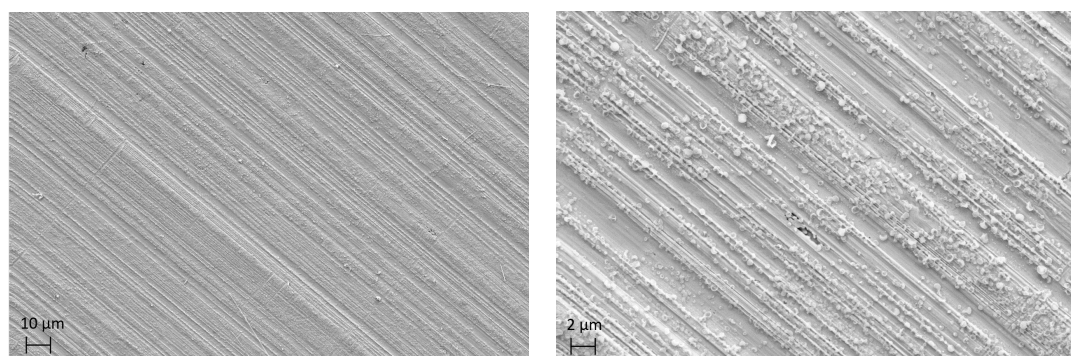
Pictures taken after depositing lithium for three minutes on the copper are shown in Fig. 4.21. Images of the copper after lithium had been plated then stripped can be observed in Fig. 4.22. In other words these are pictures after one cycle. Two images are included for each sample, one at 1000 magnification and the second one with 5000 magnification.

Additional SEM images for every samples are found in Appendix B, Fig. B.1 and Fig. B.2. These includes images in arbitrary magnifications depending on what was thought to provide the greatest complementary information for each sample.

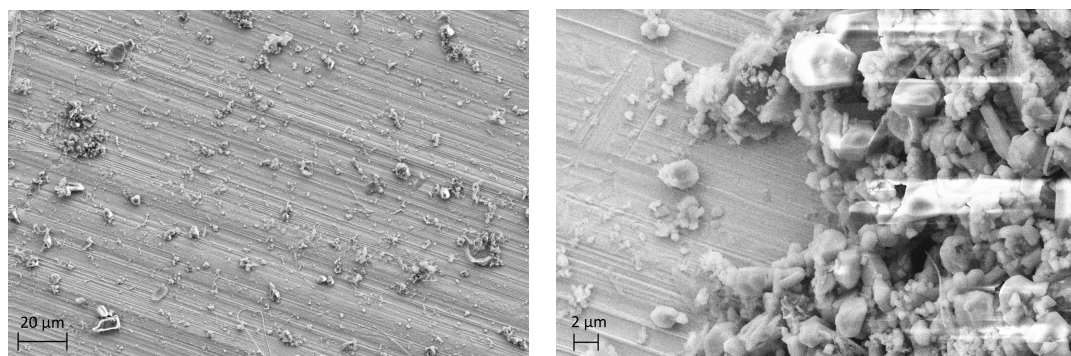
4.4.1 3 minutes deposition



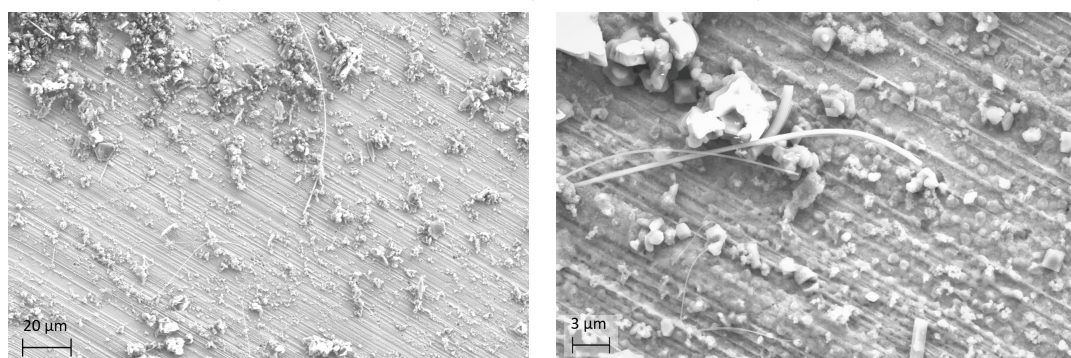
a) 3.2M LiFSI-TEGDME, Left) Mag: 1k , Right) Mag: 5K



b) 3.2M LiFSI+LiNO₃-TEGDME, Left) Mag: 1k , Right) Mag: 5K



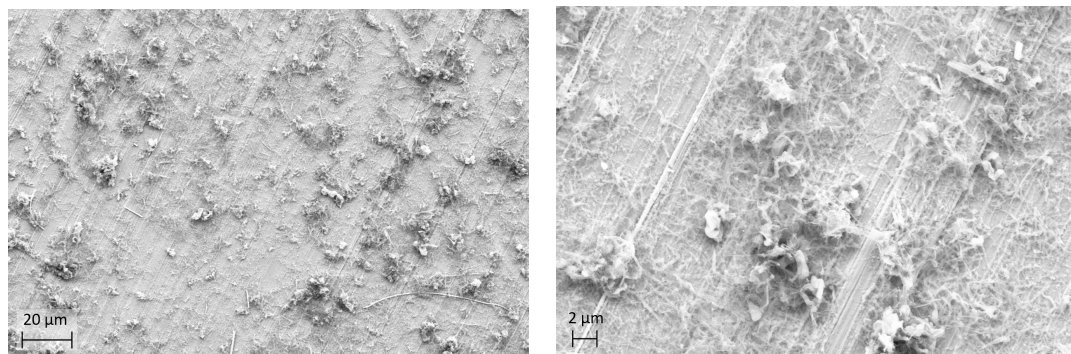
c) 3.2M LiFSI-DME, Left) Mag: 1k , Right) Mag: 5K



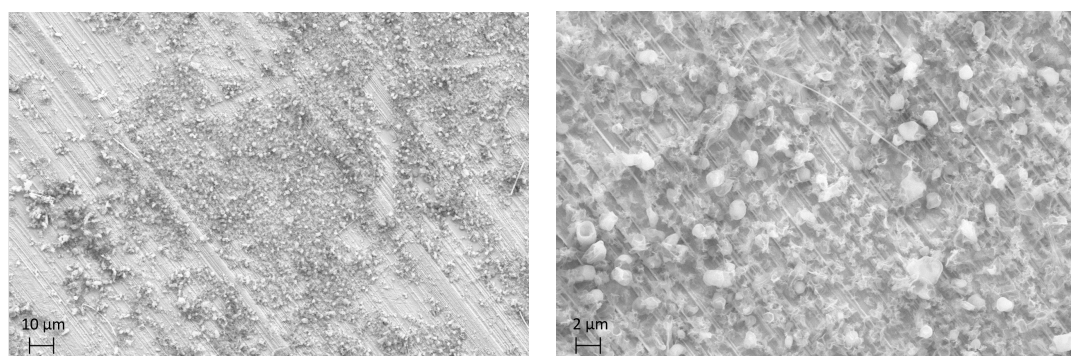
d) 3.2M LiFSI+LiNO₃-DME, Left) Mag: 1k , Right) Mag: 5K

Figure 4.21: SEM-images taken of the copper surface after 3 minutes of plating, taken with 1000x and 5000x magnification

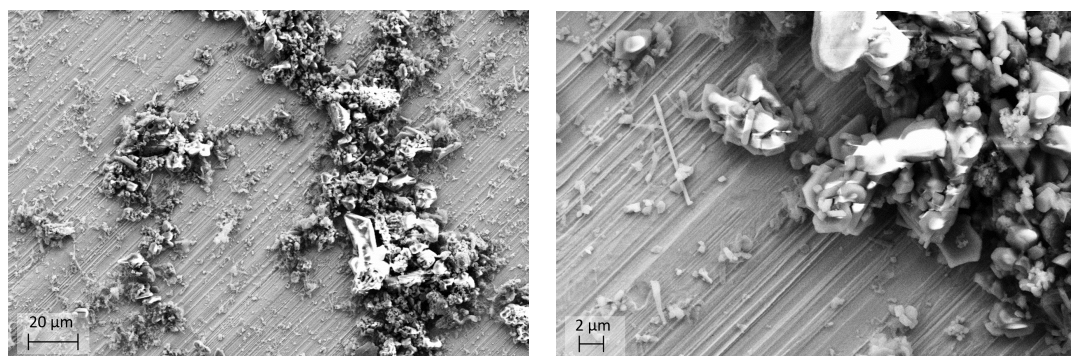
4.4.2 One charge discharge cycle/stripped



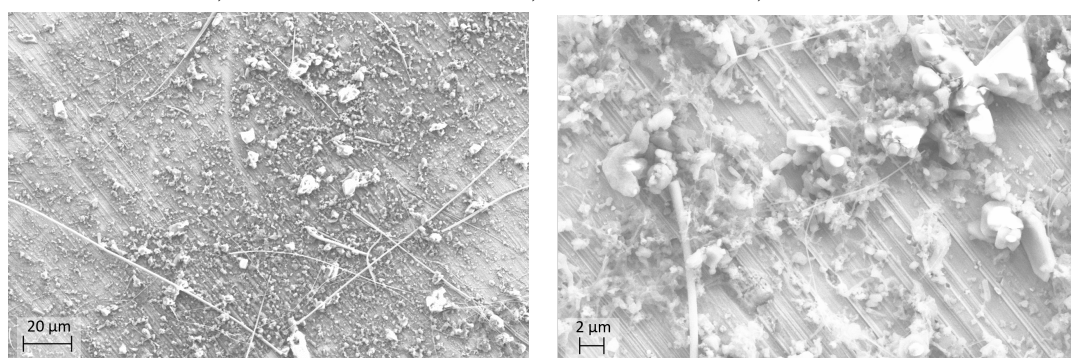
a) 3.2M LiFSI-TEGDME, Left) Mag: 1k , Right) Mag: 5K



b) 3.2M LiFSI+LiNO₃-TEGDME, Left) Mag: 1k , Right) Mag: 5K



c) 3.2M LiFSI-DME, Left) Mag: 1k , Right) Mag: 5K



d) 3.2M LiFSI+LiNO₃-DME, Left) Mag: 1k , Right) Mag: 5K

Figure 4.22: SEM images taken of the copper surface after one charge/discharge cycle, with the four electrolytes

4.5 XRD

XRD measurements of delithiated LFP cathodes were performed. The LFP was a 100 % delithiated, before the cell was opened and the LFP-cathode were put into the X-ray Diffractometer.

The results from XRD of the LFP cathodes delithiated with each of the electrolytes, are presented in Fig. 4.23. This graph includes an entirely lithiated LFP meant to be used as a reference. Individual X-ray diffractograms for each sample are found in Appendix C.

The aforementioned figures include database 2theta-values (peak positions) for the two phases, LiFePO_4 and FePO_4 , respectively, obtained from the PDF-diffraction database. The PDF IDs are:

- FePO_4 : PDF 04-011-8635
- LiFePO_4 : PDF-04-010-3115

Unit cells of LFP and FP extracted from the PDF database are found in Appendix C.

To perform the XRD measurements, the respective cells had to be opened first. The visual observations done on these cells are presented in Fig. 4.24, them being fully discharged once, meaning a lot of lithium was plated on the copper surface.

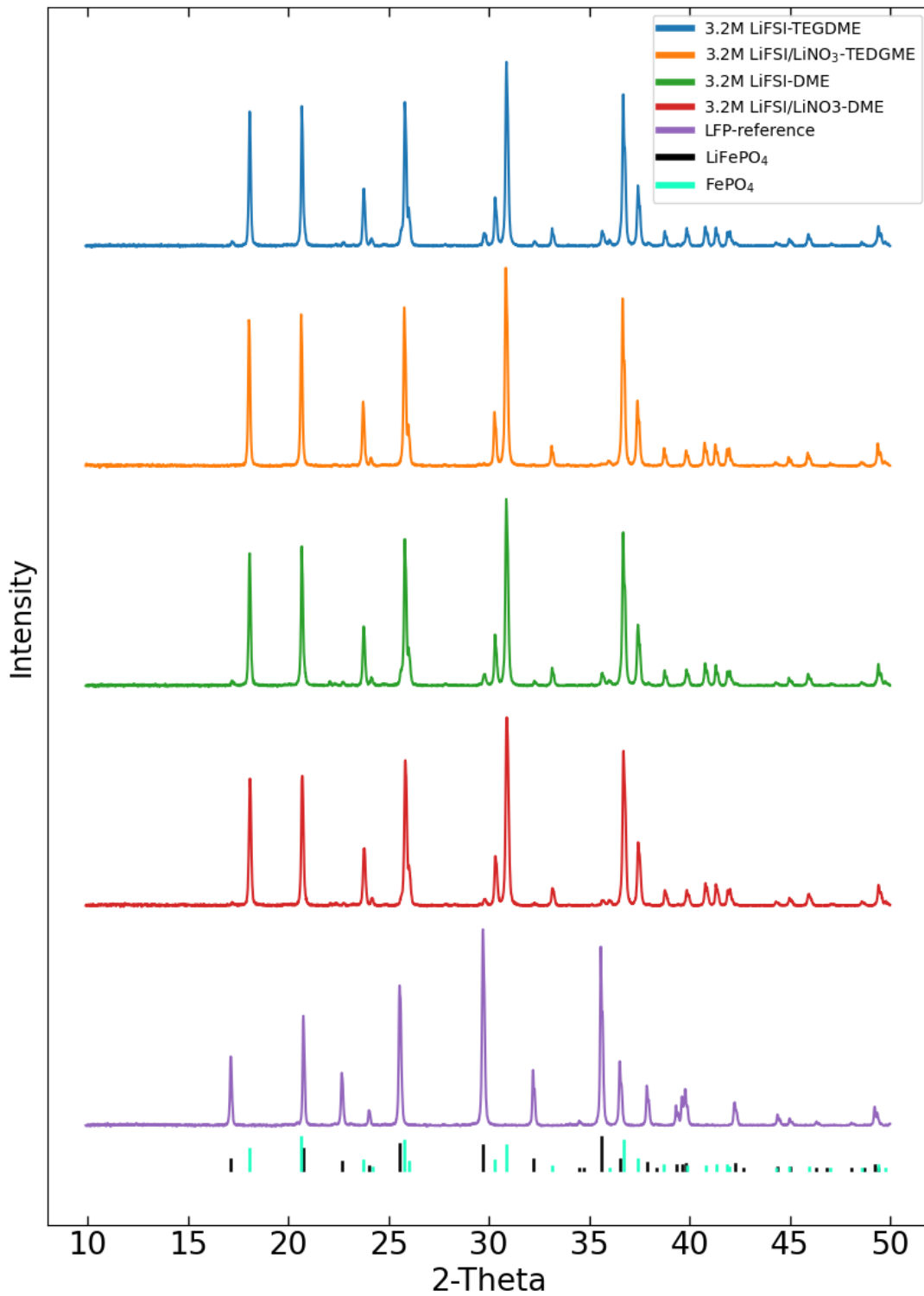


Figure 4.23: X-ray diffractograms of delithiated LFP cathodes cycled with all four electrolytes, including one lithiated LFP reference. Background has been subtracted. Peak positions of the two phases are from the PDF-database

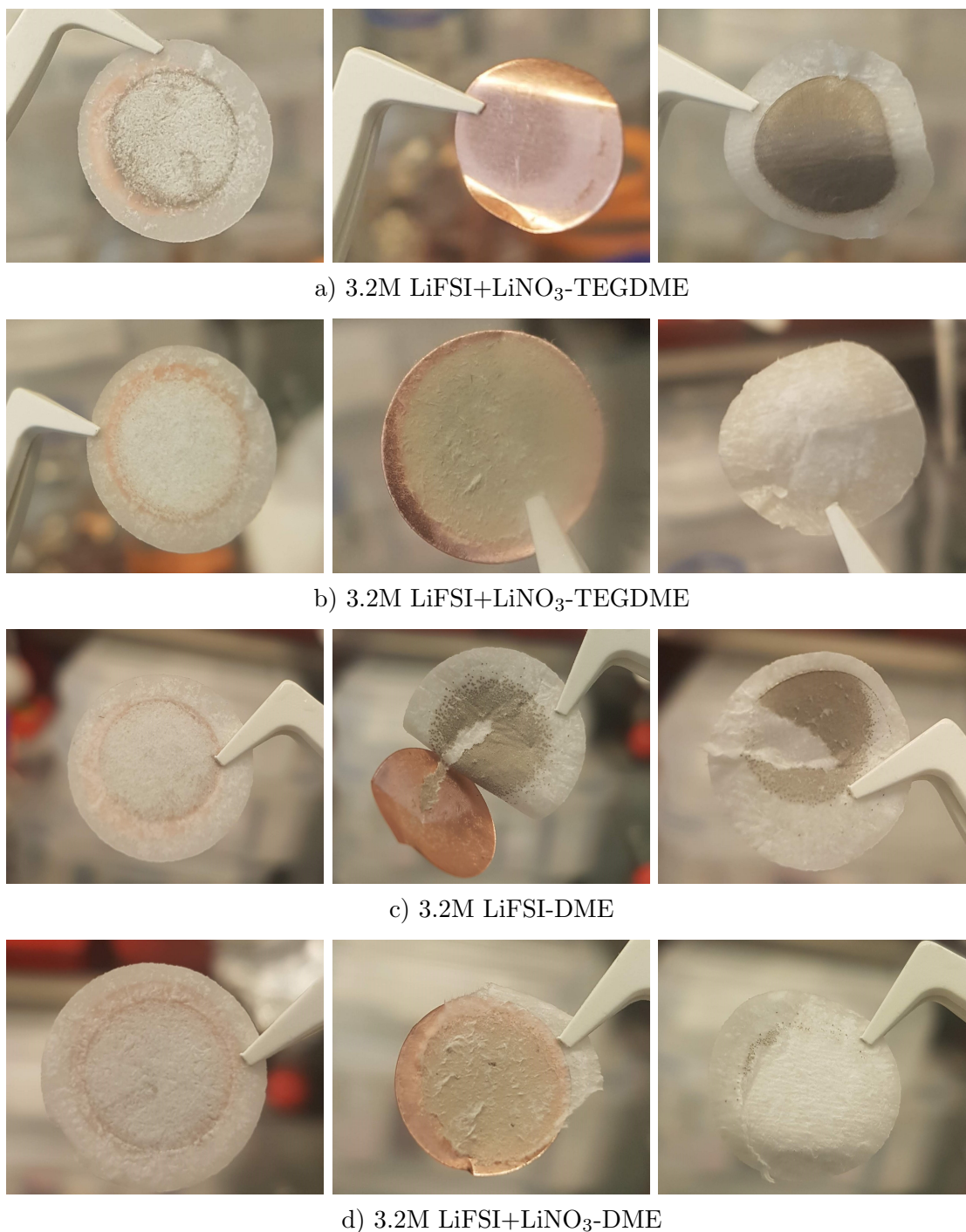


Figure 4.24: Images taken of the opened cells after one discharge for each electrolyte composition. Left: Copper foil and separator, Middle: Copper foil after removing separator, Right: Separator after being removed from the copper. When tearing the separator and copper apart from each other, the lithium deposition is observed to remain on the copper surface in some cases (b and d), while sticking to the separator in other cases (a and c)

5 Discussion

5.1 Comparison of ether solvents

The results obtained from galvanostatic cycling indicate clear differences between the two solvents. Both cycling program 1 and 2 favors DME as the ideal solvent. A general higher coulombic efficiency and a longer lifetime are achieved, which can be observed in Fig. 4.1 and 4.2 for cycling program 1 and Fig. 4.8 for cycling program 2.

The average CE in Program 1, as seen in Table 4.1, is over 2% higher for the DME electrolyte compared to the equivalent electrolyte with TEGDME, and with LiNO_3 the CE is more than 1% higher for the electrolyte containing DME. This increase in CE makes up a significant difference that directly influences the lifetime of the cell. A higher average CE for the DME-based electrolyte is also observed in Program 2, though not as considerable, with a 0.2 % increase between the TEGDME and DME-based electrolytes with LiNO_3 additive, seen in Table 4.2. A significant difference was observed between the two electrolytes without LiNO_3 additive, which is due to the LiFSI in TEGDME electrolyte not being stable, something discussed in more detail later.

Another clear distinction between the two ether solvents is the difference in the coulombic efficiency for the initial cycles, especially the first cycle. This is observed both for Program 1 and 2. Fig. 4.5 reveals the average initial CE of being about 81 and 83 % for the TEGDME based electrolytes with and without LiNO_3 , respectively, while being approximately 89 % for both DME-based electrolytes. The average CE in the initial cycles in Program 2 are shown by Fig. 4.11 to be about 84 % for LiFSI + LiNO_3 in TEGDME. while being 93 % for LiFSI + LiNO_3 in DME.

This coulombic efficiency and the respective capacity loss in the first cycle are tightly connected to the SEI formation. The lower initial CE in the TEGDME electrolytes indicates more lithium consumption and therefore, forming a thicker SEI layer. A thick SEI layer is not ideal as it represents more capacity loss, thereby being detrimental to the overall lifetime of the cell. Additionally, a thicker SEI layer causes an

increased resistance, leading to higher overpotential and more energy losses.

From the cyclic voltammetry, the initial cathodic scan from OCV to 0 V, presented in Fig. 4.18, indicates SEI formation for all electrolyte systems. The peaks in cathodic current represent the formation of different electrolyte decomposition products, making up the SEI layer. The current peaks indicate a distinction in the SEI composition between the TEGDME and DME-based electrolytes. The exact species making up the SEI layer is unknown, but during SEM-imaging charging was experienced only during imaging of DME samples, which might imply a SEI containing more organic species.

Relatively broad anodic peaks were observed for all electrolytes, as shown in Fig. 4.20, indicating SEI-formation during the first cycle for all samples. Additionally, Fig. 4.20 clearly shows the anodic peak current being lower in the first cycle, which can be explained by a limited amount of lithium being available to strip due to SEI formation.

The results show a significant distinction in the kinetic performance between the two ether solvents, benefiting DME. The CV demonstrates that the DME-based electrolytes are able to reach much higher cathodic and anodic currents compared to TEGDME using the same scan rate. In other words, more lithium is plated and stripped. This distinction is illustrated in Fig. 4.19 and further proves that the kinetics of the plating/stripping reaction is much faster in the DME solvent.

The ohmic resistances measured from EIS measurements, presented in Table 4.4, is the most concrete result, showing that DME gives lower resistance. The resistance is tightly connected to the TEGDME experiencing higher overpotentials during cycling, as shown in Fig. 4.6 and 4.12. However, even though the TEGDME-based electrolyte exhibits a higher resistance, 12-15 Ω is still considered tolerable as a high current density, i.e. 1.5 mA/cm² (2.3 mA) would only cause an ohmic overpotential of $I \cdot R = 30$ mV.

However, similarly, the overpotential associated with the TEGDME-based electrolytes is getting way higher than the resistance indicates. The overpotential also increases during charging shown in Fig. 4.6 and Fig. 4.12. The higher-than-expected

overpotential can partially be attributed to the SEI layer contributing to increased internal resistance in the cell. However, Fig. 4.13 clearly shows that the overpotential is notably higher on the LFP cathode compared to the Cu/Li electrode. Resistance originating from the LFP-electrolyte interface is therefore seen as the likely reason to be the main ohmic contribution. The increase in overpotential can also be explained by the the LFP-electrolyte interface. The viscosity of the electrolyte makes wetting deep into the LFP-cathode difficult, leading to a high overpotential when delithiating the innermost lithium.

Even though most cells containing either electrolyte cycled fine, stability issues were observed in electrolytes containing both DME and TEGDME. The LiFSI-TEGDME electrolyte turned out to be particularly unstable when exposed to the cycling conditions of Program 2, as it was unable to charge properly. A closer look at the first two cycles extracted from Fig. 4.12 is presented in Fig. 5.1, showing that the voltage curves during delithiation see a sudden drop followed by irregular and fluctuating movement in the voltage profile. The reason why this occurs is unclear, but reasons such as; decomposition of electrolyte and or corrosion of aluminium current collector was seen as possible reasons, given the reported disadvantages associated with ether solvents [83, 84, 85, 38].

However, the brief testing done with the higher capacity LFP-cathode, at 3.5 mAh/cm^2 , instead of 2.0 mAh/cm^2 provided some valuable results. The sudden drop in the voltage profile occurred more or less after it had delithiated for about five to six hours, equal to about 65-75% of the total eight-hour discharge. When cycling at the same C-rate for the LFP with 75% more capacity, the drop in voltage profile happened earlier, typically after just 3-4 hours. This gave a reason to believe that it had something to do with the amount of lithium plated, as it happened more or less at the same capacity charged, being approximately 1.4 mAh/cm^2 .

The delithiation at Program 1 supports the assumption that it has to do with the lithium. If there were any presence of corrosion or decomposition, one would expect it to occur at both cycling programs, not only in Program 2, as the voltage reaches the same values in Program 1, if not higher, due to being charged at a higher rate. As seen in Fig. 4.6, no irregular voltage profiles are observed, which could be explained

by the 30% DoD in Program 1 compared to the 80% in Program 2. The apparent connection between the sudden drop in voltage profile and lithium plating naturally makes dendrite formation a probable candidate causing the unstable cycling.

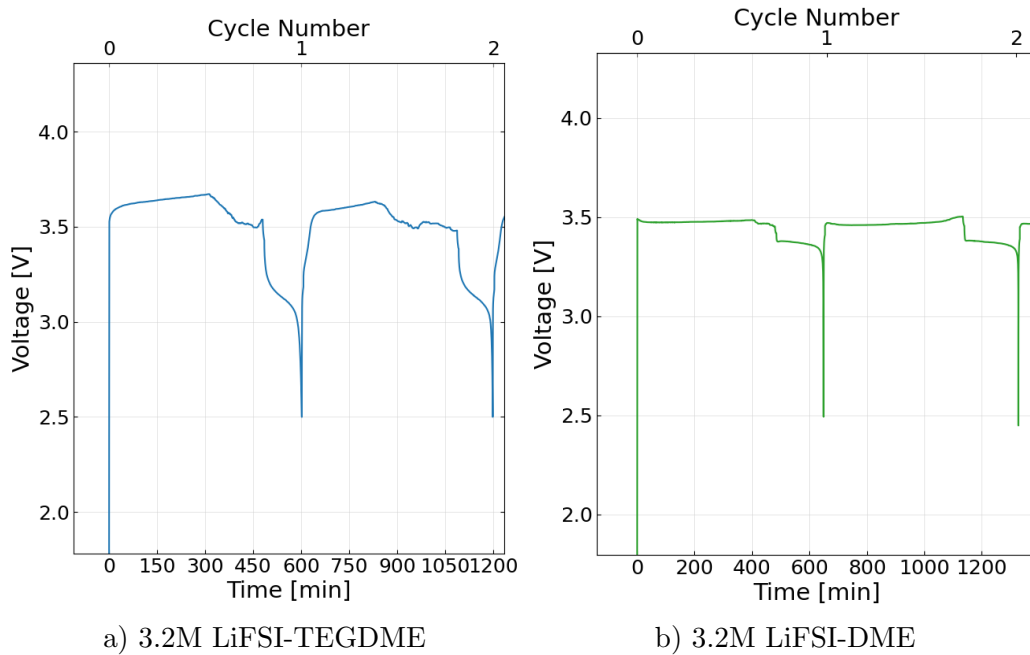


Figure 5.1: Voltage profile of the initial cycle of the two electrolytes without LiNO_3 additive, extracted from Fig. 4.12

The three electrode cycling done on PAT-cells and the X-ray diffractograms of cycled delithiated LFP materials provided further information. Fig. 4.13a establishes that the instability is occurring at the counter electrode, being the LFP. Thin dendrite structures touching or influencing the potential could potentially be the explanation for this.

The X-ray diffractograms clearly show an LFP-peak remaining in the LiFSI-TEGDME sample, meaning that the LFP was not delithiated properly. Based on Dodd's work [69], the amount of lithium left in the LFP can be estimated at around 10%, but as the LFP is not homogeneously delithiated and the calculated X-ray penetration depth is about $20 \mu\text{m}$, and the LFP is about $100 \mu\text{m}$, this can be expected to be significantly more.

The X-ray diffractogram of the LFP cycled in LiFSI-DME electrolyte also indicates some lithium left in the cathode. While being a smaller amount, it should not be

overlooked.

Even though the LiFSI in TEGDME clearly was the most unstable, some of the cells containing LiFSI in DME showed similar tendencies. The cells experiencing a sudden drop in voltage followed by an irregular voltage profile for the remaining delithiation, as shown in Fig. 5.1b. However, this was unlike LiFSI-TEGDME not experienced in all cells, and the cells experiencing this drop managed to recover and cycle stably with a lifetime just as long, unlike the LiFSI-TEGDME cells. The enormous standard deviation for cycle 1 in this electrolyte observed in Fig. 4.11 can be explained by this phenomenon. The explanation for the recovery is unknown, but a possibility is that the DME-LIFSI cells manage to create a stable SEI, but only after two cycles, while the LiFSI-TEGDME never tends to form a stable SEI layer.

The cyclic voltammetry support this possibility. As seen in Fig. 4.20c, the anodic peak current is lower in the two initial cycles. This behavior is unlike the stable electrolytes containing LiNO_3 , where the anodic peak current only was lower in the first cycle, indicating SEI still being formed in cycle 2 for LiFSI-DME electrolyte. In Fig. 4.20a, the anodic current is generally much lower than the cathodic current density for all cycles, indicating lower reversibility due to continuous SEI formation, which also fits with the galvanostatic cycling results.

As discussed, the sudden weird behavior of voltage profiles occurring for the LiFSI-TEGDME and LiFSI-DME electrolyte, as shown in Fig. 5.1, is believed to be caused by dendrites. From Bai and his group's work, this looks pretty likely [14]. Given his work, the point where the sudden drop occurs is expected to be the transition from mossy lithium to dendritic lithium. It seems likely to be due to reaching "Sand's capacity" as it is not experienced in the cycling program having lower DoD. The voltage profile drop occurring later in the LiFSI-DME electrolyte means this electrolyte has a longer Sand's time (and Sand's capacity) than LiFSI-TEGDME. The eventual formation of a stable SEI layer in LiFSI-DME makes it able to recover from this, unlike the cell containing LiFSI-TEGDME.

In addition to the challenges experienced during the initial cycle, the LiFSI-DME

electrolyte, sees sudden drops in CE, which is reflected in Fig. 4.3 and 4.9. Possible explanations for this are that large chunks of SEI break or large lithium pieces get loose, causing dead lithium, resulting in a low CE and a significant capacity drop. However, judging from the voltage profiles, Fig. 4.12c shows the voltage profile at cycle nine looking remarkably similar to the issues experienced in the first cycle, leading one to believe it could be the same reason.

The lifetime did not seem to be affected by the sudden drop in CE, as they had more or less the same lifetime as equivalent cells where such values were not observed. This similar lifetime is reason to believe these occasionally low CE values are not a correct indicator of the capacity loss in these cells.

The SEM images provide additional information as to what could be the reason for the sudden CE drop. As seen in Fig. 4.21, the plated lithium in LiFSI-DME has a rather rough and uneven morphology, noticeably more uneven than LiFSI-TEGDME.

The observation of large chunks of deposited material makes it difficult to neglect the possibility that large pieces of lithium can loosen and result in substantial capacity losses. However, it can also indicate easier dendrite formation, making it difficult to conclude anything with certainty.

The noticeable rougher deposition of lithium in DME is somewhat surprising. Given the better cycling performances of the DME-based electrolyte, one might expect it to have a more uniform morphology. Still, the results clearly show that it is more complicated than first assumed.

Another result worth mentioning was an observed gradient in the amount of deposited material on the Cu surface, with more material deposits along where the corresponding edges of LFP were located during cycling. This effect was much more evident on the cells with DME, which is likely connected to the lower resistances of the DME-based electrolytes, seen in Table 4.4.

5.2 Effect of LiNO₃ additive

One of the primary aims was to look at the effect adding LiNO₃ had on the performance of the battery cells, investigating the impact it had on both ether solvents containing the LiFSI salt. The galvanostatic cycling revealed LiNO₃ is improving the coulombic efficiency and lifetime. Still, as importantly, it improved the stability of the cells, with cells cycling without any of the problems experienced in the LiNO₃-free electrolytes.

Fig. 4.1 shows the clear improvements attributed to the addition of LiNO₃ in Program 1, giving over 3 and 2 % improvements in the average CE for LiFSI in TEGDME and LiFSI in DME respectively, presented in Table 4.1. This improvement led to the LiFSI + LiNO₃ in DME electrolyte to achieve an average coulombic efficiency of 99% with a lifetime of over 200 cycles.

The cells cycled on Program 2 also saw a drastic improvement with the LiNO₃, improving the coulombic efficiencies and eliminating the occurrences of voltage drops previously experienced with no LiNO₃ content. In Program 2, adding LiNO₃ made the TEGDME-based electrolyte going from not being able to cycle properly to cycle with an average CE of 98.6 %. A similar improvement is seen with adding LiNO₃ to the LiFSI in DME. It improved the average CE, and eliminated the issues experienced, such as the unusual behavior during the first cycle and the sudden drops in CE when cycling. This improvement caused the electrolyte to cycle stable with high CE for all cycles. This improvement is displayed in Fig. 4.9, as one can observe the higher coulombic efficiencies with more minor variances overall. The same effect is also clearly observable for Program 1 in Fig. 4.3.

The X-ray diffractograms presented in Fig. 4.23 reveals there being less lithium left in the cathode material cycled with the LiNO₃ containing electrolytes, as the LiFePO₄-peaks are less pronounced, more or less non-observable compared to their LiNO₃-less counterpart. This result indicates the cells with LiNO₃ are able to delithiate better, which is preferred, being an indication of better battery performance. One can easily observe the resolved stability issues by LiNO₃ addition in the voltage profiles for Program 2.

For the TEGDME-based electrolytes, the comparison between Fig. 4.6a and b shows LiNO_3 resolving the voltage drop issues thought to be caused by dendrite formation. Fig. 4.13 further confirms this, showing the previously unstable LFP counter electrode being able to cycle excellently with the addition of LiNO_3 . By comparing Fig. 4.6c and d, one also sees the improvements as the first cycle is went excellent reflected by an average initial CE of 93 %, giving less capacity loss, as presented in Fig. 4.11. All the following cycles before failure also cycle fine, unlike the samples containing DME electrolyte without any additive.

As dendrite formation is the probable cause for the issues experienced with the electrolytes not containing any additive, the LiNO_3 is believed to limit or eliminate dendrite formation. The prevention of dendrite formation is likely to be linked with the SEI layer, with LiNO_3 contributing to a better performing SEI-layer able to protect the lithium metal better, which is in agreement with previously reported work done on the influence of LiNO_3 [1, 50, 45].

Though it is not very noticeable, the cyclic voltammograms (Fig. 4.18) does reveal that adding LiNO_3 makes a difference in the initial decomposition products, eventually forming the SEI. Between the TEGDME-based electrolytes, there are observable distinctions in cathodic current from about 2 V to 1V. The DME-based electrolytes seem more similar, but one can argue that there is a difference at around 1.6 V and 1 V. These distinctions imply different species formed, with LiNO_3 likely contributing to an improved SEI.

The lower anodic currents relative to the cathodic currents during the first cycle, observed in Fig. 4.20 for the LiNO_3 -containing electrolytes, also imply the formation of a good SEI as the following cycles seem to cycle reversibly. However, Fig. 4.20d shows the current generally decreasing for increasing cycle number. This decrease indicate a relatively poor conductivity and high interfacial resistance due to the SEI that has formed, which is not preferred.

Fig. 4.5 shows that the electrolytes containing LiNO_3 have a generally lower CE in the initial cycle than the same electrolytes without any additive. Again this implies more formation of SEI during the initial cycle.

The SEM images presented in Fig. 4.21 and 4.22 also reveal that LiNO_3 has an overall improved effect on the morphology in both solvent-based systems. LiFSI - TEGDME has a web-like structure with a relatively large concentration of deposited material, while LiFSI + LiNO_3 - TEGDME has a uniform and sphere-like morphology. One could see the same kind of improvements in the DME-based electrolytes, with the morphology shifting towards being more uniform with the addition of LiNO_3 .

The better morphology can also be confirmed by the pictures taken of the opened cells, shown in Fig. 4.24. The fact that the lithium remains on the copper surface in both electrolytes containing LiNO_3 , while being stuck in the separator in both electrolytes without any LiNO_3 is a clear evidence that the lithium depositions has better contact with the copper and that it has not grown dendrite like structures into the separator material. This is believed to be the reason why the lithium is stuck in the two electrolytes without LiNO_3 as poor contact with copper substrate and branched lithium structures into the separator made ram in the separator when the copper and separator was taken apart from each other.

The improved morphology and better SEI provided by adding LiNO_3 are probable reasons for experiencing better cell performances. The improved SEI protects the lithium metal better and prevents dendrite growth from occurring, effectively increasing the Sand's time/Sand's capacity. The better morphology leads to less lithium exposure towards the electrolyte resulting in better coulombic efficiencies and a longer lifetime.

5.3 The importance of cycling conditions

Altering the cycling conditions to investigate its effect on cycling performance was also a major focus of this work. All cycling programs 1-5 used in this work provided valuable information on the effects of current density, relative difference between charge and discharge rate, and depth of discharge.

The LiFSI + LiNO_3 in DME was the electrolyte chosen for the investigation, as it was the best performing electrolyte in Program 1 and 2. Consequently, when discussing the cycling conditions this is the only electrolyte considered.

The results presented in Fig. 4.14 gives a clear indication that an asymmetric charge/discharge protocol is beneficial. As the symmetrical program were tested with a very low rate compared to the other programs, one would expect this to give the better performance, but this is not the case. All asymmetrical programs, which all cycled at higher rates compared to the symmetrical program, gives similar or better performance.

All three asymmetrical programs has as good or higher average CE and similar or longer lifetime compared to the symmetrical. Having a slower charge and faster discharge is therefore proven to be beneficial. This agrees with previous reported work related to optimal cycling parameters when using lithium metal [2, 59].

However, one can observe a rather surprising result when comparing the three asymmetrical programs. Fig. 4.17 shows one of the programs, Program 3, giving an undoubtedly better performance compared to the rest. This cycling program is the medium charge/discharge rate program. Fig. 4.16 shows that this program gives the best performance with an average CE of 99.4 % lasting for more cycles, with many cycles having efficiencies over 99.6 %. The fact that it is the program with the intermediate current density is a fascinating discovery that suggest that the slow program has too low rates and the fast program having too high rates. This is definitely something that should be investigated further, to gain more knowledge on the mechanisms determining the performance.

The DoD was set as 80 % in all programs except Program 1 were DoD was about 34 %. As the only program with a different DoD also was symmetric and at a different rate, comparing these programs determining the effect of DoD should be taken with a grain of salt. Still, given the results from all cycling conditions tested it is fair to say that a lower DoD provide improved performance. A lower DoD contributing to lower capacity loss, and a longer lifetime in equivalent full cycles, something which is in agreement with previous work [59].

With a higher DoD there is a high chance lithium would grow more and more dendritic as more is plated. Even if this will not cause the cell to fail, it would expose more lithium towards the electrolyte, resulting in more capacity loss per

lithium, the more lithium is plated per area. This idea suggests that using an even thinner LFP with $< 2\text{mAh}/\text{cm}^2$ would be beneficial.

The DoD should also be chosen with respect to the corresponding lithium reservoir that would be remaining in the cathode. In that sense an 80 % DoD seems a bit too high, even considering the best performing electrolyte on the best performing cycling program using 80 % DoD. With the lower CE values experienced the first few cycles due to SEI formation, almost all of the reservoir is gone after just a few cycles in the 80 % DoD programs. With almost no lithium left for cycling after SEI is formed, it causes the cells to have a lifetime of 20-30 cycles, while the cells in Program 1 lasts over 200 cycles.

The other solution would be to alter the electrolyte to be able to form a stable SEI without consuming as much lithium. This require the CE in the initial cycles to be higher. This is clearly the ideal solution, but if this is actually achievable is unsure. Another thing is to try to alter the cut-off voltage to alter the lithium reservoir left on the copper, but this is not tested here as the same cut of has been used in all programs. The more realistic solution, given the electrolytes reported in this work, would be to decrease the DoD below 80 %. Decreasing it just to i.e. 70% would drastically increase the lifetime as the remaining lithium reservoir after SEI formation would be much larger, thereby contributing to much longer lifetime.

In retrospect, it is clear that this analysis is a bit lackluster when discussing the implications of some of the influencing parameters, i.e. that more symmetrical programs should have been tested at higher rates and that the DoD should be the only variable changed in some of the programs to provide quantitative results of its effect.

5.4 The anode free cell configuration, The LFP-Cu system

The capacity loss derived from CE and the lifetime should be directly correlated. However, by comparing the measured coulombic efficiencies with the observed lifetimes of each cell, one could see that the realized lifetime of each cell is higher than what the coulombic efficiency suggests. This behavior suggests that there is cross

talk in the cells.

When cycling a cell, the coulombic efficiency is the yield of charge from one charge/discharge cycle. A 99% CE would imply a 1% irreversible loss of capacity. Fig. 4.4, 4.10 and 4.15, represents the total capacity loss and are directly calculated from the coulombic efficiencies of the respective cells. If this was the actual capacity loss of lithium, one would see a clear decrease in CE-values, and therefore a further decrease in the respective capacity, when the total capacity went under the cycle/charge capacity. The charge capacity is marked with a dashed line in the respective figures.

The expected failure or decrease when the capacity drops under the DoD is a result of the setup and end conditions of the cycling programs used. The programs delithiate the LFP at a certain time equal to the cycle capacity, even though there isn't sufficient lithium in the LFP to cover the entire charge capacity.

This expected decrease when reaching the cycle capacity is not observed. The expected behavior seems to happen much later for all electrolytes. The sudden drop in DME around the cycle capacity observed in Fig. 4.4 is just a coincidence in this specific sample, as it is exactly when the unexpected stability issue occurs, which causes a large drop in one cycle. One can observe the capacity decreasing linearly after this, until it actually fails at around 100 cycles.

Fig. 5.2 display the expected lifetime given the CE, marked with a dashed line, compared to the actual experienced lifetime, marked with a solid line.

Nanda et al. reported an average coulombic efficiency of 96 % CE, using a anode-free Cu-Li₂S cell, corresponding to 1.7 % capacity retention after 50 cycles [63]. Still, they received a 51.5 % capacity retention after 50 cycles, which is explained by the polysulfide shuttle effect. They also reported that this phenomenon would not occur when using a cathode such as i.e. LFP, which contradicts the results presented here. Given the assumption that there is no cross talk, the only explanation is that the capacity of the LFP is significantly higher than specified. Although a certain error margin is possible, the capacity needed to justify the results makes this rather unlikely. Though not as evident as in Nanda's groups work, cross talk is believed to have some influence in the anode free Cu-LFP cell as well.

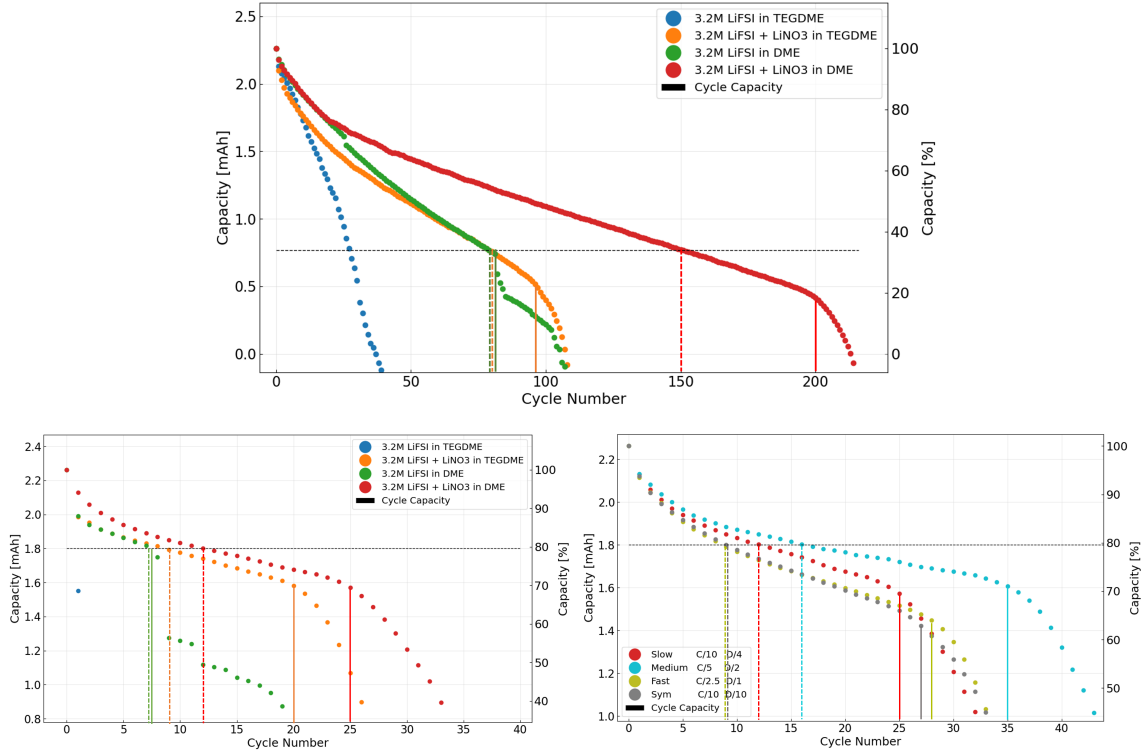


Figure 5.2: CE-capacity retention, vs actual lifetime. Extracted from Fig. 4.4, 4.10, and 4.15. The dashed lines are marking the expected lifetime given the CE values, as this is at the time the capacity crosses the cycle capacity. The solid lines marked the actual lifetime, seen by a non linear drop in capacity, caused by the actual lithium reserve being lower than the DoD

Given the lifetime of the cell, the initial capacity and the DoD capacity one could calculate the linear average CE needed to provide such a lifetime. The equation becomes:

$$TotalCapacity \cdot (avgCE)^{n_{cycles} * DoD} = CycleCapacity \quad (5.1)$$

Given this one could quantitatively calculate the difference between measured coulombic efficiency and the coulombic efficiency needed for the actually observed lifetimes.

A respective improvements given the actual lifetimes observed, for the $LiNO_3$ containing electrolytes, is presented in Table 5.1.

Table 5.1: Linear CE values given measured CE and observed lifetime. Lifetime CE being taken from Fig. 5.2, seen as the dashed line, which is the expected lifetime given the CE values. Actual lifetime is the lifetime observed for each cell. Avg CE and Avg CE* are calculated directly from the lifetimes marked in Fig. 5.2 using Eq. 5.1

Electrolyte	Cycling Prog	Lifetime CE	Avg CE	Actual Lifetime	Avg CE*
LiFSI + LiNO ₃ - TEGDME	1	80	96.1	96	96.7
LiFSI + LiNO ₃ - DME	1	150	97.9	200	98.4
LiFSI + LiNO ₃ - TEGDME	2	9	96.9	20	98.6
LiFSI + LiNO ₃ - DME	2	12	97.6	25	98.9
LiFSI + LiNO ₃ - DME	3	16	98.2	35	99.2
LiFSI + LiNO ₃ - DME	4	9	96.9	28	99.0
LiFSI + LiNO ₃ - DME	5	9	96.9	27	98.9

Another important parameter not investigated in this work is the influence of separator. Bai et al. reported that having a stiff, permeable and nanoporous separator is crucial for these systems, to prevent dendritic growth better [14]. The usage of glass fiber may not be the best solution, as it may not be the ideal separator to block dendrites. Glass fiber is also very thick, making it unsuitable for commercial use. Different separators should therefore be considered in further work when testing the anode free lithium metal batteries.

6 Conclusion

The investigation of anode-free lithium metal batteries was the topic of this work. The aim of the work was to compare the use of two ether solvents, study the effect of LiNO_3 additive, and investigate the importance cycling parameters have on the performance of the cell.

Of the two ether solvents investigated (TEGDME and DME), DME proved to be the optimal solvent. Overall, DME provided improved reversibility, longer lifetime, and better stability compared to TEGDME. However, DME led to a considerably rougher morphology in the deposited lithium compared to TEGDME.

Adding LiNO_3 is shown to have a significant effect on the performance of the cells. The electrolytes containing LiNO_3 exhibit much higher efficiencies and longer lifetimes, with the best electrolyte, $\text{LiFSI} + \text{LiNO}_3$ in DME, being able to cycle with an average CE of 98.92 % for over 200 cycles. LiNO_3 is shown to improve the stability of the electrolytes, which is believed to be linked with dendrite growth. The addition of LiNO_3 is also shown to promote more uniform lithium morphologies when plated on the copper surface.

Cycling conditions are clearly demonstrated to affect the cycling stability. The results confirm that a slower charge and faster discharge is beneficial for the reversibility of the cell. Of the asymmetrical cycling protocols, the one with the intermediate rates is clearly shown to give the best performance, with an average CE of 99.4%. A lower DoD is also shown to be beneficial, and given the electrolytes used, 80 % DoD is concluded to be slightly too high, with a DoD of 60-70% believed to be optimal.

The CE values and observed lifetimes of the cells are not in accordance with each other, which is possibly the result of cross talk in the cell.

7 Further work

As LiFSI + LiNO₃ in DME was identified to be the optimal electrolyte in this work, further investigation could be to further optimize this electrolyte composition. Testing new concentrations of LiFSI salt and LiNO₃ is a possibility. Introducing additional additives and multiple salts in addition to LiFSI should be done in further investigation potentially to achieve superior performances.

In this work, all asymmetric cycling protocols had the same relative difference between charge and discharge rate, D/C = 2.5. Further work should be done looking more closely into this, preferably investigating several rates with different D/C ratios. The same goes for DoD, and given a similar system, this work suggests investigating cells using DoD of 60-70 %.

Additional suggestions for further work include studying the effect of separators more closely as it was not explored extensively in this work. Thinner and more permeable separators can potentially control dendrite growth better. Another proposition is to further investigate the electrodes such as the copper foil and LFP, to look at their influence in the cell. Given this work, the use of a thinner LFP is suggested, e.g, with an areal capacity of 1.0 - 1.5 mAh/cm².

Bibliography

- [1] Heng Zhang, Gebrekidan Gebresilassie Eshetu, Xabier Judez, Chunmei Li, Lide M. Rodriguez-Martínez, and Michel Armand. Electrolyte Additives for Lithium Metal Anodes and Rechargeable Lithium Metal Batteries: Progress and Perspectives. *Angewandte Chemie International Edition*, 57(46):15002–15027, 2018. _eprint: <https://onlinelibrary.wiley.com/doi/pdf/10.1002/anie.201712702>.
- [2] Jiangfeng Qian, Brian D. Adams, Jianming Zheng, Wu Xu, Wesley A. Henderson, Jun Wang, Mark E. Bowden, Suochang Xu, Jianzhi Hu, and Ji-Guang Zhang. Anode-Free Rechargeable Lithium Metal Batteries. *Advanced Functional Materials*, 26(39):7094–7102, 2016. _eprint: <https://onlinelibrary.wiley.com/doi/pdf/10.1002/adfm.201602353>.
- [3] Jun Liu, Zhenan Bao, Yi Cui, Eric J. Dufek, John B. Goodenough, Peter Khalifah, Qiuyan Li, Bor Yann Liaw, Ping Liu, Arumugam Manthiram, Y. Shirley Meng, Venkat R. Subramanian, Michael F. Toney, Vilayanur V. Viswanathan, M. Stanley Whittingham, Jie Xiao, Wu Xu, Jihui Yang, Xiao-Qing Yang, and Ji-Guang Zhang. Pathways for practical high-energy long-cycling lithium metal batteries. *Nature Energy*, 4(3):180–186, March 2019. Number: 3 Publisher: Nature Publishing Group.
- [4] A. J. Louli, A. Eldesoky, Rochelle Weber, M. Genovese, Matt Coon, Jack deGooyer, Zhe Deng, R. T. White, Jaehan Lee, Thomas Rodgers, R. Petibon, S. Hy, Shawn J. H. Cheng, and J. R. Dahn. Diagnosing and correcting anode-free cell failure via electrolyte and morphological analysis. *Nature Energy*, 5(9):693–702, September 2020. Bandiera_abtest: a Cg_type: Nature Research Journals Number: 9 Primary_atype: Research Publisher: Nature Publishing Group Subject_term: Electrochemistry;Energy;Energy storage Subject_term_id: electrochemistry;energy;energy-storage.
- [5] John B. Goodenough and Youngsik Kim. Challenges for Rechargeable Li Batteries †. *Chemistry of Materials*, 22(3):587–603, February 2010.
- [6] Jakob Asenbauer, Tobias Eisenmann, Matthias Kuenzel, Arefeh Kazzazi, Zhen Chen, and Dominic Bresser. The success story of graphite as a lithium-ion anode material – fundamentals, remaining challenges, and recent developments including silicon (oxide) composites. *Sustainable Energy & Fuels*, 4(11):5387–5416, 2020. Publisher: Royal Society of Chemistry.
- [7] John B. Goodenough and Kyu-Sung Park. The Li-Ion Rechargeable Battery: A Perspective. *Journal of the American Chemical Society*, 135(4):1167–1176, January 2013. Publisher: American Chemical Society.
- [8] Wenchen Ren, Wei Ma, Shufen Zhang, and Bingtao Tang. Recent advances in shuttle effect inhibition for lithium sulfur batteries. *Energy Storage Materials*, 23:707–732, December 2019.

-
- [9] Ali Eftekhari. Low voltage anode materials for lithium-ion batteries. *Energy Storage Materials*, 7:157–180, April 2017.
- [10] Jun Lu, Zhongwei Chen, Feng Pan, Yi Cui, and Khalil Amine. High-Performance Anode Materials for Rechargeable Lithium-Ion Batteries. *Electrochemical Energy Reviews*, 1(1):35–53, March 2018.
- [11] Xin Shen, He Liu, Xin-Bing Cheng, Chong Yan, and Jia-Qi Huang. Beyond lithium ion batteries: Higher energy density battery systems based on lithium metal anodes. *Energy Storage Materials*, 12:161–175, May 2018.
- [12] Hee Jung Chang, Andrew J. Ilott, Nicole M. Trease, Mohaddese Mohammadi, Alexej Jerschow, and Clare P. Grey. Correlating Microstructural Lithium Metal Growth with Electrolyte Salt Depletion in Lithium Batteries Using ^7Li MRI. *Journal of the American Chemical Society*, 137(48):15209–15216, December 2015. Publisher: American Chemical Society.
- [13] C. Brissot, M. Rosso, J. N. Chazalviel, and S. Lascaud. Dendritic growth mechanisms in lithium/polymer cells. *Journal of Power Sources*, 81-82:925–929, September 1999.
- [14] Peng Bai, Ju Li, Fikile R. Brushett, and Martin Z. Bazant. Transition of lithium growth mechanisms in liquid electrolytes. *Energy & Environmental Science*, 9(10):3221–3229, October 2016. Publisher: The Royal Society of Chemistry.
- [15] E. Peled. The Electrochemical Behavior of Alkali and Alkaline Earth Metals in Nonaqueous Battery Systems—The Solid Electrolyte Interphase Model. *Journal of the Electrochemical Society*, 126(12):2047, December 1979. Publisher: IOP Publishing.
- [16] Yaguang Zhang, Ning Du, and Deren Yang. Designing superior solid electrolyte interfaces on silicon anodes for high-performance lithium-ion batteries. *Nanoscale*, 11(41):19086–19104, October 2019. Publisher: The Royal Society of Chemistry.
- [17] Dingchang Lin, Yayuan Liu, and Yi Cui. Reviving the lithium metal anode for high-energy batteries. *Nature Nanotechnology*, 12(3):194–206, March 2017. Number: 3 Publisher: Nature Publishing Group.
- [18] Ghulam Yasin, Muhammad Arif, Tahira Mehtab, Xia Lu, Donglin Yu, Noor Muhammad, M. Tariq Nazir, and Huaihe Song. Understanding and suppression strategies toward stable Li metal anode for safe lithium batteries. *Energy Storage Materials*, 25:644–678, March 2020.
- [19] Doron Aurbach. Review of selected electrode–solution interactions which determine the performance of Li and Li ion batteries. *Journal of Power Sources*, 89(2):206–218, August 2000.
- [20] Haiping Wu, Hao Jia, Chongmin Wang, Ji-Guang Zhang, and Wu Xu. Recent Progress in Understanding Solid Electrolyte Interphase on Lithium
-

-
- Metal Anodes. *Advanced Energy Materials*, 11(5):2003092, 2021. _eprint: <https://onlinelibrary.wiley.com/doi/pdf/10.1002/aenm.202003092>.
- [21] Rongxiang Hu, Huayu Qiu, Huanrui Zhang, Peng Wang, Xiaofan Du, Jun Ma, Tianyuan Wu, Chenglong Lu, Xinhong Zhou, and Guanglei Cui. A Polymer-Reinforced SEI Layer Induced by a Cyclic Carbonate-Based Polymer Electrolyte Boosting 4.45 V LiCoO₂/Li Metal Batteries. *Small*, 16(13):1907163, 2020. _eprint: <https://onlinelibrary.wiley.com/doi/pdf/10.1002/sml.201907163>.
- [22] Haitao Wang and Yongbing Tang. Artificial Solid Electrolyte Interphase Acting as “Armor” to Protect the Anode Materials for High-performance Lithium-ion Battery. *Chemical Research in Chinese Universities*, 36(3):402–409, June 2020.
- [23] Seho Sun, Seungcheol Myung, Gaeun Kim, Dongsoo Lee, Hyunsu Son, Minchul Jang, Eunkyung Park, Byoungkuk Son, Yeon-Gil Jung, Ungyu Paik, and Taeseup Song. Facile ex situ formation of a LiF–polymer composite layer as an artificial SEI layer on Li metal by simple roll-press processing for carbonate electrolyte-based Li metal batteries. *Journal of Materials Chemistry A*, 8(33):17229–17237, August 2020. Publisher: The Royal Society of Chemistry.
- [24] Rui Xu, Xue-Qiang Zhang, Xin-Bing Cheng, Hong-Jie Peng, Chen-Zi Zhao, Chong Yan, and Jia-Qi Huang. Lithium Metal Anodes: Artificial Soft–Rigid Protective Layer for Dendrite-Free Lithium Metal Anode (Adv. Funct. Mater. 8/2018). *Advanced Functional Materials*, 28(8):1870049, 2018. _eprint: <https://onlinelibrary.wiley.com/doi/pdf/10.1002/adfm.201870049>.
- [25] Dingchang Lin, Yayuan Liu, Zheng Liang, Hyun-Wook Lee, Jie Sun, Haotian Wang, Kai Yan, Jin Xie, and Yi Cui. Layered reduced graphene oxide with nanoscale interlayer gaps as a stable host for lithium metal anodes. *Nature Nanotechnology*, 11(7):626–632, July 2016. Number: 7 Publisher: Nature Publishing Group.
- [26] Tamene Tadesse Beyene, Hailemariam Kassa Bezabh, Misganaw Adigo Weret, Teklay Mezgebe Hagos, Chen-Jui Huang, Chia-Hsin Wang, Wei-Nien Su, Hongjie Dai, and Bing-Joe Hwang. Concentrated Dual-Salt Electrolyte to Stabilize Li Metal and Increase Cycle Life of Anode Free Li-Metal Batteries. *Journal of The Electrochemical Society*, 166(8):A1501, May 2019. Publisher: IOP Publishing.
- [27] Yanpeng Guo, Huiqiao Li, and Tianyou Zhai. Reviving Lithium-Metal Anodes for Next-Generation High-Energy Batteries. *Advanced Materials*, 29(29):1700007, 2017. _eprint: <https://onlinelibrary.wiley.com/doi/pdf/10.1002/adma.201700007>.
- [28] Yingying Lu, Zhengyuan Tu, and Lynden A. Archer. Stable lithium electrodeposition in liquid and nanoporous solid electrolytes. *Nature Materials*, 13(10):961–969, October 2014.
-

Bandiera_abtest: a Cg_type: Nature Research Journals Number: 10 Primary_atype: Research
Publisher: Nature Publishing Group Subject_term: Batteries Subject_term_id: batteries.

- [29] Huadong Yuan, Jianwei Nai, He Tian, Zhijin Ju, Wenkui Zhang, Yujing Liu, Xinyong Tao, and Xiong Wen David Lou. An ultrastable lithium metal anode enabled by designed metal fluoride spansules. *Science advances*, 6(10):eaaz3112, March 2020.
- [30] Jianming Zheng, Joshua A. Lochala, Alexander Kwok, Zhiqun Daniel Deng, and Jie Xiao. Research Progress towards Understanding the Unique Interfaces between Concentrated Electrolytes and Electrodes for Energy Storage Applications. *Advanced Science*, 4(8):1700032, 2017. eprint: <https://onlinelibrary.wiley.com/doi/pdf/10.1002/advs.201700032>.
- [31] Wu Xu, Jiulin Wang, Fei Ding, Xilin Chen, Eduard Nasymbulin, Yaohui Zhang, and Ji-Guang Zhang. Lithium metal anodes for rechargeable batteries. *Energy & Environmental Science*, 7(2):513–537, January 2014. Publisher: The Royal Society of Chemistry.
- [32] D. Aurbach, M. L. Daroux, P. W. Faguy, and E. Yeager. Identification of Surface Films Formed on Lithium in Propylene Carbonate Solutions. *Journal of the Electrochemical Society*, 134(7):1611, July 1987. Publisher: IOP Publishing.
- [33] Fei Ding, Wu Xu, Gordon L. Graff, Jian Zhang, Maria L. Sushko, Xilin Chen, Yuyan Shao, Mark H. Engelhard, Zimin Nie, Jie Xiao, Xingjiang Liu, Peter V. Sushko, Jun Liu, and Ji-Guang Zhang. Dendrite-Free Lithium Deposition via Self-Healing Electrostatic Shield Mechanism. *Journal of the American Chemical Society*, 135(11):4450–4456, March 2013. Publisher: American Chemical Society.
- [34] Doron Aurbach, Yosef Gofer, Moshe Ben-Zion, and Pinchas Aped. The behaviour of lithium electrodes in propylene and ethylene carbonate: The major factors that influence Li cycling efficiency. *Journal of Electroanalytical Chemistry*, 339(1):451–471, November 1992.
- [35] Fei Ding, Wu Xu, Xilin Chen, Jian Zhang, Mark H. Engelhard, Yaohui Zhang, Bradley R. Johnson, Jarrod V. Crum, Thomas A. Blake, Xingjiang Liu, and Ji-Guang Zhang. Effects of Carbonate Solvents and Lithium Salts on Morphology and Coulombic Efficiency of Lithium Electrode. *Journal of The Electrochemical Society*, 160(10):A1894, September 2013. Publisher: IOP Publishing.
- [36] Y. Gofer, M. Ben-Zion, and D. Aurbach. Solutions of LiAsF₆ in 1,3-dioxolane for secondary lithium batteries. *Journal of Power Sources*, 39(2):163–178, January 1992.
- [37] Shuhong Jiao, Xiaodi Ren, Ruiguo Cao, Mark H. Engelhard, Yuzi Liu, Dehong Hu, Donghai Mei, Jianming Zheng, Wengao Zhao, Qiuyan Li, Ning Liu, Brian D. Adams, Cheng Ma, Jun Liu, Ji-Guang Zhang, and Wu Xu. Stable cycling of high-voltage lithium metal batteries

in ether electrolytes. *Nature Energy*, 3(9):739–746, September 2018. Number: 9 Publisher: Nature Publishing Group.

- [38] Xiaodi Ren, Lianfeng Zou, Shuhong Jiao, Donghai Mei, Mark H. Engelhard, Qiuyan Li, Hongkyung Lee, Chaojiang Niu, Brian D. Adams, Chongmin Wang, Jun Liu, Ji-Guang Zhang, and Wu Xu. High-Concentration Ether Electrolytes for Stable High-Voltage Lithium Metal Batteries. *ACS Energy Letters*, 4(4):896–902, April 2019. Publisher: American Chemical Society.
- [39] Ethan P. Kamphaus, Stefany Angarita Gomez, Xueping Qin, Minhua Shao, and Perla B. Balbuena. Effects of Solid Electrolyte Interphase Components on the Reduction of LiFSI over Lithium Metal. *ChemPhysChem*, 21(12):1310–1317, 2020. eprint: <https://chemistry-europe.onlinelibrary.wiley.com/doi/pdf/10.1002/cphc.202000174>.
- [40] Gebrekidan Gebresilassie Eshetu, Thomas Diemant, Sylvie Grugeon, R. Jürgen Behm, Stephane Laruelle, Michel Armand, and Stefano Passerini. In-Depth Interfacial Chemistry and Reactivity Focused Investigation of Lithium–Imide- and Lithium–Imidazole-Based Electrolytes. *ACS Applied Materials & Interfaces*, 8(25):16087–16100, June 2016. Publisher: American Chemical Society.
- [41] Hong-Bo Han, Si-Si Zhou, Dai-Jun Zhang, Shao-Wei Feng, Li-Fei Li, Kai Liu, Wen-Fang Feng, Jin Nie, Hong Li, Xue-Jie Huang, Michel Armand, and Zhi-Bin Zhou. Lithium bis(fluorosulfonyl)imide (LiFSI) as conducting salt for nonaqueous liquid electrolytes for lithium-ion batteries: Physicochemical and electrochemical properties. *Journal of Power Sources*, 196(7):3623–3632, April 2011.
- [42] D. Aurbach, I. Weissman, A. Zaban, and O. Chusid. Correlation between surface chemistry, morphology, cycling efficiency and interfacial properties of Li electrodes in solutions containing different Li salts. *Electrochimica Acta*, 39(1):51–71, January 1994.
- [43] Ya-Xia Yin, Sen Xin, Yu-Guo Guo, and Li-Jun Wan. Lithium–Sulfur Batteries: Electrochemistry, Materials, and Prospects. *Angewandte Chemie International Edition*, 52(50):13186–13200, 2013. eprint: <https://onlinelibrary.wiley.com/doi/pdf/10.1002/anie.201304762>.
- [44] Jennifer Heine, Peter Hilbig, Xin Qi, Philip Niehoff, Martin Winter, and Peter Bieker. Fluoroethylene Carbonate as Electrolyte Additive in Tetraethylene Glycol Dimethyl Ether Based Electrolytes for Application in Lithium Ion and Lithium Metal Batteries. *Journal of The Electrochemical Society*, 162(6):A1094, March 2015. Publisher: IOP Publishing.
- [45] Jing Guo, Zhaoyin Wen, Meifen Wu, Jun Jin, and Yu Liu. Vinylene carbonate–LiNO₃: A hybrid additive in carbonic ester electrolytes for SEI modification on Li metal anode. *Electrochemistry Communications*, 51:59–63, February 2015.

-
- [46] Cao Cuong Nguyen and Brett L. Lucht. Comparative Study of Fluoroethylene Carbonate and Vinylene Carbonate for Silicon Anodes in Lithium Ion Batteries. *Journal of The Electrochemical Society*, 161(12):A1933, September 2014. Publisher: IOP Publishing.
- [47] Snehashis Choudhury and Lynden A. Archer. Lithium Fluoride Additives for Stable Cycling of Lithium Batteries at High Current Densities. *Advanced Electronic Materials*, 2(2):1500246, 2016. eprint: <https://onlinelibrary.wiley.com/doi/pdf/10.1002/aelm.201500246>.
- [48] Doron Aurbach, Elad Pollak, Ran Elazari, Gregory Salitra, C. Scordilis Kelley, and John Affinito. On the Surface Chemical Aspects of Very High Energy Density, Rechargeable Li–Sulfur Batteries. *Journal of The Electrochemical Society*, 156(8):A694, June 2009. Publisher: IOP Publishing.
- [49] Han Jin, Huayun Liu, Hao Cheng, Peng Zhang, and Miao Wang. The synergistic effect of lithium bis(fluorosulfonyl)imide and lithium nitrate for high-performance lithium metal anode. *Journal of Electroanalytical Chemistry*, 874:114484, October 2020.
- [50] Shizhao Xiong, Kai Xie, Yan Diao, and Xiaobin Hong. Properties of surface film on lithium anode with LiNO₃ as lithium salt in electrolyte solution for lithium–sulfur batteries. *Electrochimica Acta*, 83:78–86, November 2012.
- [51] Shuru Chen, Jianming Zheng, Donghai Mei, Kee Sung Han, Mark H. Engelhard, Wengao Zhao, Wu Xu, Jun Liu, and Ji-Guang Zhang. High-Voltage Lithium-Metal Batteries Enabled by Localized High-Concentration Electrolytes. *Advanced Materials*, 30(21):1706102, 2018. eprint: <https://onlinelibrary.wiley.com/doi/pdf/10.1002/adma.201706102>.
- [52] Mengyun Nie, Daniel P Abraham, Daniel M Seo, Yanjing Chen, Arijit Bose, and Brett L Lucht. Role of Solution Structure in Solid Electrolyte Interphase Formation on Graphite with LiPF₆ in Propylene Carbonate. *J. Phys. Chem. C*, page 9, 2013.
- [53] Toshihiko Mandai, Kazuki Yoshida, Kazuhide Ueno, Kaoru Dokko, and Masayoshi Watanabe. Criteria for solvate ionic liquids. *Physical Chemistry Chemical Physics*, 16(19):8761–8772, April 2014. Publisher: The Royal Society of Chemistry.
- [54] Kazuki Yoshida, Megumi Nakamura, Yuichi Kazue, Naoki Tachikawa, Seiji Tsuzuki, Shiro Seki, Kaoru Dokko, and Masayoshi Watanabe. Oxidative-Stability Enhancement and Charge Transport Mechanism in Glyme–Lithium Salt Equimolar Complexes. *Journal of the American Chemical Society*, 133(33):13121–13129, August 2011. Publisher: American Chemical Society.
- [55] Dennis W. McOwen, Daniel M. Seo, Oleg Borodin, Jenel Vatamanu, Paul D. Boyle, and Wesley A. Henderson. Concentrated electrolytes: decrypting electrolyte properties and reassessing Al corrosion mechanisms. *Energy & Environmental Science*, 7(1):416–426, December 2013. Publisher: The Royal Society of Chemistry.
-

-
- [56] Jiangfeng Qian, Wesley A. Henderson, Wu Xu, Priyanka Bhattacharya, Mark Engelhard, Oleg Borodin, and Ji-Guang Zhang. High rate and stable cycling of lithium metal anode. *Nature Communications*, 6(1):6362, February 2015. Number: 1 Publisher: Nature Publishing Group.
- [57] Chao Shen, Petru Andrei, and Jim P. Zheng. Stable cycling of lithium-sulfur batteries by optimizing the cycle condition. *Electrochimica Acta*, 326:134948, December 2019.
- [58] Thomas S. Bryden, Alexander Holland, George Hilton, Borislav Dimitrov, Carlos Ponce de León Albarrán, and Andrew Cruden. Lithium-ion degradation at varying discharge rates. *Energy Procedia*, 151:194–198, October 2018.
- [59] A. J. Louli, Matt Coon, M. Genovese, Jack deGooyer, A. Eldesoky, and J. R. Dahn. Optimizing Cycling Conditions for Anode-Free Lithium Metal Cells. *Journal of the Electrochemical Society*, 168(2):020515, February 2021. Publisher: The Electrochemical Society.
- [60] Matthew Genovese, A. J. Louli, Rochelle Weber, Sam Hames, and J. R. Dahn. Measuring the Coulombic Efficiency of Lithium Metal Cycling in Anode-Free Lithium Metal Batteries. *Journal of The Electrochemical Society*, 165(14):A3321, October 2018. Publisher: IOP Publishing.
- [61] A. J. Louli, Matthew Genovese, Rochelle Weber, S. G. Hames, E. R. Logan, and J. R. Dahn. Exploring the Impact of Mechanical Pressure on the Performance of Anode-Free Lithium Metal Cells. *Journal of The Electrochemical Society*, 166(8):A1291–A1299, 2019.
- [62] Liangdong Lin, Liumin Suo, Yong-sheng Hu, Hong Li, Xuejie Huang, and Liquan Chen. Epitaxial Induced Plating Current-Collector Lasting Lifespan of Anode-Free Lithium Metal Battery. *Advanced Energy Materials*, 11(9):2003709, 2021. _eprint: <https://onlinelibrary.wiley.com/doi/pdf/10.1002/aenm.202003709>.
- [63] Sanjay Nanda, Abhay Gupta, and Arumugam Manthiram. A Lithium–Sulfur Cell Based on Reversible Lithium Deposition from a Li₂S Cathode Host onto a Hostless-Anode Substrate. *Advanced Energy Materials*, 8(25):1801556, 2018. _eprint: <https://onlinelibrary.wiley.com/doi/pdf/10.1002/aenm.201801556>.
- [64] Jian Li, Ya Wang, Lihua Wang, Bin Liu, and Hongming Zhou. A facile recycling and regeneration process for spent LiFePO₄ batteries. *Journal of Materials Science: Materials in Electronics*, 30(15):14580–14588, August 2019.
- [65] Chunwen Sun, Shreyas Rajasekhara, John B. Goodenough, and Feng Zhou. Monodisperse Porous LiFePO₄ Microspheres for a High Power Li-Ion Battery Cathode. *Journal of the American Chemical Society*, 133(7):2132–2135, February 2011. Publisher: American Chemical Society.
-

-
- [66] Ghassan Zubi, Rodolfo Dufo-López, Monica Carvalho, and Guzay Pasaoglu. The lithium-ion battery: State of the art and future perspectives. *Renewable and Sustainable Energy Reviews*, 89:292–308, June 2018.
- [67] Wei-Jun Zhang. Structure and performance of LiFePO₄ cathode materials: A review. *Journal of Power Sources*, 196(6):2962–2970, March 2011.
- [68] Critical Raw Materials Resilience: Charting a Path towards greater Security and Sustainability, March 2020.
- [69] Joanna Lynn Dodd. *Phase Composition and Dynamical Studies of Lithium Iron Phosphate*. phd, California Institute of Technology, 2007.
- [70] Nobuyuki Imanishi, Alan C. Luntz, and Peter Bruce. *The Lithium Air Battery: Fundamentals*. Springer New York, Springer, New York, NY, 2014 edition, 2014.
- [71] Peter G. Bruce, Stefan A. Freunberger, Laurence J. Hardwick, and Jean-Marie Tarascon. Li–O₂ and Li–S batteries with high energy storage. *Nature Materials*, 11(1):19–29, January 2012. Number: 1 Publisher: Nature Publishing Group.
- [72] Yasin Emre Durmus, Huang Zhang, Florian Baakes, Gauthier Desmaizieres, Hagay Hayun, Liangtao Yang, Martin Kolek, Verena Küpers, Jürgen Janek, Daniel Mandler, Stefano Passerini, and Yair Ein-Eli. Side by Side Battery Technologies with Lithium-Ion Based Batteries. *Advanced Energy Materials*, 10(24):2000089, 2020. eprint: <https://onlinelibrary.wiley.com/doi/pdf/10.1002/aenm.202000089>.
- [73] Tobias Placke, Richard Kloepsch, Simon Dühnen, and Martin Winter. Lithium ion, lithium metal, and alternative rechargeable battery technologies: the odyssey for high energy density. *Journal of Solid State Electrochemistry*, 21(7):1939–1964, July 2017.
- [74] Jürgen Janek and Wolfgang G. Zeier. A solid future for battery development. *Nature Energy*, 1(9):1–4, September 2016. Number: 9 Publisher: Nature Publishing Group.
- [75] Richard T. Jow, Kang Xu, Oleg Borodin, and Makoto Ue, editors. *Electrolytes for Lithium and Lithium-Ion Batteries*. Modern Aspects of Electrochemistry. Springer-Verlag, New York, 2014.
- [76] M. H. Cho, J. Trottier, C. Gagnon, P. Hovington, D. Clément, A. Vijh, C. S. Kim, A. Guerfi, R. Black, L. Nazar, and K. Zaghbi. The effects of moisture contamination in the Li–O₂ battery. *Journal of Power Sources*, 268:565–574, December 2014.
- [77] Meng Zhao, Bo-Quan Li, Xue-Qiang Zhang, Jia-Qi Huang, and Qiang Zhang. A Perspective toward Practical Lithium–Sulfur Batteries. *ACS Central Science*, 6(7):1095–1104, July 2020. Publisher: American Chemical Society.
-

-
- [78] Zhiyu Wang, Yanfeng Dong, Hongjiang Li, Zongbin Zhao, Hao Bin Wu, Ce Hao, Shaohong Liu, Jie Qiu, and Xiong Lou. Enhancing lithium-sulphur battery performance by strongly binding the discharge products on amino-functionalized reduced graphene oxide. *Nature communications*, 5:5002, September 2014.
- [79] Zhi Wei Seh, Weiyang Li, Judy J. Cha, Guangyuan Zheng, Yuan Yang, Matthew T. McDowell, Po-Chun Hsu, and Yi Cui. Sulphur–TiO₂ yolk–shell nanoarchitecture with internal void space for long-cycle lithium–sulphur batteries. *Nature Communications*, 4(1):1331, January 2013. Number: 1 Publisher: Nature Publishing Group.
- [80] Marzieh Barghamadi, Adam S. Best, Anand I. Bhatt, Anthony F. Hollenkamp, Mustafa Musameh, Robert J. Rees, and Thomas R  ther. Lithium–sulfur batteries—the solution is in the electrolyte, but is the electrolyte a solution? *Energy & Environmental Science*, 7(12):3902–3920, November 2014. Publisher: The Royal Society of Chemistry.
- [81] Kazuhide Ueno, Kazuki Yoshida, Mizuho Tsuchiya, Naoki Tachikawa, Kaoru Dokko, and Masayoshi Watanabe. Glyme–Lithium Salt Equimolar Molten Mixtures: Concentrated Solutions or Solvate Ionic Liquids? *The Journal of Physical Chemistry B*, 116(36):11323–11331, September 2012. Publisher: American Chemical Society.
- [82] NIST X-ray Attenuation Databases.
- [83] Rongrong Miao, Jun Yang, Zhixin Xu, Jiulin Wang, Yanna Nuli, and Limin Sun. A new ether-based electrolyte for dendrite-free lithium-metal based rechargeable batteries. *Scientific Reports*, 6(1):21771, February 2016. Number: 1 Publisher: Nature Publishing Group.
- [84] Varvara Sharova, Arianna Moretti, Thomas Diemant, Alberto Varzi, R. J  rgen Behm, and Stefano Passerini. Comparative study of imide-based Li salts as electrolyte additives for Li-ion batteries. *Journal of Power Sources*, 375:43–52, January 2018.
- [85] Gabriela Horwitz, Ernesto J. Calvo, Lucila P. M  ndez De Leo, and Ezequiel de la Llave. Electrochemical stability of glyme-based electrolytes for Li–O₂ batteries studied by in situ infrared spectroscopy. *Physical Chemistry Chemical Physics*, 22(29):16615–16623, July 2020. Publisher: The Royal Society of Chemistry.

Appendices

A Supplementary results, electrochemical cycling

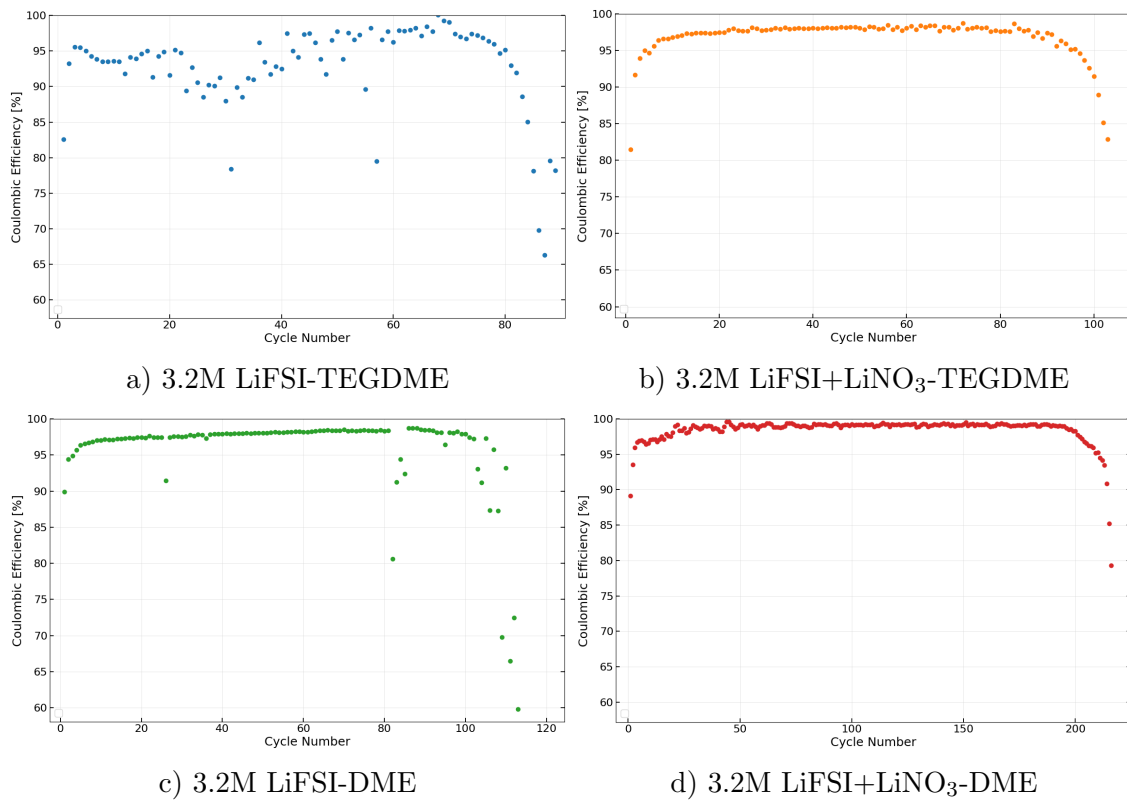


Figure A.1: Individual coulombic efficiencies for the selected samples cycled at Program 1

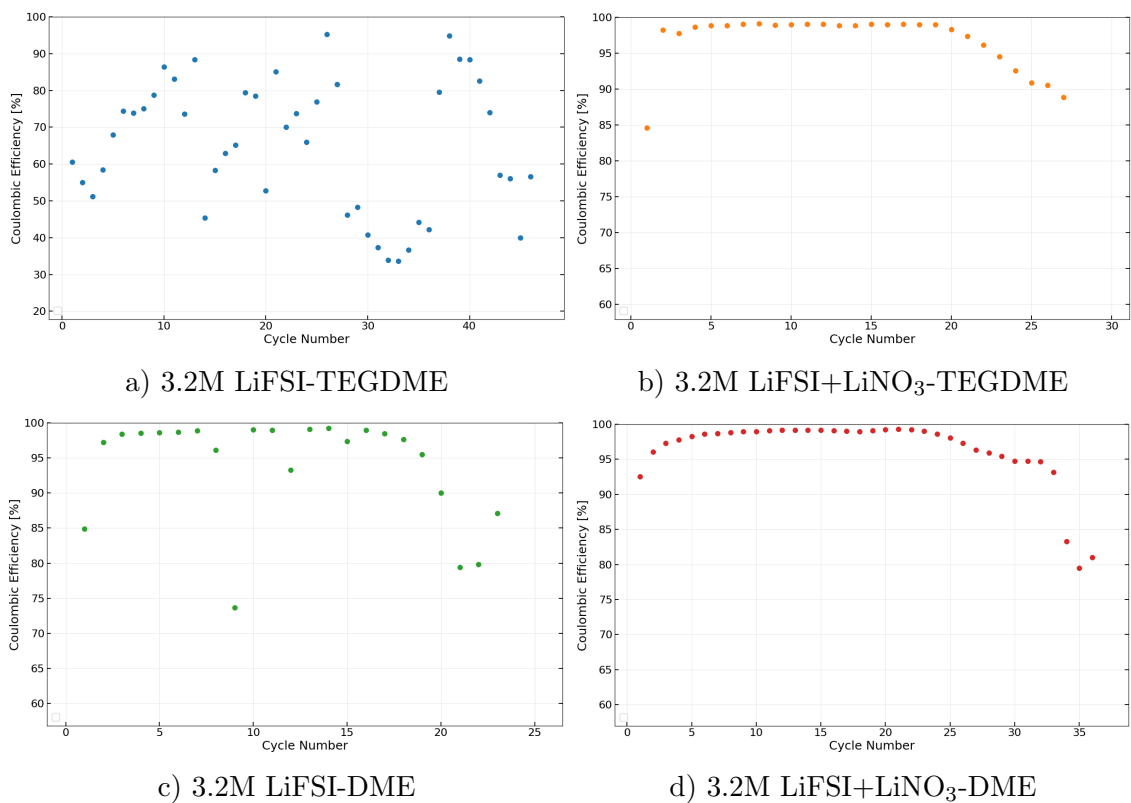


Figure A.2: Individual coulombic efficiencies for the selected samples cycled at Program 2

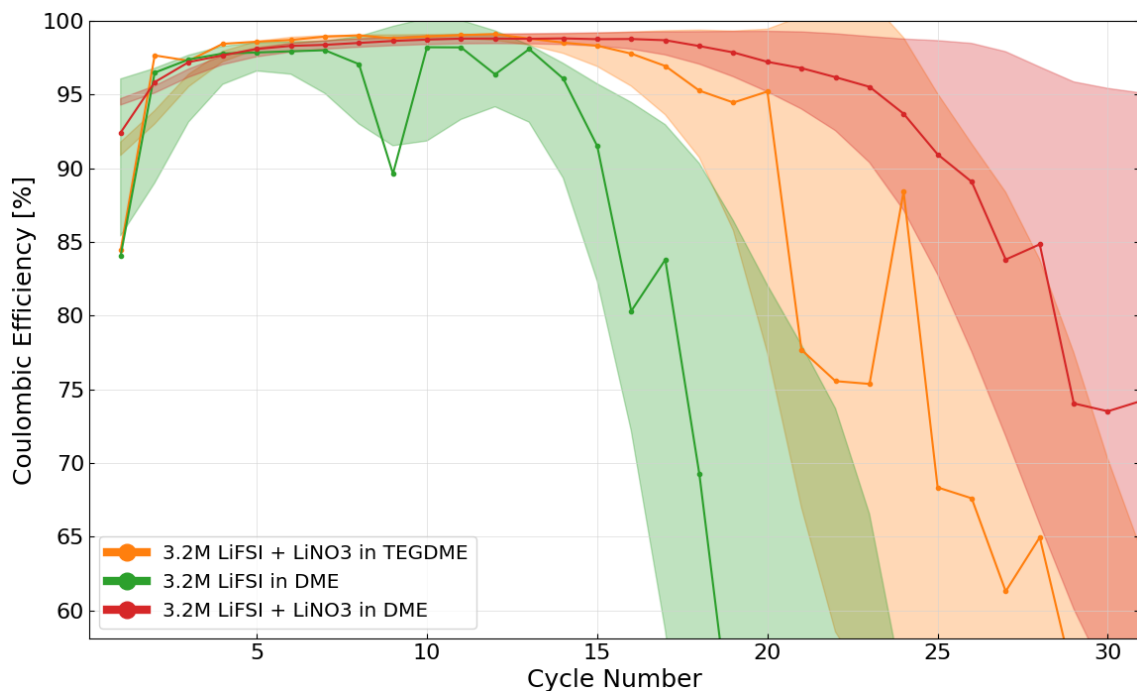


Figure A.3: Program 2, average coulombic efficiencies with standard deviation

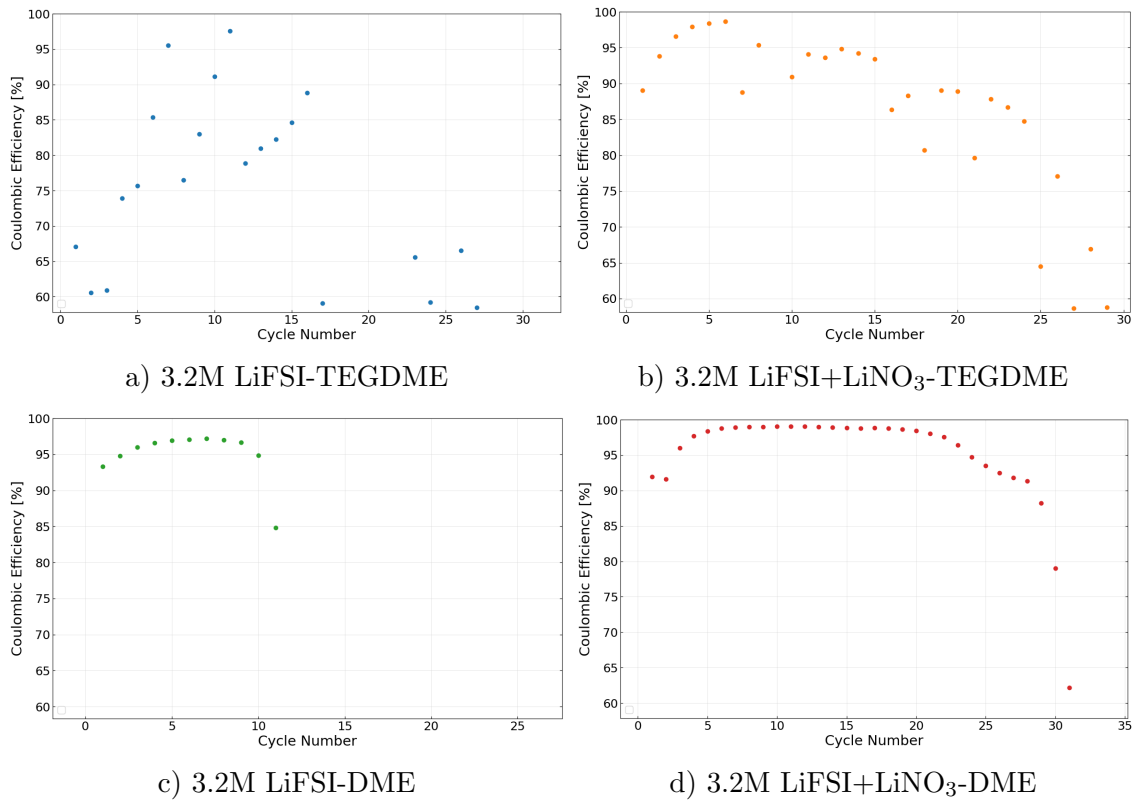


Figure A.4: Coulombic efficiencies of PAT-cells, cycled on Program 2*

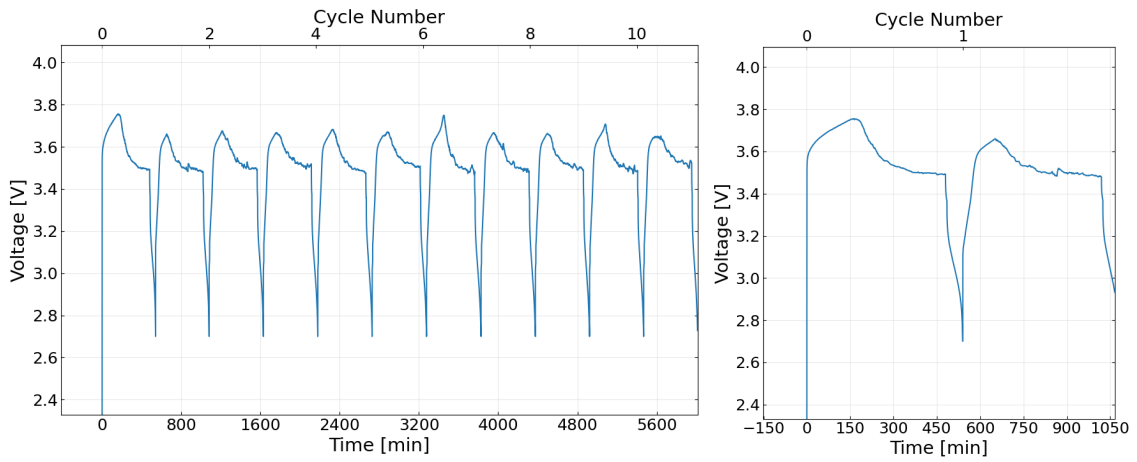


Figure A.5: Voltage curve, 3.2M LiFSI-TEGDME with 3.5mAh LFP, Program 2

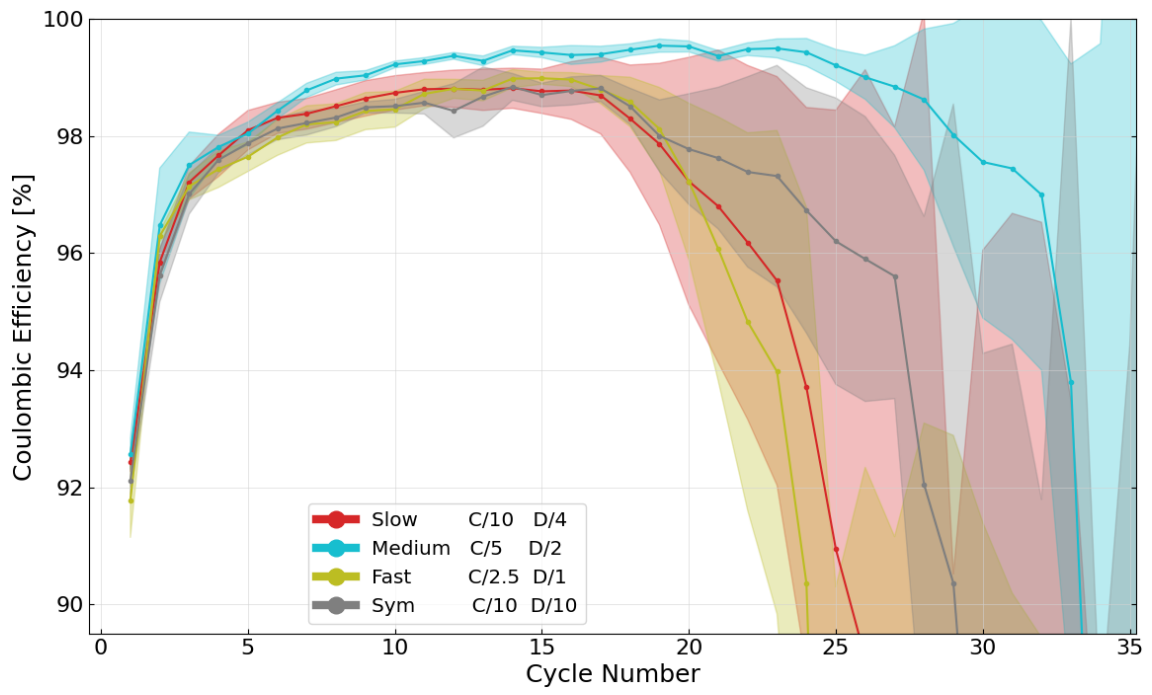
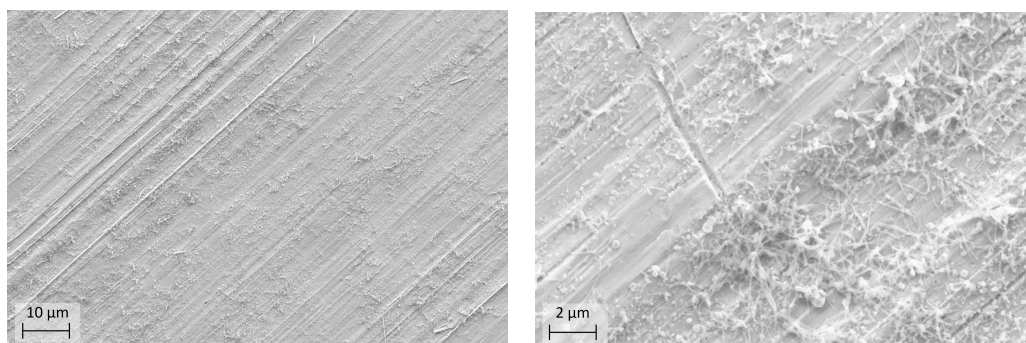


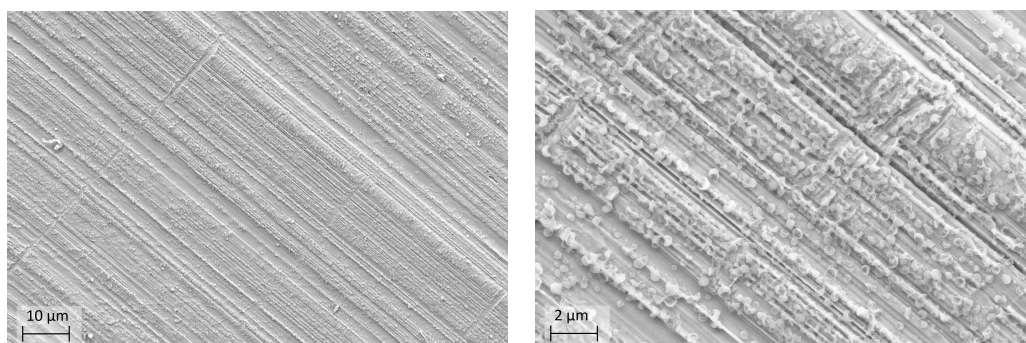
Figure A.6: Average coulombic efficiencies with standard deviation for each of the cycling programs

B Supplementary results, SEM

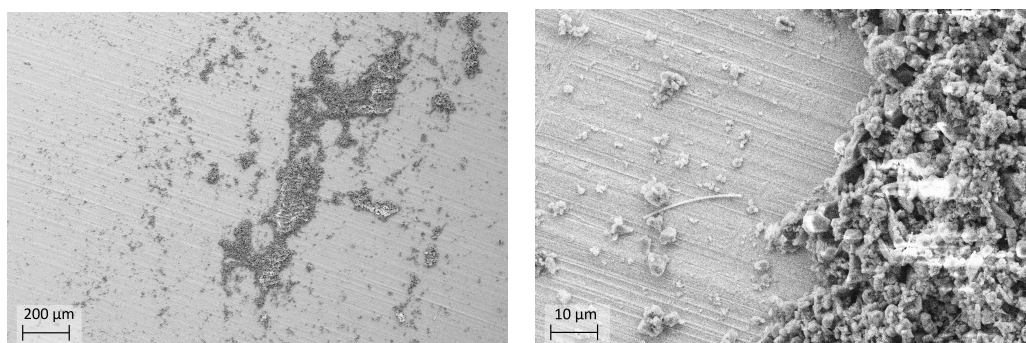
3 minutes deposition



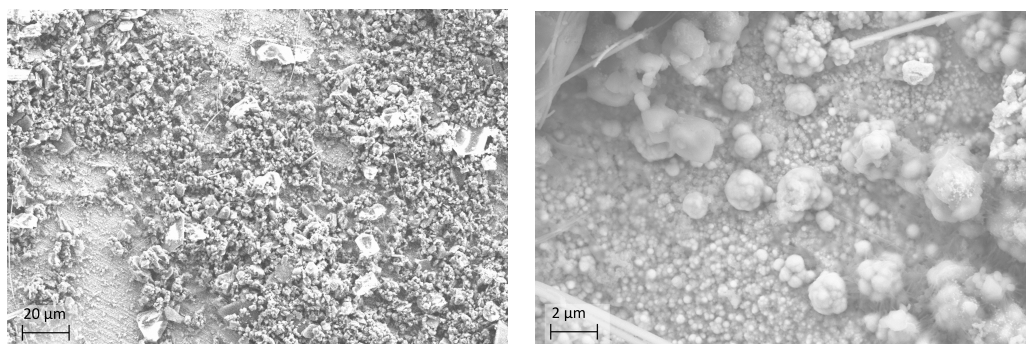
a) 3.2M LiFSI-TEGDME, (Left) Mag: 2k , (Right) Mag: 10K



b) 3.2M LiFSI+LiNO₃-TEGDME, (Left) Mag: 2k , (Right) Mag: 10K



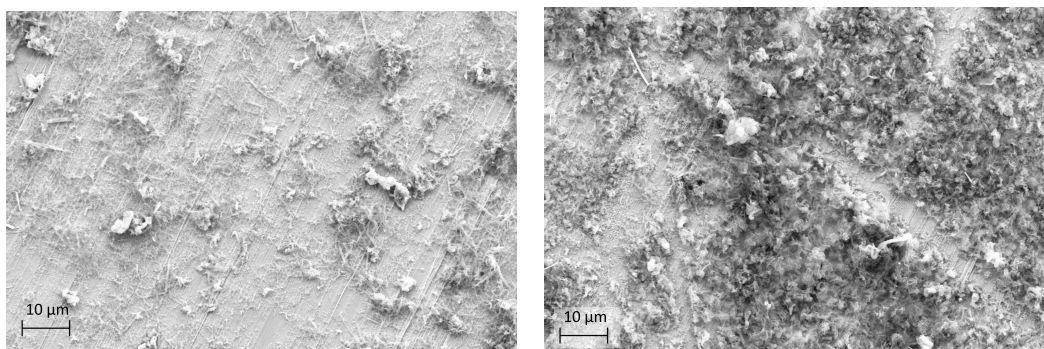
c) 3.2M LiFSI-DME, (Left) Mag: 100x , (Right) Mag: 2K



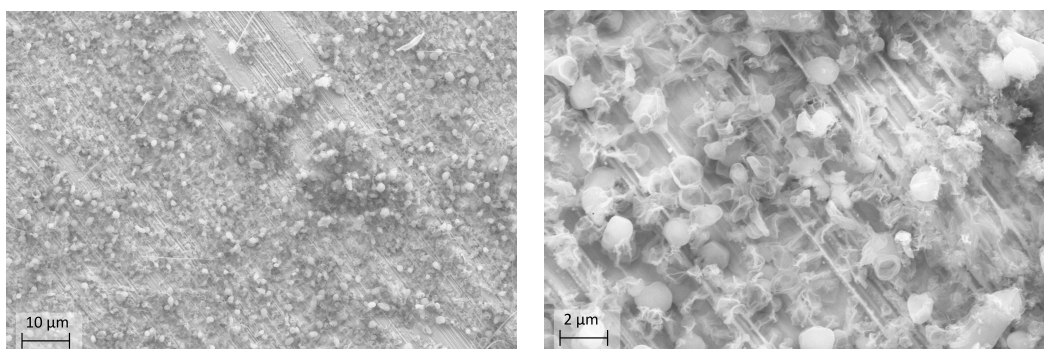
d) 3.2M LiFSI+LiNO₃-DME, (Left) Mag: 1k , (Right) Mag: 10K

Figure B.1: Additional SEM images taken of the copper surface after 3 minutes plating, all four electrolytes

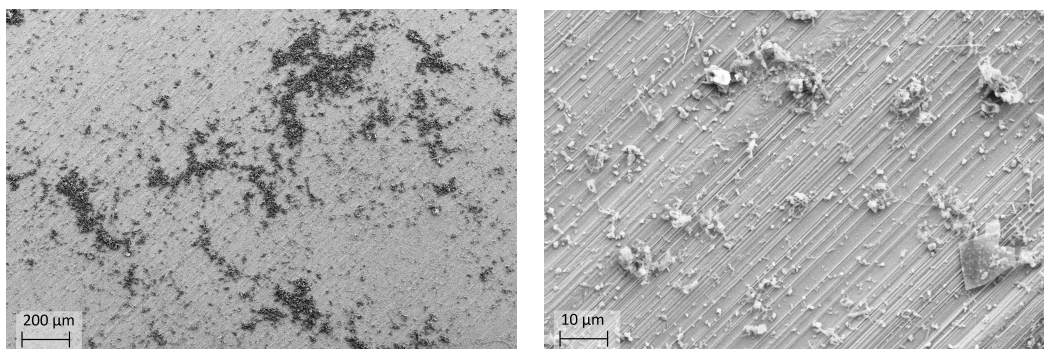
One charge discharge cycle/stripped



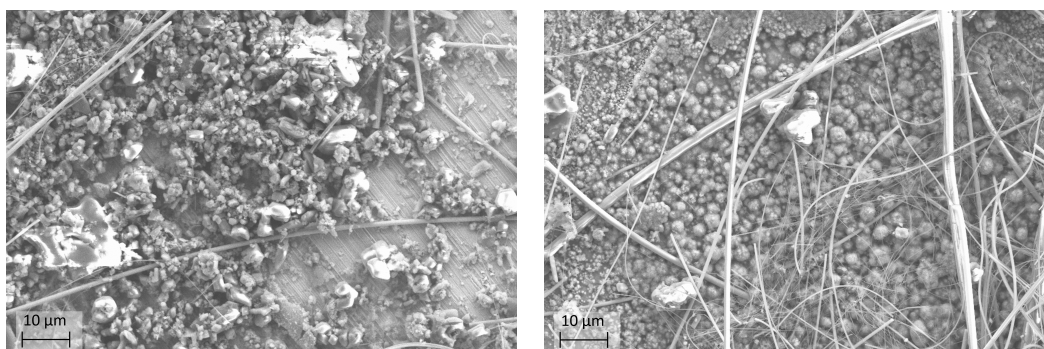
a) 3.2M LiFSI-TEGDME, Left) Mag: 2k , Right) Mag: 2K



b) 3.2M LiFSI+LiNO₃-TEGDME, Left) Mag: 2k , Right) Mag: 10K



c) 3.2M LiFSI-DME, Left) Mag: 100x , Right) Mag: 2K



d) 3.2M LiFSI+LiNO₃-DME, Left) Mag: 2k , Right) Mag: 2K

Figure B.2: Additional SEM images taken of the copper surface after one charge/discharge cycle, with the four electrolytes

C Supplementary results, XRD

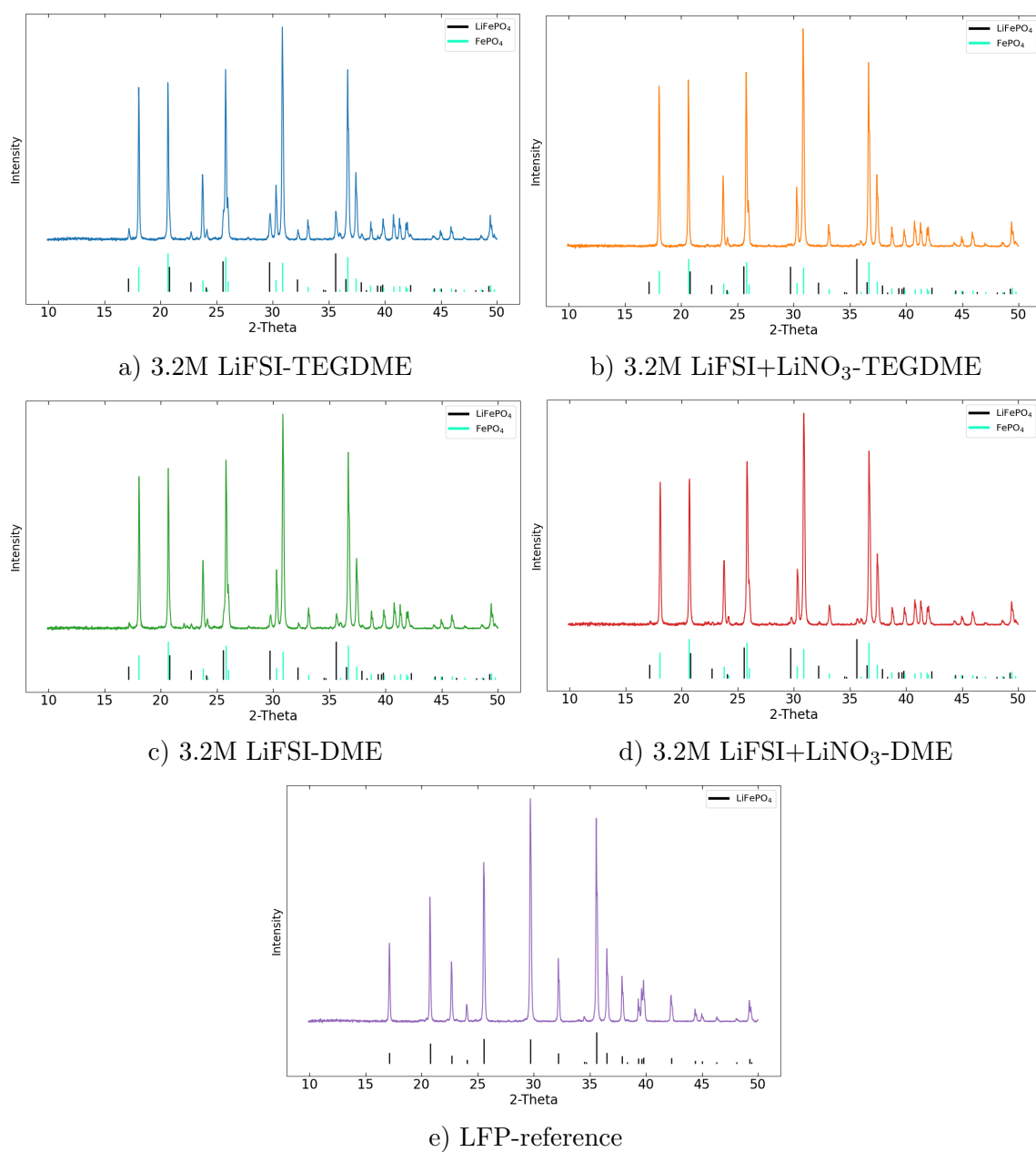


Figure C.1: Individual X-ray diffractograms of delithiated LFP cathodes cycled with all four electrolytes, including one lithiated LFP reference

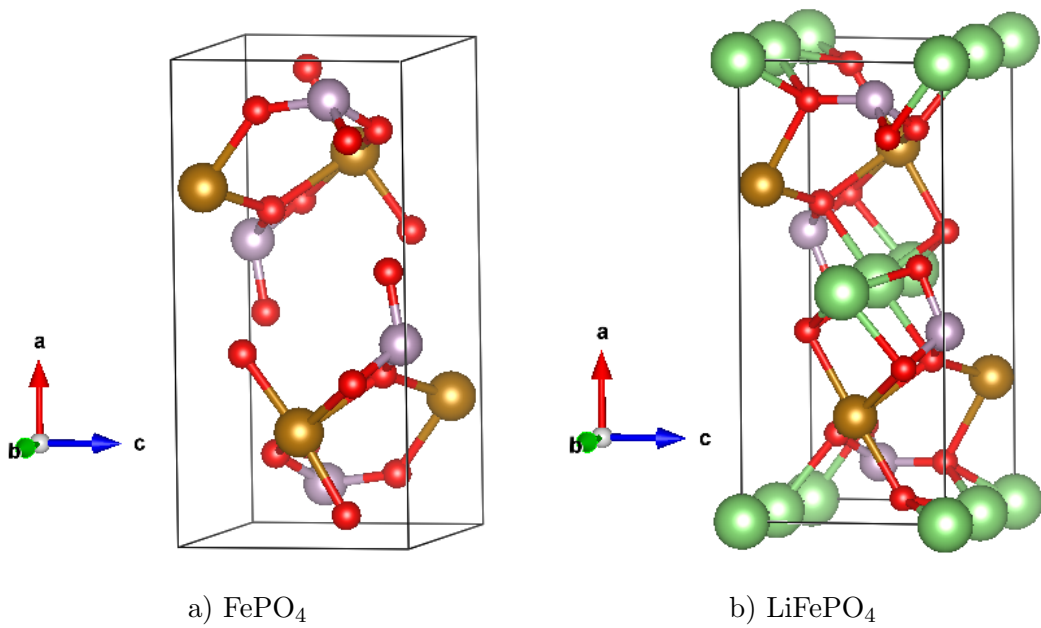


Figure C.2: The unit cells of FePO_4 and LiFePO_4 from the PDF database IDs used. Graphs extracted from the Vesta software.

